FACTA UNIVERSITATIS

Series
ARCHITECTURE AND CIVIL ENGINEERING
Vol. 22, № 1, 2024

22 | 1

FACTA UNIVERSITATIS

SERIES **ARCHITECTURE AND CIVIL ENGINEERING**
Vol. 22, Nº 1, 2024

UNIVERSITY OF NIŠ

INSTRUCTIONS FOR CONTRIBUTORS

Contributions should be (preferably) in English, French or German.

Under the paper title, the name(s) of the author(s) should be given while the full name, official title, institute or company affiliation and the like should be placed at the end of the paper together with the exact mail and e-mail address, as well as short (running) title of paper.

Manuscript format. A brief abstract of approximately 100 to 150 words in the same language and a list of up to six key words should precede the text body of the manuscript. All the authors apart from foreign ones should also submit a complete manuscript in Serbian. Manuscripts should be prepared as doc. file, Word version 6.0 or higher. Manuscript should be prepared using a Word template (downloaded from web address http://casopisi.junis.ni.ac.rs/index.php/FUArchCivEng/about/submissions#onlineSubmissions).

Manuscript length. Brief articles and discussions (10 pages or less) are encouraged. Otherwise, papers should present well-focused arguments of approximately 16 pages.

Style requirements. **Letters, figures and symbols** should be clearly denoted.

Equations should be typewritten and, with the number, placed in parentheses at the right margin. References to equations should be in the form "Eq. (2)" or simply (2). For equations that cannot be entered in a single line, use the Equation Editor in MS Word. In equations and in the text, *italicize* symbols that are used to represent variables or parameters, including subscripts and superscripts. Only use characters and symbols that are available in the Equation Editor, in the *Symbol font* or in *Times New Roman*.

All illustrations (figures, photographs, line drawings, graphs) should be numbered in series and all legends should be included at the bottom of each illustration. All figures, photographs, line drawings and graphs, should be prepared in electronic form and converted in TIFF or JPG (max quality) file types, in 300 dpi resolution, for superior reproduction. Figures, line drawings and graphs prepared using elements of MS Drawing or MS Graph must be converted in form of pictures and unchangeable. All illustrations should be planned in advance so as to allow reduction to 12.75 cm in column width. Please review all illustrations to ensure that they are readable.

All **tables** should be numbered with consecutive Arabic numbers. They should have descriptive captions at the top of each table and should be mentioned in the text.

The **references** should be numbered in the order in which they appear in the text, at the end of the manuscript, in the same way as the following examples:

1. Kollbruner C. F., Hajdin N., Stipanić B.: *Contribution to the Analysis of Cable-Stayed Bridges* N. 48, Schulthess Verlag, Zürich, 1980, pp. 66-77.
2. Đuranović P.: Organizacija upravljanja projektima, Izgradnja N° 1/96, Beograd, 1996, str. 45-52.
3. Živković D.: Influence of front excavation on the state and deformity of montage lining of hydraulic pressure tunnels, Ph. D. University of Niš, 1988, pp. 95-108.
4. Kurtović-Folić N.: Typology of Architectural Forms-Strong and Weak Typological Characteristics, Facta Universitatis, University of Niš, Vol. 1, N° 2, 1995, pp. 227-235.

References should be quoted in the text by the corresponding number in square brackets.

Electronic submission. Papers for consideration should be submitted to the Series Editor in electronic form via the Journal's home page: http://casopisi.junis.ni.ac.rs/index.php/FUArchCivEng/index.

Contents

Review Paper

THE COLORFUL FACADE DECORATIONS OF THE SECESSION STYLE IN SOFIA. SOFIA MINERAL BATHS AND THE RECOVERING OF MISSING ELEMENTS

UDC 721:7.035.93(497.2)

Blagovesta Ivanova

University of Structural Engineering & Architecture (VSU) "Lyuben Karavelov",
Department of Urban Planning, Theory and History of Architecture, Sofia, Bulgaria

ORCID iD: Blagovesta Ivanova   https://orcid.org/0000-0003-2994-2037

Abstract. *The report presents the national specific of the Secession style in the colourful ceramic decoration of some buildings in Sofia. The most representative between them are the church of St "Nikolay Novi Sofiiski", buildings of the Synodal Palace, the Central Mineral Baths, and the Higher Theological School at the Holy Synod, built and decorated between 1900 and 1922. They are the works of the architects Friedrich Grünanger, Yurdan Milanov and Petko Momchilov.*

The accent of the research is the ceramic decoration of the facades of the Central Mineral Baths in Sofia, by the project of Haralampi Tachev. The details of the types of ornaments are presented and analysed. The graphic designs for the restoration of the missing elements were considered. The impact of colour in the design of the facades is analysed. The peculiarities in the decoration and the connection of this style with the medieval elements, were examined.

The connection of the facade solutions with the Bulgarian historical traditions of the early Middle Ages and Byzantium is explained through examples from Preslav, the capital of the First Bulgarian Kingdom. This way the coloured ceramic tiles of the facades of the Central Mineral Baths are represented as an expression of the Bulgarian medieval tradition in the Secession style in Sofia.

The colour facade interpretations of the buildings in Vienna, Paris and Prague of that period are presented for comparison and demonstration of the national differences, decisions and tasks of the Secession style.

Key words: *ceramic and mosaic facade decoration, Sofia, Mineral Baths, buildings, Prague, Vienna, Paris.*

1. Introduction and Definition of the Peculiarities of Secession Style.
Several Reflections and Examples of Secession in Europe and in Bulgaria

The Secession style is one of the most interesting artistic phenomena in the European and American architecture and arts in the late 19th and early 20th c. According to its nature, it is multifaceted and is nationally colored. The national specificity in each country is related to the modern expression of the past styles or traditions, which are also expressed in the materials used.

The most representative examples in architecture in Vienna are: the decorative golden domed Secession Building (1897-98) [1] by architect Joseph Maria Olbrich (1867-1908); the glass-covered atriums in the interiors (Post Office Saving Bank, 1904-06); the metal (most popular is Karlsplatz station of the Vienna Stadtbahn (1894–99)), and ceramic decorations (Ceramic ceiling decoration and stained glass of Rumbach Street synagogue, 1870-73; Majolica House, 1898-99) by Otto Wagner (1841-1918) [2].

Fig. 1 Secession Building, Vienna, 1897-98, architect Joseph Maria Olbrich. The Great Building collection. Photography: Howard Davis.
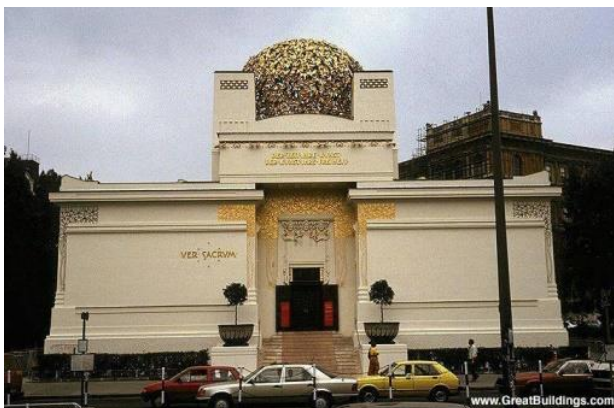
Fig. 2 Post Office Saving Bank, Vienna, 1904-06, architect Otto Wagner. The Great Building collection. Photography: Claudio Divizia.

Fig. 3 Majolica House, Vienna,1898-99, Otto Wagner. The Great Building collection.
Photography: Tibisay de Hoyos. http://www.greatbuildings.com/

The Secession in Paris is also expressed with the steel constructions, wall painting and mosaics, golden ornaments, covered passages and the domes of the large stores, decorated with colored glasses as: Bon Marche (1876, engineer Alexandre-Gustave Eiffel and architect Louis-Auguste Boileau) [3], Samaritaine (1905-10, architect Frantz Jourdain; 1926-28, Jourdain and Henry Sauvage,) [4] and Printemps (1865, Jules and Paul Sédille; domed hall 1904 Rene Binet) [5].
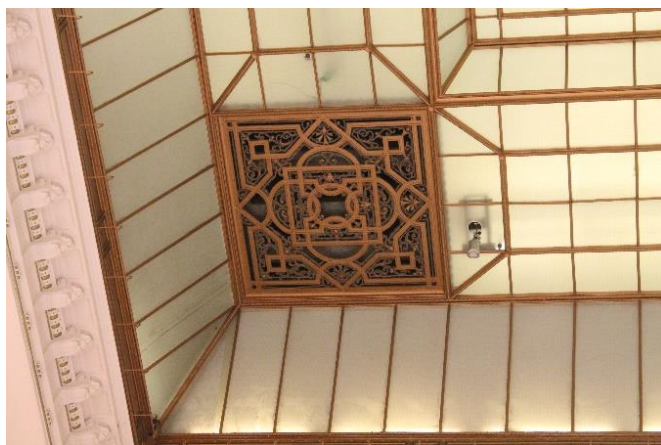
Fig. 4 Bon Marche, interior, Paris, 1876, engineer Alexandre-Gustave Eiffel and architect Louis-Auguste Boileau. Photography: Blagovesta Ivanova.

Fig. 5 Printemps, interior, Paris, 1865, Jules and Paul Sédille; domed hall 1904 Rene Binet. Photography: Blagovesta Ivanova.

Fig. 6 Samaritaine, interior, Paris,1905-10, architect Frantz Jourdain; 1926-28, Jourdain and Henry Sauvage. Photography: Blagovesta Ivanova.

One of the most famous Secession-style buildings in Prague is the Municipal House (1912, according to the project of architect Antonín Balšánek and Osvald Polívka as a centre of the Czech cultural life). The lunette mosaic in this building is the work of Karel Špillar representing the apotheosis of Prague. Stucco relief medallions, depicted the types of Czech folk costumes [6], which is an expression of national identity are placed between the windows. According to the thematic scope of the compositions, it is closest to the building of the mineral baths in Sofia.

Fig. 7 The Municipal House, detail from the façade, Prague, 1912, according to the project of architect Antonín Balšánek and Osvald Polívka. Photography: Blagovesta Ivanova.

Fig. 8 The Central Mineral bath, detail from the façade, Sofia, 1907-1915, architect Petko Momchilov. Photography: Blagovesta Ivanova.

Romantic inspiration from the past styles and eras, and the using of the gold are distinctive for the Secession. The means of expression in the shaping of the buildings

facades are diverse. They represent relief ornaments or mosaics, or ceramic tiles, in which has been read the reflection of the past. In its stylistic features, Secession was inspired by the East (ceramics), Egypt (stylized forms) and Byzantium (gold and mosaic techniques). Its difference from the Eclecticism is the bold use of the line and the modern understanding of the forms.

Ivaylo Nachev makes a successful summarized definition of the ornamentation in the Secession, defining its character as a connection with the "organic principle in nature" [7]. According to the same author "Secession becomes, in some sense, an expression and the platform of the growing modernization and Europeanization of the Bulgarian culture." [8], on a cultural level.

Secession in Bulgaria expresses the romantic returning to the past periods of the national culture, similar to the European one. The using of multicolor and ceramic elements (mainly chamotte) is based on the Bulgarian medieval tradition, associated with the architecture of the second Bulgarian capital Preslav (in the 10th century). It is expressed not only in the decorative art work elements. It can be seen in the compositions of the facades formed with decorative or real mixed masonry (i. e. alternation of "brick" friezes in the "smooth stone masonry"), and the using of bifora and triforium located under the semicircular arches in the window openings, too.
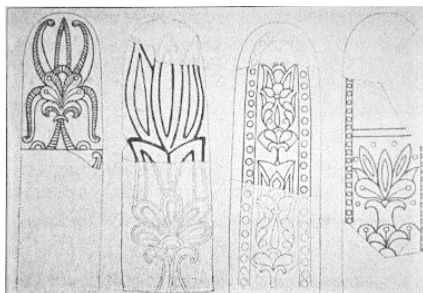
Fig. 9 Restored decoration of water liliies from Patleyna, [24], 330.
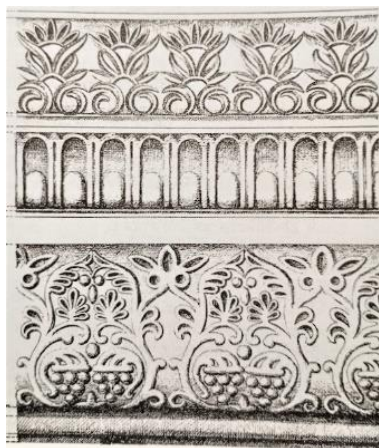
Fig. 10 Ornaments from the cornice from the Golden church in Preslav, [24], 211. (right)

Fig. 11 Palmette of metal works from Preslav, [24], 306.

2. OBJECT OF THE STUDY

The study is dedicated to the decoration of the Secession-style facades in Sofia. The most famous are the buildings of the church "Nikolay Novi Sofiyski" (1896-1900), the Higher Theological School at the Holy Synod (1904-1908), the Synodal Palace (1904-1910) and the Central Sofia Mineral Baths (1907-1915). The common features in the decoration of their facades is the used of ceramics. It is an expression of the romantic view of Bulgarian medieval architecture and art. [9]

The highlight of the study is the decoration of the building of the Sofia Mineral Bath and the result of new technological possibilities for the restoration of the ceramic decorations destroyed by time.

3. METHODOLOGY AND RESEARCH OBJECTIVES

Historical methodology and comparative analysis were used in the research. By historical methodology we understand the historical tracing of the objects of the research and the researches of other investigators about this problem. By comparative analysis we understand the indication of examples for comparison. In regard to the style of Secession, they are sought after in synchronous European analogues. The principle of diachronic observation is applied too. Relevant examples were searched through it. In this way, the goal of the research was achieved: an analysis of the decorative artistic elements of the Central Mineral Baths in Sofia as a synthesis with the architecture; an observation of the details as separate ceramic elements and the richness of their ornaments; the typological connection of the design of the facades with the medieval architectural heritage of Bulgaria; the displaying of the national specificity of secession; defining of the features of the Bulgarian Secession through a vivid architectural representative such as the Central Mineral Baths in Sofia, compared to the other European images in terms of the forms and materials used.

4. Previous Researches about the Secession Decorations of Buildings in Sofia

The facade decorations of the mentioned buildings are analyzed in the study of architect Petar Yokimov, dedicated to the Secession in Bulgarian architecture. In it, he examines the national specificity in the context of European secession. [10]

Valuable archival information about the ceramic studio in Sofia (little is known about the ceramic studios in Sofia from the end of the 19th and the beginning of the 20th century) and about the production of the ceramic cornice of the church "St. Nikola Novi Sofiyski" was published by church historian Hristo Temelski. According to the archival data that he indicates, its production was assigned to the "First Bulgarian Anonymous Joint Stock Company for Clay Products", which was unable to cope with their production. Thus, the author of the colored cornices of the church became the unknown sculptor Julius Silvai.[11] The data for the facade decorative decoration of the Synodal Palace were obtained from the same researcher. He points out that the designs for this mosaic decoration have been the work of Professor Haralampi Tachev and Gospodin Zhelyazkov. Floor, wall decorative tiles and majolica for the building of the Synodal Palace have been supplied from the Novi Khan (Elin Pelin) station factory. [12]

Temelski points out that in 1922, for the decoration of the building of the Higher Theological School, it was decided to "immediately plaster the external walls, assigning H. Tachev to make a color sample of the ceramic tiles and the plaster of the facade in the old Bulgarian style, by selecting the necessary tones for the harmony of the plaster with the tiles; the same Tachev have to present samples of ornaments for the medallions above the windows of the northern and western facades and present a project for a fresco on the pediment under the dome on the north facade. The members of the Synod have propose to paint the medallions on the facades depict the heads of "historic figures of our church enlightenment from all periods of our church history". [13] In the reference to "Old Bulgarian style" and "historical figures" in the above quote, the connection of the Secession with the Bulgarian medieval tradition in architecture is evident.

The subject of Violeta Vasilchina's article is the most detailed study of Tachev's work on the execution of the ceramic decoration of Sofia Mineral Baths facades and his co-work with the contractor of decorative ceramics, the painter Stefan Dimitrov. The article examines the general architectural and artistic approach, the style of the decorative solution of the building of the Mineral Baths and its importance for the construction of the new look of Sofia. [14]

Haralampi Tachev (1875-1944), who is the artist of the decoration projects of the mentioned buildings, is one of the famous artistic names in Bulgarian culture from the first decades of the 20th c. He is known as one of the best decorators such as the creator of the coat of arms of Sofia in 1900.[15],[16].

5. Analysis

Before the analyzing of the decoration of the facades of the Sofia Mineral Baths, it is necessary to note the names of the architects worked at that time and in that style. Designer of the earliest Secession buildings decorated with colorful ceramic panels on the facades - "St. Nikolay Novi Sofia" is Anton Tornyov [17] (1868-1943, graduated in Stuttgart). The architect of the building of the Higher Theological School in Sofia was Friedrich Grünanger (1856-1929, graduated from the Academy of Fine Arts in Vienna).

The architects of the Holy Synod are Petko Momchilov (1864-1923, studied architecture at the German Higher Technical School in Prague) and Yurdan Milanov (1867-1932, graduated from the Higher Technical School in Vienna). The architect of the building of the Sofia's Central Mineral Baths is Petko Momchilov. The common line of their creativity is their academic education is the Austrian school of architecture and art. [18] Friedrich Grünanger is older than Momchilov and Milanov and in his work he is closer to the style of Baroque, and the tendencies of Eclecticism and Neoclassicism. Momchilov and Milanov are innovators. In the buildings of the Holy Synod and the Mineral Baths, the opportunities for inspiration from the Bulgarian medieval architecture have been used. Peter Yokimov defines their style as a late historicism, with the domination of the decorative [19] principles.

In one of his letters, the artist-designer of the decorative ceramic panels on the facades of the Sofia Mineral Baths, Petko Momchilov, describes the motifs of the different panels. They can be have figural motifs, as well as a motives with a figures and ornaments, and have a national style ornaments. According to him, they should be monochrome, dichromic, tricolor and polychrome. [20]

Fig. 12 Decorative panels with floral ornaments and water lily, central in the triangular panels near the triforia. Bottom a frieze with swans and beasts, Central Mineral baths, Sofia. Photography: Blagovesta Ivanova.

Fig. 13 Graphic documentation for the restoring of the frize with swans and beasts, Archive photography, Sofia Museum of History.

The Sofia Mineral Baths were declared an architectural monument of national importance in 1978. In 1988, the building was stopped from operation. In 2015, after restoration, its central part became the Regional History Museum of Sofia.

The restoration documents [21] allow for detailed tracking of the specific fragments of the tiles made of chamotte, which were projected by the artist Haralampi Tachev. Brick-coloured tiles (brown), are used in the window openings framing the arches of the domes' drums, and between them there are located masonry imitating panels (green relief circles), which are inherent for the Moesian architectural school. The cornices of the domes (located around the arches' window openings) are intricately composed. The banded frieze consists of blue royal lilies on an ochre background, separated by a brown zig zag. The cornice is framed with a blue ribbon and creates the feeling of growth of lilies from it. The lower row of the "window holes" represents deaf arches (niches) located at the level of the dome drum. Their walls are decorative panels with stylized plant ornaments. Ornaments build a complex tangle system.

In her research, Violeta Vasilchina notes that the lower coloured decorations are more complex, and the higher ones are more elementary. [22] This feature is related to the perception of the eye. The graphic documentation of the recovery of the lost elements and the restoration, show that this is indeed the case. [22] From separate elements we can determine the types of neo-Byzantine elements that Haralampi Tachev used. These are palmettes motives, "royal lilies" type, numerous stylized teratological elements, floral and braided elements combined with swans, lion bodies and water lilies. All of them are executed in relief. The colours are blue, green, ochre and brown.
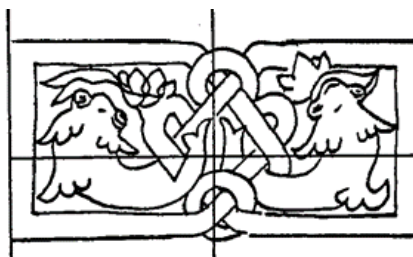
Fig. 14 Tile decoration of the front of the arch of the dome's drum. Archive photography, Sofia Museum of History.
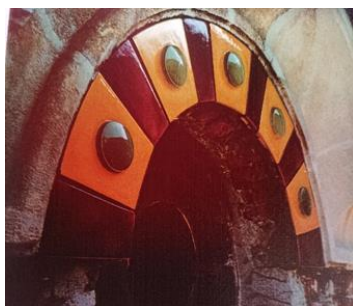
Fig. 15 Graphic documentation for the restoring of the frieze with beasts, Archive photography, Sofia Museum of History.

The origin of some of these motives is related to the creation of a new image in the second decade of the 20th c. built on the basis of traditional Preslav's architecture sculptural

stone and ceramic painted elements. One possible typological example is the artistic elements in the architectural decoration of the "Golden Church" in Preslav, dated 907 [24], as well as other examples from the architecture of the second medieval Bulgarian capital, Preslav.

The compositional elements in the panels in the Sofia Mineral Baths are repeated on every one secular facade and in their different parts. Thus, for example, the two water lilies, which are located on a small rectangular tile, are included as a central element on one of the triangular (corner) panels in the windows. From the documentation of the graphic reconstructions, it appears that the same modules are included in the small modules and in the large modules of the frieze. The elements are united in more complex groups and they are located on the walls above, around and below the windows of the building. All of them are adapted to the tectonics of the walls, and are organically included in the wall's decorative system. Through them, the synthesis between the form, material and colour of the building was achieved. The masonry of the building imitatively represents the mixed masonry characteristic of the High Middle Age period. It is characterized not only by the horizontal alternation of the brick and stone (in the 20th c., brick and white plaster), but also with the composing of the high windows, with the foreheads of the arches (imposts), as well as blind niches, such as we see on the facades of the Mineral Baths in Sofia.

In the lower register around the entrance to the niches of the Central mineral baths in Sofia, there are images in medallions of Apollo Medicus and Ulpia Serdica.
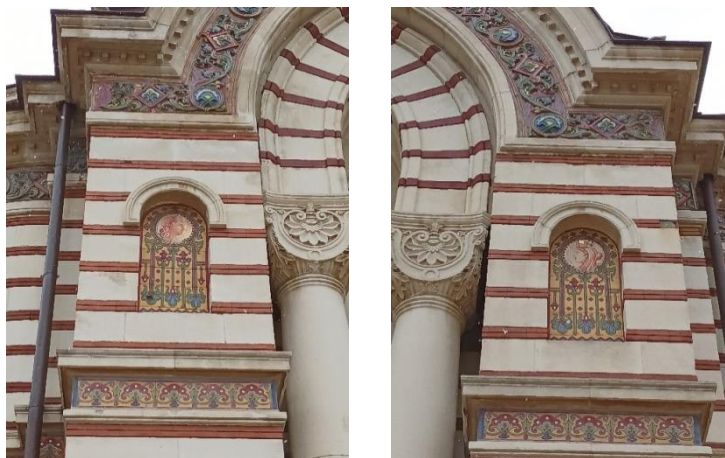
Fig. 16, 17 Ceramic panels "Apolon Medicus" and "Ulpia Serdica", central façade of Sofia mineral baths. Photography: Blagovesta Ivanova.

On the left and right sides of the facade, between the windows in the niches under semi-circular arches, there are female heads. Below the images are vertical plant ornaments like as mentioned panels.

For the restoration in 2000, the missing decorative parts were made. Graphic drawings show in detail the variety of fireclay elements.

5. CONCLUSION

The decorative decoration of the central mineral baths in Sofia is the richest and most complex among the other buildings from the reviewed period. The decoration shows the possibilities of complex synthesis in the unification of color, relief, strict tectonics and fine ornamentation.

REFERENCES

1. Charles, Victoria, Klaus H. Carl: The Viennese Secession. Parkstone International, 2011.
2. Mallgrave, Harry, ed.: Otto Wagner: reflections on the raiment of modernity. Getty Publications, 1996.
3. Miller, Michael: The Bon Marche. Burgeois Culture and the Department Store 1865-1920. Princeton University Press, 1981.
4. Vayron, Olivier Dômes et signes spectaculaires dans les couronnements des grands magasins parisiens : Dufayel, Grand-Bazar de la rue de Rennes, Printemps, Samaritaine. Livraisons de l'Histoire de l'Architecture (in French) (29), (10 June 2015), 89–112. doi:10.4000/lha.478
5. Laura S. Strumingher: Le printemps de Paris, History of European Ideas, Taylor, 1990, 12,1, 149-151, DOI: 10.1016/0191-6599(90)90142-2
6. Knotková, Veronika, Svatošová Hana: The old town hall in Prague: an unresolved architectural challenge. City Halls and Civic Materialism. Routledge, 119-134, 2014.
7. Начев, Ивайло: Сецесионовата архитектура в българската столица София в началото на XX век: влияния, творци, рецепция, памет. Сецесион & Компаративистика. Сборник в чест на проф. Цветана Георгиева. Киев – София, 2019, 141-158. [Nachev, Ivaylo: Secession architecture in the Bulgarian capital Sofia at the beginning of the 20th century: influences, artists, reception, memory. Secession & Comparative Studies. Collection in honor of Prof. Tsvetana Georgieva. Kyiv - Sofia, 2019, 141-158.] The same article is published in: Nachev, Ivaylo: The secession architecture in the Bulgarian capital city of Sofia in the beginning of the 20th century: influences, architects, reception, memory. Dzialo, e-списание в областта на хуманитаристиката, X-XXI, 2019, № 13, https://www.abcdar.com (date of visit 10.06.2023).
8. Nachev, Ivaylo: The secession architecture in the Bulgarian capital city of Sofia in the beginning of the 20th century: influences, architects, reception, memory. Dzialo, e-списание в областта на хуманитаристиката, X-XXI 2019, № 13, https://www.abcdar.com (date of visit 10.06.2023).
9. Ковачев, Атанас, Ташева Стела: Болгаро-российские взаимодействия в архитектуре Болгарии в начале XX века: нео-византийская стилистика и национальный романтизм. - Academia. Архитектура и строительство 4, 27-31, 2019. [Kovachev, Atanas, Tasheva Stela: Bulgarian-Russian Interactions in Bulgarian Architecture in the Early 20th Century: Neo-Byzantine Stylistics and National Romanticism. - Academy. Architecture and Construction 4, 27-31,]DOI 10.22337/2077-9038-2019-4-27-31
10. Йокимов, Петър: Сецесионът и българската архитектура. София, 47, 2005.[Yokimov, Petar: Secession and Bulgarian architecture. Sofia, 47, 2005.]
11. Темелски, Христо. Храмът Св. Николай Нови Софийски. София, 52-53, 2000. [Temelski, Christo. The temple of St. Nikolay Novi Sofia. Sofia, 52-53, 2000.]
12. Темелски, Христо: Синодалната палата. [Temelski, Hristo: The Synodal Palace.] https://draganbachev.com/2021/04/01/%D1%81%D0%B8%D0%BD%D0%BE%D0%B4%D0%B0%D0%BB%D0%BD%D0%B0%D1%82%D0%B0-%D0%BF%D0%B0%D0%BB%D0%B0%D1%82%D0%B0/,   01.04.2021. (date of visit 06.06.2023).
13. Темелски, Христо: Паметник на Българската екзархия или Висше богословско училище. Двери на православието. [Temelski, Hristo: Monument of the Bulgarian Exarchy or Higher Theological School. Doors of Orthodoxy.] https://dveri.bg/component/com_content/Itemid,392/catid,145/id,7650/view,article/, 15.11.2008. (date of visit 10.06.2023).

14. Vasilchina, Violeta: The challenges of the decorative project. (Haralampi Tachev and the Sofia's Mineral Baths Ceramics). Cultural heritage of Sofia. Problems and perspectives. Serdica-Sredec-Sofia. Vol. 5, 124-130, 2020,.

15. Георгиева, Милена: За облика на сецесиона в декоративната живопис на Харалампи Тачев (1875–1941). Изкуствоведски четения 2, 64-7, 2016. [Georgieva, Milena: On the appearance of the Secession in the decorative painting of Haralampi Tachev (1875–1941). Art Studies Readings 2, 64-7, 2016.]

16. Georgieva, Milena: Carrying out a Mediator's Mission. The South Slavic Concept (1904-1912) in the Works of Bulgarian Artist Haralampy Tachev. Colloquia Comparativa Litterarum. Vol. 3, No. 1, 50-69, 2017.

17. Hajdu, Ada: Bulgarian versus Byzantine The Unrealized Museum of the Bulgarian Revival and National Style Debates in Architecture, ca. 1900. Periodization in the Art Historiographies of Central and Eastern Europe. New York, 2022. https://doi.org/10.4324/9781003178415

18. Танчев Иван: Австро-унгарският принос в подготовката на българска интелигенция с европейско образование (1878–1912 г.)(Втора част). Исторически преглед, № 3-4, 165-209, 2012. [Tanchev, Ivan: The Austro-Hungarian contribution to the preparation of the Bulgarian intelligentsia with European education (1878–1912) (Part Two). Historical Review, No. 3-4, 165-209, 2012.]

19. Йокимов, Петър: Сецесионът и българската архитектура. София, 53, 2005. [Yokimov, Petar: Secession and Bulgarian architecture. Sofia, 53, 2005.]

20. Vasilchina, Violeta. The challenges of the decorative project. (Haralampi Tachev and the Sofia's Mineral Baths Ceramics). - Cultural heritage of Sofia. Problems and perspectives. Serdica-Sredec-Sofia. Vol. 5, 126, 2020.

21. Централна минерална баня. ОП „Стара София" със Софийски исторически музей. Архив, Sofia History Museum, ръкопис, 2000. [Central mineral bath. OP "Old Sofia" with Sofia Historical Museum. Archive, Sofia Museum of History, manuscript, 2000.]

22. Vasilchina, Violeta: The challenges of the decorative project. (Haralampi Tachev and the Sofia's Mineral Baths Ceramics). - Cultural heritage of Sofia. Problems and perspectives. Serdica-Sredec-Sofia. Vol. 5, 126-127, 2020.

23. Централна минерална баня. ОП „Стара София" със Софийски исторически музей. Архив, ръкопис, 2000. [Central mineral bath. OP "Old Sofia" with Sofia Historical Museum. Archive, Sofia Museum of History, manuscript, 2000.]

24. Мавродинов, Никола: Старобългарското изкуство. Изкуството на първото българско царство. София, 202, 209, 211, 2013. [Mavrodinov, Nikola: Old Bulgarian art. The art of the first Bulgarian kingdom. Sofia, 202, 209, 211, 2013.]

RAZNOBOJNA FASADNA DEKORACIJA ZGRADA U STILU SECESIJE U SOFIJI. SOFIJSKA MINERALNA KUPATILA I RESTAURACIJA NEDOSTAJUĆIH ELEMENATA

Rad predstavlja nacionalne specifičnosti stila secesije u raznobojnoj keramičkoj dekoraciji nekih zgrada u Sofiji. Najreprezentativniji među njima su crkva Svetog „Nikolaja Novog Sofijskog", zgrade Sinodalnog dvora, Centralne mineralne banje i Više bogoslovske škole pri Svetom Sinodu, građene i ukrašene između 1900. i 1922. godine. arhitekte Fridriha Grinangera, Jourdana Milanova i Petka Momčilova.

Akcenat istraživanja je keramička dekoracija fasada Centralnih mineralnih kupatila u Sofiji, po projektu Haralampija Tačeva. Prikazani su i analizirani detalji o vrstama ornamenata. Razmotreni su grafički dizajni za restauraciju nedostajućih elemenata. Analiziran je uticaj boje na dizajn fasada. Ispitane su posebnosti u dekoraciji i povezanost ovog stila sa srednjovekovnim elementima.

Povezanost fasadnih rešenja sa bugarskom istorijskom tradicijom ranog srednjeg veka i Vizantije objašnjena je na primerima iz Preslava, glavnog grada Prvog bugarskog carstva. Na ovaj način su obojene keramičke pločice fasada Centralnih mineralnih kupatila predstavljene kao izraz bugarske srednjovekovne tradicije u stilu secesije u Sofiji.

Prikazane su kolorističke interpretacije fasada građevina u Beču, Parizu i Pragu tog perioda radi poređenja i demonstracije nacionalnih razlika, odluka i zadataka secesijskog stila.

Ključne reči: keramički i mozaički ukrasi fasade, Sofija, mineralna kupatila, zgrade, Prag, Beč, Pariz

ON ROTATIONAL INVARIANCE OF HIGHER-ORDER MOMENTS OF REGULAR POLYHEDRA

UDC 514.113.5:531.232

Márton Módis, Flórián Kovács

Budapest University of Technology and Economics, Department of Structural Mechanics, Budapest, Hungary

ORCID iDs: Márton Módis   N/A
         Flórián Kovács   https://orcid.org/0000-0002-8374-8035

Abstract. *This paper covers aspects of establishing a relationship between the highest-order rotation-invariant moments of inertia and the order of symmetry of Platonic polyhedra. Moments of inertia about arbitrary, but centroidal axes are considered. After an introductory part which summarizes the possible applications of higher-order moments of area and inertia, the revision of the already solved two-dimensional version of this problem is presented, in other words the highest-order rotation-invariant moments of area about the origin of regular m-gons are studied. As a continuation, some aspects of the possible decomposition of spatial finite rotations into a sequence of rotations about given axes will be covered which are of great importance by the extension of the two-dimensional problem into three dimensions. Finally, the solution of the 3D problem will be presented, emphasizing the differences between the behavior of the even- and odd-order moments which is present in the 2D case, too, and also between the behaviour of the invariant moments of the tetrahedral and the octahedral or icosahedral solids. As a last part, possible applications will be presented.*

Key words: *moments of area and inertia, higher-order moments, rotation-invariant moments, rotation of inhomogeneous bodies, functionally graded materials.*

1. INTRODUCTION

Application of moments of area and inertia up to the second-order is common in the everyday engineering practice. Applying higher-order moments of area and inertia, however, is not as frequent, even though they might appear in basic engineering problems, such as rotation of objects with inhomogeneous density distribution, stability analysis or bending problem of beams with varying material properties inside their cross-sections etc.

This paper covers aspects of the rotation-invariance of higher-order moments of inertia of regular polyhedra based on the research of Domokos [1] who established the relationship between the highest-order moment of area about the centroid of a regular polygon and the number of its sides. The main goal of this paper is to extend these results to three dimensions, in other words, to derive the relationship between the highest-order rotation-invariant moment of inertia about arbitrary but centroidal axis and the order of symmetry of the Platonic polyhedra.

First of all, it will be clarified what the authors understand under the concept of rotation-invariant moments. In two dimensions, moments of area are defined as an integral of a polynomial expression over a planar domain and their rotation-invariance is understood in this paper as the value of this integral does not change under any rotation about the centroid of the domain. The axis of rotation is trivial in two dimensions, it has to pass through the centroid and be normal to the domain. Turning to 3D cases, moments of inertia have to be analyzed which are integrals over a spatial domain of polynomial expressions. According to the terminology of this paper, they will be denoted invariant if their value does not change under any rotation about arbitrary but centroidal axes. Note that in 3D the axis of rotation is not as trivial as in planar cases. From now on, when it is clearly specified whether a 2D or 3D case is analyzed, instead of the denominations "moments of area" and "moments of inertia" simply "moments" will be used for short. Similarly, since only the rotational invariance of the moments is examined, "rotational" might be omitted and just the expression "invariant" or "invariance" will be applied.

As a next part of the introduction, some concrete applications of higher-order moments are presented.

Let us start by the most direct application, so the analysis of the rotational movement of objects. Sulikashvili [2] analyzed the rotation of a cube, a cone and a cylinder in a central Newtonian field. The conclusion of the paper is that the third- and fourth-order moments of area have influence on the stability of the rotation.

It was mentioned at the very beginning of the introduction that if material properties, such as Young's modulus, change inside the cross-section of a structure according to some kind of function, then even by the simple bending of a Euler-Bernoulli beam higher-order moments of area may show up. Materials of this kind are called functionally graded materials. Horgan and Chan [3] analyzed a circular cross-section under torsion, where the shear modulus varied along the radius. If the variation can be described as a polynomial function, by the calculation of the shear stiffness higher-order polar moments will appear. Examples of functionally graded materials will be presented later in this paper, too.

The outline of the paper is as follows: after the short revision of the 2D case and its some basic aspects of extending it to three dimensions (Section 2), highest-order invariant moments of regular polyhedra will be presented in Section 3 and finally examples (Section 4) and conclusion (Section 5) close the paper.

2. The Necessary Theoretical Backgrounds

2.1. About the invariance of moments of area

An n-th moment of area in the xy plane about the centroid of A can be defined as follows:

$$\mu_{j,n-j} = \iint_A x^j \, y^{n-j} \, dxdy,$$

(1)

where n and j are nonnegative integers, $j \le n$. Since regular m-gons are examined, let A be a symmetric domain in the xy plane having C_m symmetry (in other words, m-fold rotational symmetry). To simplify the problem, instead of integrals over the domain A, a set of points having also C_m symmetry will be analyzed, so instead of the integration we will have a discrete summation as follows:

$$M_{j,n-j} = \sum_{i=0}^{m-1} x_i^j \, y_i^{n-j} = r^n \sum_{i=0}^{m-1} cos^j \left(\varphi_0 + i\frac{2\pi}{m} \right) sin^{n-j} \left(\varphi_0 + i\frac{2\pi}{m} \right).$$

(2)

Note that in (2) a change to a polar coordinate system has been made, where r is the distance between each point of the discrete set and the centroid of the set, φ_0 is an initial angle enclosed by the first member of the discrete set and the horizontal x axis. Also note that for this discrete case, instead of μ, the letter M has been introduced. For invariance, it has to be proven that (2) cannot depend on φ_0.

Without getting much into the details, extending the trigonometric power expressions into a weighted sum of either sines or cosines of multiple angles and applying trigonometric product-to-sum formulae, depending on the parity of j and n-j we obtain the following:

$$M_{j,n-j} = r^n \left(c_0 + \sum_{i=0}^{m-1} \sum_{k=1}^{\left[\frac{n+1}{2}\right]} c_k \, cos \left((2k - (n \bmod 2)) \left(\varphi_0 + i\frac{2\pi}{m} \right) \right) \right),$$

(3)

for $n - j$ even and

$$M_{j,n-j} = r^n \left(\sum_{i=0}^{m-1} \sum_{k=1}^{\left[\frac{n+1}{2}\right]} c_k \, sin \left((2k - (n \bmod 2)) \left(\varphi_0 + i\frac{2\pi}{m} \right) \right) \right),$$

(4)

for $n - j$ odd. In the expressions c_0 and the coefficients c_k can be determined based on [4], the square brackets mean the floor function. A very important remark is that we will always get a series of either pure sines or pure cosines.

Note that the order of the summations in (3) or (4) can be interchanged and once the summation with respect to i becomes the inner one, closed formulae for both of the expressions with cosines and sines are provided in [5]. Once we have closed formulae for the summations with respect to i in (3) and (4), we are able to evaluate them and what we get is either constant zero (in this case obviously the summation with respect to k vanishes, too) or m (in this case the summation with respect to k will not vanish and dependence on

φ_0 remains. These latter cases are the non-invariant moments, while the former ones are the desired invariant moments.

It can be proven that the non-invariant moments are obtained if n is such that either n itself or positive integers n-2, n-4,… are divisible by m. At this point we claim that nth-order moments are only considered invariant if all of the moments of order n are invariant. Note that this approach verifies the well-known fact that invariant odd-order moments are constant zero (note that in (4) we do not have c_0), however, even-order invariant moments can be nonzero as well.

Let the following table summarize the relationship between m and n (which is now the highest-order invariant moment).

Table 1 The invariance of moments of area of regular polygons

Polygon (m)	Order of the highest invariant moments (n)
Regular triangle (m = 3)	4
Square (m = 4)	any odd-order (highest even: 2)
Regular pentagon (m = 5)	8
Regular hexagon (m = 6)	any odd-order (highest even: 4)
⋮	⋮

2.2. The decomposition of finite spatial rotations

Platonic polyhedra belong to symmetry groups Td, Oh or Ih (tetrahedral, octahedral and icosahedral groups) which groups contain cyclic subgroups of maximum order 3, 4 or 5, respectively. This means that in order to determine the highest-order invariant moment of inertia of a tetrahedron, octahedron (or its dual, the cube) or icosahedron (or its dual, the dodecahedron), the planar cases with three-, four- or fivefold cyclic symmetry, respectively, are good starting points, these case are to be extended into three dimensions.

Without getting much into the details, based on references [6] and [7] it can be proven that an arbitrary finite spatial rotation can be decomposed into a sequence of three consecutive rotations about three different three-, four- or fivefold axes of symmetry of point groups Td, Oh or Ih, which are attached to the rotating body. This means that we are always able to handle a rotation about an arbitrary but centroidal axis as a sequence of rotations about current axes of symmetry. This statement is of key importance when extending the invariance of planar moments into three dimensions.

3. THE INVARIANCE OF MOMENTS OF INERTIA

Given a volume V in the xyz coordinate system, its nth-order moments of inertia about any of its centroidal axes can be calculated as follows:

$$\mu_{j,k,n-j-k} = \iiint_V x^j \, y^k z^{n-j-k} dx dy dz.$$

(5)

As we did before in the planar case, instead of integrating over the continuous domain V, discrete sets of points will be analyzed, in which the points are located at the vertices of a regular polyhedron. Changing the integration to summation leads:

$$M_{j,k,n-j-k} = \sum_{i=0}^{p-1} x_i^j \, y_i^k \, z_i^{n-j-k},$$

(6)

where p is the number of points in the set, namely, p = 4, 6 (8), 12 (20) for tetrahedral, octahedral or icosahedral symmetry, respectively. Note that here a coordinate transformation also could be performed, i.e., to spherical coordinates. However, developing a solution similar to the 2D case based on spherical coordinates would be much more complicated, so the problem will be analysed from a different approach.

We emphasize that rotational invariance means here that the axis of rotation can be arbitrary but centroidal. As we mentioned before (see previous section), instead of an arbitrary axis of rotation, we are able always to consider a rotation about an axis of symmetry (see Fig. 1).
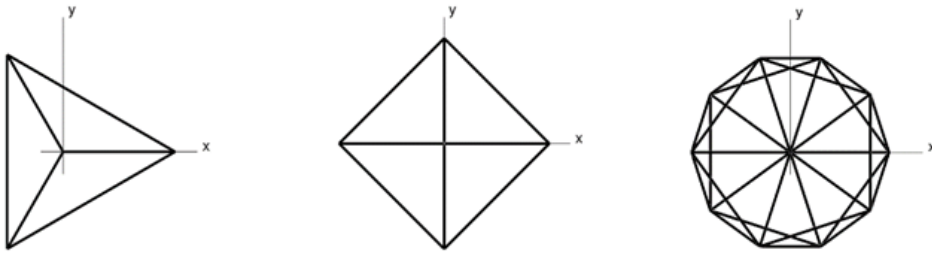
Fig. 1 View of a tetrahedron, an octahedron and an icosahedron from a three-, four- and fivefold axis of symmetry

Let us consider first the case of tetrahedra. In this case our set contains four points and we are able to interpret any rotation about an arbitrary centroidal axis as a sequence of rotations about three out of its four threefold axes of symmetry. Letting the z axis coincide with the current axis of rotation, what we get in the xy plane is nothing else, than a regular triangle, so the planar case corresponding to m = 3 is restored (see Fig. 1). According to Table 1, the highest-order invariant moments are the fourth-order moments, however, the third-order moments (n = m, n divides m) are not invariant, while for n < m, the moments are always invariant. Let us consider the case when the sum of the exponents of x and y is 3. In this case, in the xy plane we obtain a non-invariant moment and since the fourth point on the z axis has no contribution to the moment (x = y = 0), rotation about the z axis with arbitrary exponent of z results in non-invariant moments. So the highest-order rotation-invariant moments of inertia of tetrahedra are the second-order.

Turning to the other two cases, to the octahedral and icosahedral solids, the planar cases m = 4 and m = 5, respectively, can be applied, so what follows immediately from the previous section is that the order of the highest even-order moments of inertia will be the highest even number less that 4 or 5, respectively. Those numbers are 2 and 4 for the two cases (n = 4 is not invariant for m = 4 according to Table 1 and even though n = 6 is invariant for m = 5, with the same way of thinking as we excluded the fourth-order moments from the invariant ones in case of tetrahedra, it can be proven that sixth-order moments are not invariant for icosahedral solids).

Turning to the odd-order moments, according to Table 1 and for m = 4, any odd-order moment will be invariant, this will be true in three dimensions, too. It is enough to consider

Fig. 1, with the axis of rotation (now considered to be axis z) pointing towards the reader. In that view there are four nodes at the z = 0 level and other two nodes at the z axis, so evaluating (6) what we get is undoubtedly 0, if the sum of the exponents is odd.

Even though for the case m = 5 the order of the highest invariant moments is finite, we can state that in 3D all odd moments are invariant zero. To see this, consider now the right panel of Fig 1, with the axis z as the axis of rotation pointing towards the reader. We see two quintets of points forming two regular pentagons, at heights -z and z, respectively. If the sum of the exponents of x and y is odd, then an odd-order moment implies the exponent of z to be even which means that the minus sign of z in case of the lower pentagon is not of any importance. Thus, a 10-gon can be analyzed, and for even m all of the odd-order moments are zero. If the exponent of z is odd, however, then the sum of the exponents of x and y must be even. In this case we have a "positive" and a "negative" quintet of points, but since the icosahedron possesses twofold axes of symmetry perpendicular to fivefold ones, there are such twofold axes in the xy plane, too. Hence, in this case the positive and the negative quintets will cancel each other out, so a constant zero moment is obtained.

The following table summarizes the highest-order invariant moments corresponding to each Platonic polyhedra:

Table 2 The highest-order invariant spatial moments corresponding to Platonic polyhedra

Polyhedron	Order of the highest invariant moments
Tetrahedron	2
Octahedron (cube)	any odd-order (highest even: 2)
Icosahedron (Dodecahedron)	any odd-order (highest even: 4)

4. EXAMPLES

In this part some possible engineering applications will be presented. As a first example let us consider simple bending problems of Euler-Bernoulli beams. For the sake of transparency, the formula of the normal stresses from the bending moment will be assumed to have a polynomial distribution of the modulus of elasticity. Let us suppose that the bending moment acts around the y axis and the cross-section is in the yz plane.

$$\sum M_{iy} = M_y = \iint_A \sigma_x \, z dA = \iint_A E(y,z)\varepsilon_x z dA = \kappa_y \iint_A E(y,z)z^2 dA. \tag{7}$$

Note that here M_y stands for the bending moment and not for the moments, κ_y is the curvature about the y axis. Note also that the Young's modulus E can be taken out from the integral if and only if it is constant inside the cross-section (in this case we obtain the basic formula $M_y = \kappa_y EI_y$), with polynomial distributions of E, higher-order moments appear.

Let us consider a distribution of E (the origin is at the centroid, the y axis points leftwards, the z axis downwards) given by the formula below:

$$E(y,z) = E_1 + E_2 z^2. \tag{8}$$

In this case (7) takes the following form (E_1 and E_2 are known values):

$$M_y = \kappa_y \iint_A (E_1 + E_2 z^2) \, z^2 dA = \kappa_y (E_1 I_y + E_2 \mu_{0,0,4}), \tag{9}$$

so a fourth-order moment appears as well. Now let us examine two different cross-sections which are a square and a regular hexagon with the above introduced distribution of E (see Fig. 2). It is clear that, based on just the geometry, these cross-sections can only undergo simple bending, they have infinitely many principal directions. However, according to Table 1 we can state that fourth-order moments are not invariant for squares, but it is so for regular hexagons, so the hexagonal cross-section can be bent only simply, the other one, however, can undergo either simple or composite bending, depending on the orientation of the coordinate system. In other words, in case of the hexagonal cross-section, despite the fact that the modulus of elasticity varies along one axis, the bending moment vector should not necessarily be parallel to this axis to generate simple bending.
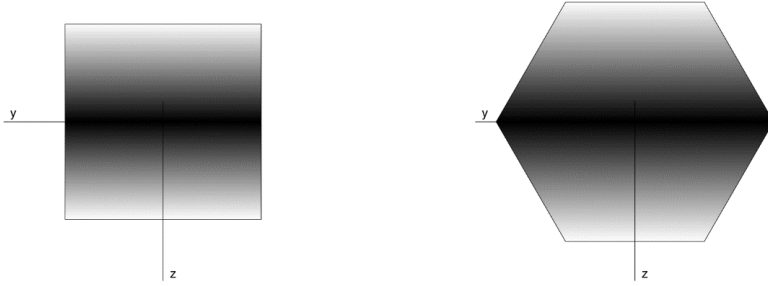
Fig. 2 A square and a hexagonal cross-section with distribution of Young's modulus shown in (8)

Similar examples in 3D also can be presented. Let us consider now rotating solid bodies with the following density distribution:

$$\varrho(x, y, z) = \varrho_0(x^2 + y^2), \tag{10}$$

where ϱ_0 is a known value. It can be seen that this type of density distribution will cause mathematically fourth-order moments of inertia which, according to Table 2, are non-invariant for octahedra but invariant for icosahedra. It is to mention that the axis of symmetry of the distribution of the density (which is now the z axis) does not have to coincide with an axis of symmetry of the icosahedral body itself, the only requirement of getting an invariant moment is that the centroid must remain at its original position.
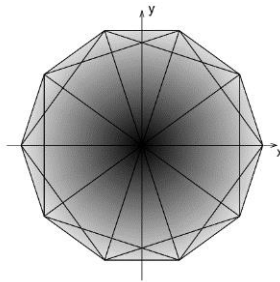
Fig. 3 The density distribution (Eq. (10)) inside an icosahedron

5. CONCLUSION

The main goal of this paper was to establish a relationship between the highest-order rotation-invariant moments of inertia about arbitrary but centroidal axes of Platonic polyhedra and their order of symmetry based on the invariance of planar moments. We can conclude that the order of the invariant spatial moments is only bounded in the case of the tetrahedron (they are invariant up to the second-order), while odd-order moments of inertia of the octahedron or icosahedron (and their duals) are always invariant, namely zero. The order of the invariant even moments, however, are bounded for the octahedron and icosahedron, too (2 and 4, respectively).

REFERENCES

1.   G. Domokos: Taylor Approximation of Operators with Discrete Rotational Symmetry. J. Appl. Math. Mech. / Zeitschrift für Angew. Math. und Mech., Vol. 72, No. 3, 221–225, 1992.
2.   R. S. Sulikashvili: The effect of third-and fourth-order moments of inertia on the motion of a solid. J. Appl. Math. Mech., Vol. 51, No. 2, 208–212, 1987.
3.   C. O. Horgan and A. M. Chan: Torsion of functionally graded isotropic linearly elastic bars. J. Elast., Vol. 52, No. 2, 181–199, 1998.
4.   https://mathworld.wolfram.com/TrigonometricPowerFormulas.html (31.05.2023.)
5.   https://en.wikibooks.org/wiki/Trigonometry/The_summation_of_finite_series (31.05.2023.)
6.   G. Piovan and F. Bullo: On coordinate-free rotation decomposition: Euler angles about arbitrary axes. IEEE Trans. Robot., Vol. 28, No. 3, 728–733, 2012.
7.   D. Brezov, C. Mladenova, and I. Mladenov: A decoupled solution to the generalized Euler decomposition problem in R3 and R2,1. J. Geom. Symmetry Phys., Vol. 33, 47–78, 2014.

O INVARIJANTNOSTI ROTACIJA MOMENATA VIŠEG REDA KOD PRAVILNIH POLIEDARA

Ovaj rad pokriva aspekte uspostavljanja odnosa između momenata inercije najvišeg reda invarijantnih rotacija i reda simetrije Platonovih poliedara. Razmatraju se momenti inercije oko proizvoljnih, ali centralnih osa. Nakon uvodnog dela koji sumira moguće primene statičkih momenata površine i inercije višeg reda, predstavljena je revizija već rešene dvodimenzionalne verzije ovog problema, odnosno proučavaju se nepromenjivi momenti invarijantnih rotacija najvišeg reda površine oko koordinantnog početka pravilnih m-uglova. U nastavku će biti obrađeni neki aspekti moguće dekompozicije prostornih konačnih rotacija u niz rotacija oko datih osa koji su od velike važnosti proširenjem dvodimenzionalnog problema na tri dimenzije. Na kraju će biti predstavljeno rešenje 3D problema, naglašavajući razlike između ponašanja momenata parnog i neparnog reda koje je prisutno i u 2D slučaju, kao i između ponašanja invarijantnih momenata tetraedarskih i oktaedarskih ili ikosaedarskih tela. Kao poslednji deo biće predstavljene moguće primene.

Ključne reči: *moment površine i inercije, moment višeg reda, invarijantni rotacijski moment, rotacija nehomogenih tela, funkcionalno gradirani materijali.*

URBAN SPATIAL ANALYSIS AND VIRTUAL MODEL NETWORK OF THE CULTURAL BUILDINGS LOCATED AT THE CULTURAL ROUTE IN SKOPJE, N. MACEDONIA

UDC 727:004.946(497.7)

Viktorija Mangaroska[1], Liljana Mangaroska[2], Kosta Mangaroski[3]

[1]International Balkan University, Faculty of Architectural Engineering, Skopje, North Macedonia
[2]Chief Museum Architect at National Museum of Republic of North Macedonia
[3]SS Cyril and Methodius University, Faculty of Architectural Engineering, Skopje, North Macedonia

ORCID iDs:	Viktorija Mangaroska	N/A
	Liljana Mangaroska	N/A
	Kosta Mangaroski	N/A

Abstract. *Urban spatial and program organization of virtual network model of the cultural buildings is one of the crucial network developments at the Cultural Route in Skopje, North Macedonia. The methodology of this scientific paper includes urban spatial diagram analysis of the virtual network modeling of the cultural buildings in Skopje: analysis and testing of the developed virtual spatial models in the context of architectural-design and urban-planning interventions, stimulating the processes for their complete inventory, systematization, valorization, integration and adaptation in the virtually created urban environment.*

The method of typological and morphological analysis where the reasons for the morphology and the emergence of cultural development are considered in the context of the relationship with cultural development as development of semantic factors. The modeling method (virtual) which is presented as an analogy and virtual simulation of the current and future conditions of cultural institutions in Skopje. Virtual realistic representation and simulation of the current situation is analyzed in this scientific paper. The situation is critically reviewed and measures are proposed that architects and designers can implement in the virtual modeling of the future state of museums and cultural institutions.

The expected outcome results of this scientific paper is to explore and define the application of virtual modeling in the planning of current and future development of the virtual museum network, in the development of the city Skopje. The research includes: defining the existing and future programming factors that influence the development of the cultural institutions, defining factors in the process of virtual modeling of the spatial organization, location and relational connection of the objects in the field of

culture in the network; defining the influence factors of the development of the facilities in the field of culture on the virtually created development of the city of Skopje.

Key words: *urban spatial analysis, virtual network modeling, cultural buildings.*

1. INTRODUCTION

According to ICOM (International Council of Museums) the museum is defined as "The museum is a non-profit institution in the service of society and its development, open to the public, conserving, researching and communicating with cultural exhibits, which are used to study, educate and research material evidence of the existence of people and their environment [1]." Museums should perform the following functions: preservation, exhibition, scientific and educational activity through the organization of exhibitions, professional lectures, performances, cultural events.

Functional and program organization of the museum institutions in Skopje include the following premises: administrative part - organization of the function through distribution of professional staff by organizational units, management, storage of a museum complex, depot - department for storage of artifacts, conservation and restoration department, organization of museum materials by collections, exhibition halls - organizing the space by exhibiting exhibits. salon - department for the sale of museum copies, museum tickets, souvenirs, library and documentation department [2].

The typology of museums as cultural buildings in the Republic of North Macedonia is specifically analyzed and classified according to the following aspects:
1. Typology of museums according to the exhibited objects:
   - Museums of applied arts,
   - Archaeological and Historical museums,
   - Ethnographic museums,
   - Natural science museums.
2. Typology of museums according to the meaning of the territory:
   - National museums,
   - Regional museums,
   - City museums.
3. Typology of museums according to the architecture and location:
   - Museums Houses in restored authentic historic buildings and sites.

2. METHODOLOGY OF THE CASE STUDY URBAN ANALYSIS OF VIRTUAL MUSEUM ARCHITECTURE

Virtual spatial models of the museum architecture and the circulation diagrams are an important tool in the architectural project design process, where architects, civil engineers, intercultural managers and potential investors will receive fast and accurate information about the facilities of the cultural institutions, the opportunity to see the ratio of the constructed with the newly designed facilities. When designing architectural objects, it enables the preparation of a large number of variant solutions for one architectural object. The virtual model is used in the process of inventory, systematization and valorization of existing cultural institutions, as well as in proposing possible future architectural solutions in the architectural design process [3].

According the spatial and functional analysis of the existing spatial and functional organization of the National Institution Museum of North Macedonia, with the virtual model the following proposal of interventions in the museum architecture can be tested in the virtual model; reconstruction of the exhibition spaces, reconstruction of administrative spaces, providing and protective measures for depots and premises for conservation and restoration, repair and reconstruction of the depot space with the most modern and sophisticated equipment for storage and storage, reconstruction and rehabilitation of the access plateau, construction of access ramps and elevators-platforms for overcoming the architectural barriers for people with special needs, increased need because the architectural project has a leveling in the levels of the exhibition halls [3].

Fig. 1 National Institution Museum of Macedonia, museum architecture, organizational and spatial structure of the program diagram

Organizational and functional structure in the museum architecture of the National Institution Museum of Macedonia (Fig. 1): 1. Historical exhibition that presents the history from the Ottoman period II World War, 2. Gallery of Icons exhibits the most important icons, iconostasis and frescoes from the post-Byzantine period and the Renaissance period, 3. Ethnology department presents the thematic units from: folk architecture, customs, musical instruments, costumes, jewelry, embroidery and weaving, 4. Complex museum- the building of Kurshumli an, where the exhibition of stone monuments - Lapidarium is located (Fig. 2). The Archaeological collection from the National Museum of Republic of North Macedonia has been transferred to the new building of the Archaeological Museum in Skopje.
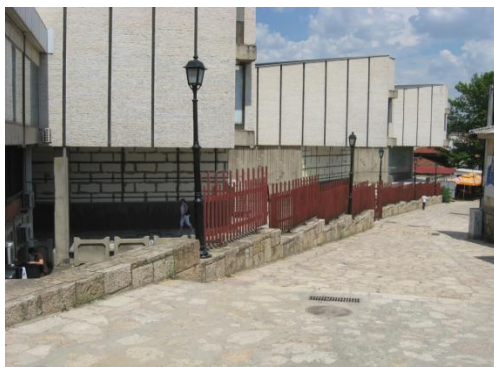
Fig. 2 National Institution Museum of Macedonia, museum architecture, visual context, and form development of the museum architecture

Methodological analysis of the cultural institutions on the Cultural Route in Skopje is defined by the: virtual modeling method that has an analogy and virtual simulation of the current and future conditions of cultural institutions in Skopje; (Fig. 3) virtual realistic representation and simulation of the current situation critically reviewed and measures proposed that architects and designers can implement in virtual modeling of the future state of cultural institutions [5]. The method of typological and morphological analysis where the reasons for morphology and the emergence of culture are considered in the context of the relationship with cultural development, development of semantic factors.
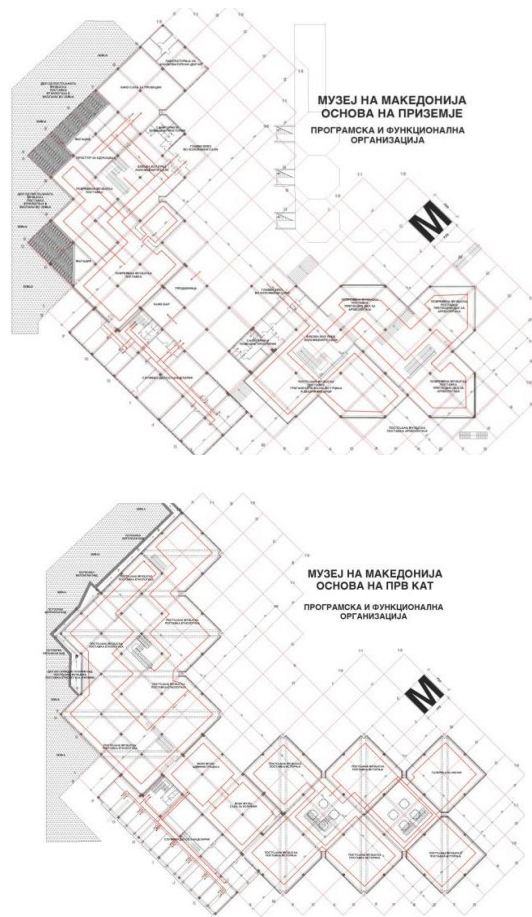
Fig. 3 Presentation of the National Institution Museum of Macedonia, museum architecture and visitors circulation diagram

Virtual network modeling of spatial and program organization of cultural buildings and museums is one of the crucial network development at the Cultural Route in Skopje, North Macedonia.

The methodology of this scientific paper includes the following principles [3]:

1. Analysis and testing of the developed virtual spatial models in the context of architectural-design and urban-planning interventions,

2. Stimulating the processes for their complete inventory,

3. Systematization, valorization, integration and adaptation of the virtually created urban environment.

Objectives of the scientific research of the virtual museum network of the Cultural Route as methodology for spatial diagram analysis are [3]: analysis of the urban and spatial connection of the museum complexes in an urban context - cultural paths, virtual model of the Cultural Route -spatial and functional organization and connection in the

museum complex, importance of the database in determining the functional aspect of architectural planning by the architect and designer, functional program and spatial analysis of museums, analysis of the trajectory of the movement and circulation of museum visitors - simeza, planning the current and future development of the architectural space through a virtual model, planning of spatial and functional organization of the interior design of the exhibitions by the architects and curators, spatial and functional planning at the city level and organization of spatial cultural buildings.

The network of cultural institutions facilitates the exchange of information, skills, knowledge and experience, by holding meetings, workshops, publications and developing cooperation programs, in order to have a wider social impact [4].

3. RESULTS FROM THE RESEARCH OF THE VIRTUAL NETWORK SPATIAL
AND PROGRAM ORGANIZATIONS OF MUSEUMS

Analysis of the spatial-urban context of the location of the Cultural Route in the city of Skopje, Macedonia is spatially defined with the following cultural buildings: starting with the beginning with the Museum of the City of Skopje in the central city area along Macedonia Street through Macedonia Square, the Stone Bridge, the Old Skopje Bazaar as an old oriental urban complex from the 16th-17th century, and final destinations the building of the Museum of N. Macedonia, the building of the Museum of Contemporary Art located at the Skopje Fortress. The analysis of the virtual museum network is focused on the museums as focal points in the urban network on the trajectory of the Cultural Route in Skopje, North Macedonia.

The following national and local museums were identified in the process of the mapping of the museums in the virtual museum network (Fig. 4): national museums: NI Museum of Macedonia – Skopje (Fig. 6), NI Museum of Contemporary Art - Skopje, NI Museum of the Macedonian Struggle for Statehood and Independence - Skopje, NI Museum of the Holocaust - Skopje, NI Art Gallery - Skopje, NI Memorial House of Mother Teresa - Skopje, NI Archaeological Museum of Macedonia, and local museums: Museum of the City of Skopje.

Fig. 4 Photo-documentation of the cultural institutions in the Cultural Route in Skopje

Morphological analysis of the cultural institutions in Skopje, North Macedonia is conducted by mapping and identification of virtual model criteria on the trajectory with cultural contents [6]:

1. Spatial criteria
  - defining the spatial urban scope
  - length of connection of cultural institutions.
  - defining the shortest and longest distance,
  - defining the diversity of contents

2. Time criteria
  - beginning, end, frequency of visit
  - time interval of visit,
  - scheduled time visits through a virtual curator,
  - the time interval of permanence - one-year, multi-year, seasonal)

3. Cultural criteria (purpose and significance of the cultural paths, cultural and content aspects of the permanent and temporary exhibitions of the cultural buildings and museums.

In the process of analyzing the spatial distances between the cultural institutions on the Cultural Route in Skopje (Fig. 5), it can be concluded that it has relatively small distances of 100 - 500 m, walking communication diagram. The communication between the cultural institutions on the Cultural Route in Skopje can take place on the pedestrian streets, paths, without crossing the pedestrian with the vehicular traffic [7]. The time required for movement of pedestrians from one object to another ranges from 10-15 minutes. The distance between cultural institutions due to the favorable configuration of the terrain, is easily accessible to people with disabilities, considering that culture should be accessible for all visitors of the cultural buildings and museums.

Distances between the cultural buildings on the Cultural Route in Skopje and analysis of the distances between the cultural buildings in the Cultural Route

Од објектот Музеј на Град Скопје (Стара железничка станица) до објектот Музеј на современа уметност	Меѓусебно растојание	Време потребно за совладување на тоа растојание со пешачење
	326,28 м	3мин 57сек
Спомен куќа на Мајка Тереза		
	235,06 м	3мин 25сек
Градска фонтана на плоштад Македонија		
	280,36 м	2мин 35сек
Плоштад Карпошево востание		
	74,31 м	0мин 55сек
Музеј на македонската револуционерна борба за самостојност		
	148,25 м	1мин 45сек
Македонски народен театар		
	126,45 м	1мин 30сек
Археолошки музеј на Македонија		
	33, 29 м	0мин 25сек
Национална галерија - Даут пашин амам		
	216,67 м	2мин 47сек
Македонска филхармонија		
	206,63 м	2мин 45сек
Национална галерија - Чифте амам		
	244,22 м	2мин 55сек
НУ Музеј на Македонија		
	679,08 м	8мин 49сек
НУ Музеј на современа уметност		
Вкупно Музеј на град Скопје - НУ Музеј на современа уметност	1769,67 М	21мин 23сек

РЕСТОЈАНИЈА ПОМЕЃУ МУЗЕИТЕ	Меѓусебно растојание	Време потребно за совладување на тоа растојание со пешачење
Музеј на град Скопје		
	326,28 м	3мин 57 сек
НУ Спомен куќа на Мајка Тереза		
	589,73 м	6мин 55 сек
Музеј на македонската револуционерна борба за самостојност		
	126,45 м	1мин 30 сек
Музеј на холокаустот		
Археолошки музеј на Македонија		
	484,14 м	5мин 55 сек
НУ Музеј на Македонија		
	679,08 м	8мин 49 сек
НУ Музеј на современа уметност		
Вкупно Музеј на град Скопје - НУ Музеј на современа уметност	1769,67 м	21мин 23сек

Fig. 5 Spatial analysis of museums in the Cultural Route; Museum of N. Macedonia
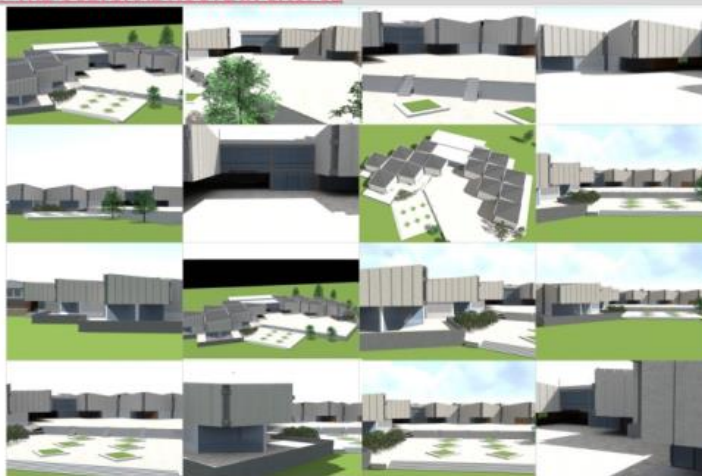
Fig. 6 Virtual Model of Museum of North Macedonia, Source: Author

The virtual network enables the connection of objects in the field of culture in a virtual context (Fig. 7), which will be of great importance in terms of: planning of activities, smooth organization of cultural events, circulation of visitors in the urban spatial matrix defined through the Cultural Route, defining the trajectory of the movement of cultural users and tourists in an urban context, which will enable a visit to several museum complexes in the city, planning the time interval of their visits to the cultural architectural buildings, opportunities for planning and development of exhibition spaces and architectural space planning by architects, museum professionals and users [8].
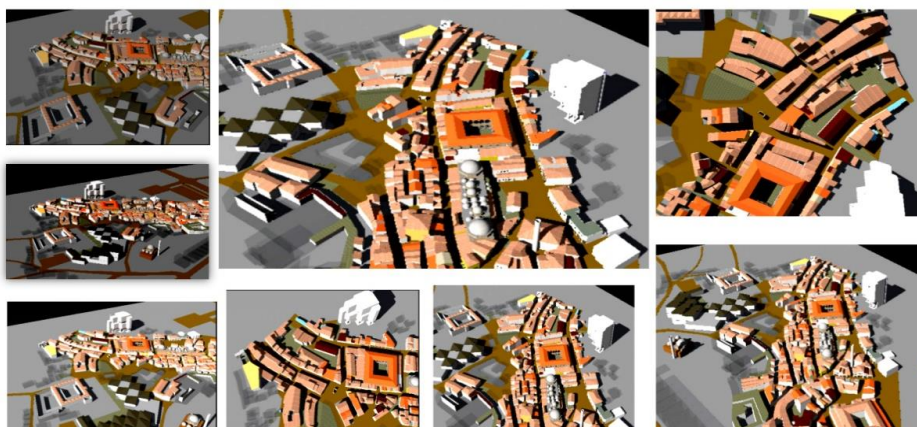
Fig. 7 Virtual Network 3D modeling of the cultural institutions and cultural heritage buildings in the Old Carsija in Skopje

4. DISCUSSION

The sustainable development of museums and cultural institutions at the virtual network of the Cultural Route in Skopje, North Macedonia include: virtual mapping of cultural buildings in Skopje through modern information and communication technologies concentration of cultural buildings in the network increasing cultural activities in the context of revitalization of cultural institutions in the long period located in the virtual network, attracting sponsorship due to the growing interest of the general population to visit cultural institutions and cultural events, involvement of project managers who will organize networked cultural activities, Skopje Art Festival, Skopje Summer Festival, increasing the interest of the media, which will actualize the presentation of the city on a regional, national and international cultural level [9].

The Strategy for Sustainable Development of the virtual network of the Cultural Route in Skopje, North Macedonia is defined by the following aspects: complete protection and revitalization of the existing, newly built and historical buildings of the Old Skopje Bazaar, construction of historical trade facilities and other business and commercial facilities next to the museums and their connection with the core of the Old Skopje Bazaar, virtual reality, visual presentations, panoramas for all museums in the Cultural Route, organization of simultaneous creative workshops in all cultural buildings for making jewelry, handicrafts in the Old Skopje Carsija, organization of simultaneous cultural events, manifestations and performances, architectural workshop for traditional construction, creating virtual network web page by entering all the information about the old and new cultural buildings and posting maps with markings of cultural institutions around the Old Skopje Bazaar.

5. CONCLUSION

This scientific paper research explores and defines the application of virtual modeling in planning of the current and future development of the virtual modeling museum network, in Skopje, North Macedonia: defining the existing and future programming factors that influence the development of the cultural institutions, defining factors in the process of virtual modeling of the spatial organization, location and relational connection between cultural buildings in the network; defining the influence factors of the development of cultural buildings on the virtually created development of the city of Skopje. With the method of virtual typological and morphological analysis considered is the urban context of the relationship with cultural development as development of semantic factors [10].

The scientific paper explores and defines the application of virtual modeling in the planning of current and future development of the virtual modeling museum network, in the development of the city Skopje, North Macedonia. The virtual modeling method is presented as an analogy and virtual simulation of current and future conditions of cultural buildings in Skopje. The situation is critically reviewed and measures are proposed that architects and designers can implement in the virtual modeling of museums [11].

The virtual methodology has a great contribution for inventory and valorization of new buildings, existing buildings, analysis of buildings based on given morphological characteristics, etc. The applicability of virtual reality and virtual modeling enables the creation of new programmatic and functional analytical virtual diagrams [12]. The new methodology of virtual modeling has an active application in the process of optimal

spatial and program organization of the new and existing facilities in the cultural buildings in Skopje. Architectural and urban design in the future will be carried out exclusively with the application of computers in a virtual world, with new modern software packages in accordance with the new achievements in computer technology.

REFERENCES

1. https://icom.museum/en/resources/standards-guidelines/museum-definition/ (14.06 2023)
2. Pleizier D., van Lammeren R., Scholten H., J.,van de Velde R., Using virtual reality as information tool in spatial planning, in Proceed. EuroConference on methods to support interaction in geovisualisation environments, 2004
3. V. Mangaroska, PhD research thesis "Virtual Modeling of spatial and functional organization of sustainable development of cultural institutions in Skopje, N. Macedonia", pp 150-210, pp 204-230, Faculty of Architecture, Ss Cyril and Methodius University Skopje, 2015
4. Piersch S., Radford A., Woodbury R., Making and Using a City Model-Adelaide, Australia in ECAADE 2001 Conference Helsinki, 2001
5. Pittman, K. A laboratory for the visualization of virtual environments. Landscape and Urban Planning, 21, 1992
6. Pletinckx, D. D. Callebaut, A. Killebrew, N. Silberman, Virtual-reality heritage presentation at Ename, IEEE Multimedia 7 (2) 45-48, 2000
7. G. Geser, Promoting Cultural Tourism, Historic Towns and Cultural Tourism in the Experience Economy- Concepts and Requirements, Salzburg Research, Culture Group, may 2007
8. Pritchard D, Enhancing Understanding Through Real-Time Urban Simulations, in conference proceedings of CUPUM 05- Computers in Urban Planning and Management,. The Design and Development of a Virtual 3D City Model, 2005
9. Poria, Y., Reichel, A., Biran, A., Heritage Site Perceptions and Motivations to Visit, Journal of Travel Research, Sage Publication, USA, 2006
10. Van Puffelen Frank, Culturele Economie in de lage landen, Amsterdam, 2000.Virtual museum of Canada. http://www.virtualmuseum.ca , 2011
11. Virtual Culture: Identity and Communication in Cybersociety, ur. Steven G. Jones, SAGE Publications, 1998
12. Virtual City Models - New Approaches in Urban Simulation and City Planning using Virtual Reality Tools Alberto Bendinger, Ingolf Jung, imk Automotive, Chemnitz, 2014

URBANA PROSTORNA ANALIZA I VIRTUALNA MREŽA MODELA KULTURNIH OBJEKATA KOJI SEN ALZE NA KULTURNOJ RUTI U SKOPLJU, S. MAKEDONIJA

Urbana prostorna i programska organizacija virtuelnog mrežnog modela kulturnih objekata jedan je od ključnih razvoja mreže Kulturne rute u Skoplju, Severna Makedonija. Metodologija ovog naučnog rada obuhvata analizu urbanističkog prostornog dijagrama modeliranja virtuelne mreže kulturnih objekata u Skoplju: analizu i testiranje razvijenih virtuelnih prostornih modela u kontekstu arhitektonsko-dizajnerskih i urbanističko-planskih intervencija, podsticanje procesa njihovog kompletnog inventorisanja, sistematizacije, valorizacije, integracije i adaptacije u virtuelno stvorenu urbanu sredinu.

Metoda tipološke i morfološke analize u kojoj se razlozi morfologije i nastanka kulturnog razvoja razmatraju u kontekstu odnosa sa kulturnim razvojem kao razvojem semantičkih faktora. Metoda modeliranja (virtuelna) koja je predstavljena kao analogija i virtuelna simulacija sadašnjeg i budućeg stanja kulturnih institucija u Skoplju. U ovom naučnom radu analizira se virtuelno realistično predstavljanje i simulacija postojećeg stanja. Kritički se sagledava situacija i predlažu mere koje arhitekti i dizajneri mogu implementirati u virtuelno modeliranje budućeg stanja muzeja i kulturnih institucija.

Očekivani rezultat ovog naučnog rada je istraživanje i definisanje primene virtuelnog modeliranja u planiranju sadašnjeg i budućeg razvoja mreže virtuelnih muzeja, u razvoju grada Skoplja. Istraživanje obuhvata: definisanje postojećih i budućih programskih faktora koji utiču na razvoj institucija kulture, definisanje faktora u procesu virtuelnog modeliranja prostorne organizacije, lokacije i relacionog povezivanja objekata iz oblasti kulture u mreži; definisanje faktora uticaja razvoja objekata u oblasti kulture na virtuelno stvoreni razvoj grada Skoplja.

Ključne reči: *urbana prostorna analiza, virtualno mrežno modeliranje, kulturni objekti*

Original Scientific Paper

ANALYSIS OF SULFATE RESISTANCE OF CONCRETE WITH RCA AFTER ONE YEAR EXPOSURE TO SULFATE SOLUTIONS

UDC 691.32/.322:661.8'053.2

Vesna Bulatović, Tiana Milović, Olivera Bukvić

University of Novi Sad, Faculty of Technical Sciences, Novi Sad, Serbia

ORCID iDs: Vesna Bulatović   https://orcid.org/0000-0001-6248-1290
             Tiana Milović   https://orcid.org/0000-0002-3905-7018
             Olivera Bukvić   https://orcid.org/0000-0001-8910-1630

Abstract. *External sulfate attack is one of the durability problems associated with concrete. Despite a perception that concrete made with recycle concrete aggregate (RCA) is of inferior quality, research has shown that RCA has the potential to satisfy the mechanical and physical requirements for a range of applications. Limited works were performed on the durability aspects of the RCA. The objective of the research described in this paper was to evaluate resistance to sulfate attack of concrete with RCA in which two types of cement (CEM I and CEM III) and two water to cement ratios (0.38 and 0.55) were combined. For the evaluation of sulfate resistance of these concretes, immersed in sodium and potassium sulfate solutions, a drop of compressive strength, length change, capillary water absorption and thermal analysis (TGA-DTA) were used. Satisfactory sulfate resistance of concrete with RCA can be achieved by applying CEM III and reducing water to cement ratios.*

Key words: *sulfate attack, recycled concrete aggregate (RCA), TGA-DTA, length change, capillary water absorption.*

1. INTRODUCTION

The construction industry contains many activities that yield a high carbon footprint i.e., manufacturing of Portland cement (OPC) and crushed aggregates, transportation of materials to the site, etc. [1]. Also, the growing demand for construction materials during the urbanization process has already affected the nature aggregate and other non-renewable resources increasingly depleted in many regions around the world. The construction of large-scale infrastructures, industrial plants, and residential buildings accompanied by the demolition of old buildings led to fast accumulation of construction and demolition wastes (C&DW), which has posed increasing threats to local environments, human health, as well as the already depleted landfills in cities. Recycled aggregate concrete (RAC) which uses recycled aggregate produced from C&DW as a partial or complete substitution to the virgin

aggregate provides a solution to both the rising demand for construction materials and the excessive discharge of C&DW [2].

Research on RAC has been carried out for many years, and it has been widely recognized that the performance of RAC prepared with recycled coarse aggregate (RCA) is obviously inferior to that of the natural aggregate concrete (NAC) at the same mixture proportions. The presence of microcracks and residual cement paste results in the high porosity, low density and high-water absorption of RCA. However, a number of modification techniques were proposed for improving the RAC performance [2].

Degradation of concrete due to sulfate attack has been recognized as a serious issue for structures since long ago. Despite extensive research in this field, there is still many doubts and space for further research. Sulfate attack is a deteriorating process where sulfates ions react with the components of cement paste resulting in concrete deterioration over time. Sulfate attack in concrete can manifest in the form of spalling, expansion, cracking, increased permeability, and strength loss. The degree of resistance against the external sulfates depends on many factors such as chemical composition of components, mineralogy, reactivity, porosity of matrix etc.

In general, it can be stated that there is a lack of papers on the durability of concrete with RCA, especially in an aggressive environment. Some of researches have begun to investigate the degradation and performance of concrete with RCA under sulfate attack. Kazmi et al. demonstrated that the resistance of concrete with RCA to sulfate attack is lower than that with natural aggregate. Qing et al. reported that the addition of RCA reduces the deterioration of concrete under sulfate attack when the RCA replacement is at a low level; however, the results are opposite if the replacement rate of RCA is increased [3].

The paper presents the results of the resistance to sulfate attack of concrete that combined different cement types (CEM I and CEM III, according to EN 197-1), water to cement ratio (0.38 and 0.55) and type of coarse aggregate (natural river (NA) and recycled concrete (RCA)). For the evaluation of sulfate resistance of these concretes, the following testing methods were used on laboratory specimens immersed in sulfate solutions (5% Na_2SO_4 or 5% $MgSO_4$) for 365 days: compressive strength, length change, capillary water absorption and thermogravimetric analysis (TGA-DTA, for samples with RCA).

2. EXPERIMENTAL INVESTIGATION

2.1. Component materials and mixture proportion

In order to investigate the effects of type cement, type aggregate and water to cement ration on sulfate resistance of concrete, four concrete mixtures were prepared with following component materials:

- Cement: Portland cement CEM I 42.5R (Lafarge-BFC Serbia, γ_{sc}=3100 kg/m^3) and Low heat/sulfate resistance cement CEM III/B 32.5N LH/SR (Lafarge-BFC Serbia, γ_{sc}=2650 kg/m^3),
- Aggregate: fine aggregate (river aggregate, 0/4 mm) and coarse aggregate (river aggregate, 4/8 and 8/16mm and recycled concrete aggregate, 4/8 and 8/16mm),
- Chemical admixture: HRWRA ("Sika ViscoCrete 3070", "Sika"- Switzerland),
- Tap water.

The basic physical properties of cement were tested according to standards EN 196-1 [4], EN 196-3 [5] and EN 196-6 [6].

Also, the basic characteristics of aggregate were examined. Recommendations and benchmark values for aggregate quality are given in standards EN 206 [7] and EN 12620 [8]. The origin of concrete mix design in RCA was unknown.

Designed compositions of concrete mixtures are shown in Table 1.

Table 1 Labels and mixture proportion of concrete in kg/m^3

Concretes (mixtures)	m_c CEM I	m_c CEM III	m_v	$m_{v,ad}$	$m_{a,f}$	$m_{a,c}$	m_{spk}	w/c
NPC1	350	-	195.5	-	930	858	-	0.55
NPC2	423	-	161	-	936	864	5.9	0.38
NMC1	-	338	186	-	936	864	0.7	0.55
NMC2	-	416	158	-	937	865	2.5	0.38
RPC1	350	-	192.5	20.2	874	803	-	0.55
RPC2	425	-	162	20.2	880	813	3.4	0.38
RMC1	-	338	186	20.5	881	813	-	0.55
RMC2	-	414	157	20.5	881	814	3.3	0.38

m_c-quantity of cement; m_v-quantity of water; $m_{v,ad}$-additional quantity of water that was calculated on the basis of RCA water absorption (2.5%); $m_{a,f}$-quantity of fine aggregate; $m_{a,c}$-quantity of coarse aggregate; m_{spk}-quantity of super-plasticizer; w/c-water-cement ratio

2.2. Curing, specimen preparation and labels

For all selected testing the following types of concrete specimens were prepared from each mixture:

- 150 mm cubes for compressive strength at age of 28 days (designated as 0)
- 100 mm diameter x100 mm height cylinders for compressive strength at 180 and 365 days after immersing the specimens into the sulfate solutions
- 100 mm x100 mm x 500 mm prisms for measuring length change
- 150 mm x150 mm x75 mm slabs for testing capillary water absorption.

All specimens were cured in lime-saturated water for 28 days. After that period, compressive strength was determined by testing three specimens from each mixture (150 mm cubes). One third of the remained specimens were transferred to containers with 5% Na_2SO_4 and another third in 5% $MgSO_4$ solution where they were stored until testing periods (90, 180 and 365 days). The last third of specimens were submerged in lime-saturated solution for the same periods (reference specimens).

For each mixture and for each solution, three specimens were tested.

Labelling was done in three series with four letters and one number in the following way: those with the first letter "E" were cured in lime-saturated water solution all the time, those with "N" were immersed in 5% Na_2SO_4 solution and those with "M" were stored in 5% $MgSO_4$ solution. The second letter in the label indicates the type of aggregate: "N" is natural aggregate and "R" is recycled concrete aggregate. The third letter refers to the type of cement: "PC" stands for CEM I and "MC" stands for CEM III. And the last letter denotes w/c ratio:"1" is for w/c=0.55 and "2" is for w/c=0.38. The value of compressive strength at the age of 28 days was taken as the initial value labelled as 0, meaning that the time of exposure to different conditions (sulfate and lime-saturated solutions) started from this point.

2.3. Methods

Compressive strength was tested according to EN 12390-3 [9] before the specimens were immersed in sulfate solutions and after storing them in these solutions for 90, 180 and 365 days.

The length change was measured continuously according to the procedure given in UNI 11307.

Testing of capillary water absorption were performed on specimens before were immersed in sulfate solutions and at chosen time.

TGA-DTA tests (Setaram, Labsys Evo) with a balance accuracy of 0.1μg, were performed on the specimens of ~30mg, crushed material, by heating in alumina crucible, 20-1000°C, at 10°C/min heating rate under argon atmosphere.

3. RESULTS AND DISCUSSION

3.1. Compressive strength

The average results of concrete compressive strength after 90, 180 and 365 days of immersion in Na_2SO_4, $MgSO_4$, and lime-saturated water are presented in Table 2. In this table are also presented the strength values prior to the exposure to sulfate solutions at 28 days (in table 0 days).

Table 2 Compressive strength (MPa) of specimens

Concrete series	0 days	90 days	180 days	365 days	Concrete series	0 days	90 days	180 days	365 days
ENPC1	46.3	54.4	55.1	56.3	ENMC1	31.8	45.3	46.4	47.7
NNPC1		55.8	42.9	27.6	NNMC1		43.4	46.1	47.8
MNPC1		56.3	52.3	48.8	MNMC1		43.3	42.5	44.3
ENPC2	72.5	79.3	87.9	90.7	ENMC2	52.8	70.0	71.4	71.7
NNPC2		80.7	79.7	84.3	NNMC2		62.6	64.7	69.2
MNPC2		81.1	71.5	76.8	MNMC2		76.0	74.7	73.4
ERPC1	43.1	53.5	54.5	57.1	ERMC1	31.3	39.7	45.9	48.8
NRPC1		49.1	35.9	22.7	NRMC1		43.2	46.7	48.8
MRPC1		54.8	49.3	40.6	MRMC1		41.6	42.5	43.5
ERPC2	61.8	78.0	82.2	84.6	ERMC2	54.1	71.2	74.4	76.9
NRPC2		79.3	74.8	76.0	NRMC2		65.7	67.7	68.1
MRPC2		77.1	73.4	74.1	MRMC2		67.8	67.5	67.9

From the results in the Table 2 it can be concluded that almost all concretes have an increase in compressive strength after all observed periods of exposure to Na_2SO_4 or $MgSO_4$ solutions (90, 180 and 365 days) corresponding to reference specimens (28 days). The exception are concretes with CEM I and w/c=0.55 immersed in Na_2SO_4 and $MgSO_4$ solutions for 180 and 365 days.

For the better understanding, relative compressive strength values are illustrated in Figure 1. These values present the relation between the compressive strength of specimens immersed in selected sulfate solution and their corresponding reference values of the same age.
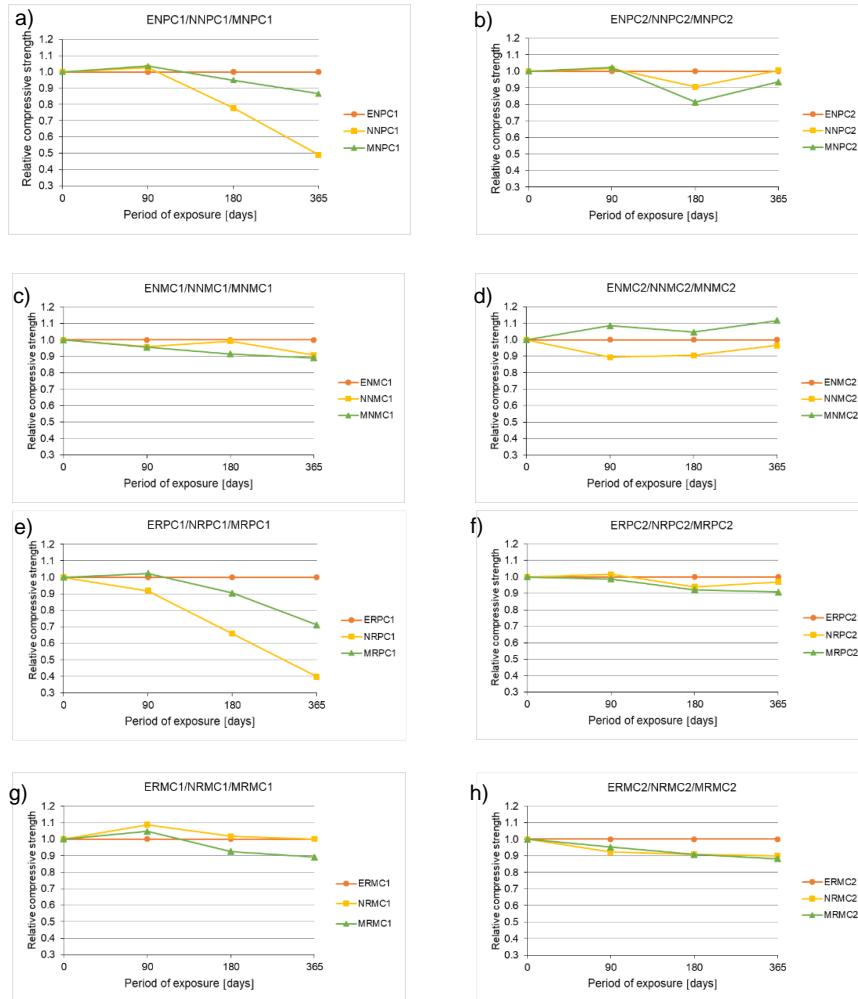
Fig. 1 Changes of compressive strength of concretes exposed to sulfate solutions in relation to corresponding strength of control specimens (a – NA, CEM I, w/c=0.55, b – NA, CEM I, w/c=0.38, c – NA, CEM III, w/c=0.55, d – NA, CEM III, w/c=0.38, e – RCA, CEM I, w/c=0.55, f – RCA, CEM I, w/c=0.38, g – RCA, CEM III, w/c=0.55, h – RCA, CEM III, w/c=0.38)

After 180 days of immersion in Na_2SO_4 or $MgSO_4$ solutions, all concretes with cement CEM I regardless of the type of aggregate and w/c ratio showed a decrease in strength compared to reference series (ENPC1, ENPC2, ERPC1, ERPC2), Figure 1. The concretes with w/c=0.55 which were immersed in 5% Na_2SO_4 solution (series NNPC1 and NRPC1) have the greatest decrease of compressive strength (22% for NNPC1, Figure 1a, and 34% for NRPC1, Figure 1e).

Concretes with CEM I regardless of the type of aggregate and w/c ratio, after 365 days of immersion in Na_2SO_4 or $MgSO_4$ solutions had a decrease in compressive strength compared to reference series. Two concretes with w/c=0.55 regardless the type of aggregate, which were immersed in 5% Na_2SO_4 solution (series NNPC1 and NRPC1) and one concrete with the same w/c and RCA immersed in 5% $MgSO_4$ (series MRPC1) had the greatest decrease of compressive strength. These decreases are 51% for NNPC1, 60% for NRPC1 and 29% for MRPC1.

The specimens of all concretes made with CEM III and stored in both sulfate solutions, showed differences in compressive strength at the age of 90, 180 and 365 days compared to reference series. Similar conclusion can be derived after 90, 180 and 365 days of exposure to both sulfate solutions: most concrete series showed a change in compressive strength, which did not exceed 10%, compared to the corresponding referent value. It can be seen that, after 365 days, the decrease in compressive strength of concrete series with RCA is slightly higher (MRMC1, NRMC2 and MRMC2) in comparison to the concrete with NA (MNMC1, NNMC2 and MNMC2).

3.2. Length change

Figure 2 shows the results of experiments monitoring the length changes of the concrete prisms subjected to 5% Na_2SO_4 and 5% $MgSO_4$ solutions, as well as the control specimens, which grouped according to the type of sulfate solution.

It can be seen that the linear expansion of concretes with CEM I, w/c=0.55 and both types of aggregate (series NNPC1, MNPC1, NRPC1, MRPC1), which have the largest values of linear expansion, depends on the type of sulfate solution. The difference between linear expansions of concretes made with RCA and NA is significant in the case of immersion in Na_2SO_4 (series NNPC1 and NRPC1). On the other hand, analysed difference is negligible when $MgSO_4$ is used (series MNPC1and MRPC1).
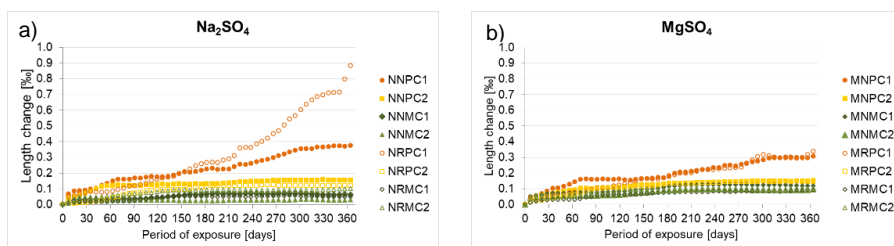
Fig. 2 Length change of concrete mixtures depends on sulfate solution a) in 5% Na_2SO_4; b) in 5% $MgSO_4$

3.3. Capillary water absorption

Results of capillary water absorption at 25 hours in kg/m^2 on all observed specimens after 180 and 365 days immersed in sulfate solutions are presented in Figure 3.
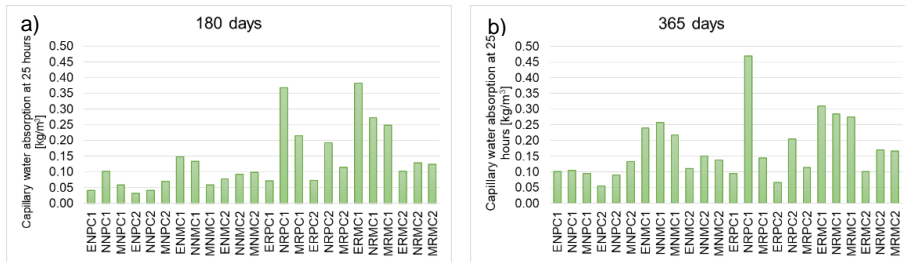
Fig. 3 Capillary water absorption of concrete mixtures depends on time exposure at 25 hours a) 180 days; b) 365 days

Due to different and complex physical processes and chemical reactions that occur during immersion specimens in sodium sulfate and magnesium sulfate solutions, analysis obtained results of capillary water absorption is not easy.

Nevertheless, on the basis of shown results some general conclusions can be drawn:

- The values of capillary water absorption are significantly affected by the type of aggregate, type of cement and the water to cement ratio.
- In general, mixtures with natural aggregate have lower values of capillary water absorption.
- The largest values of capillary water absorption, for specimens that have been exposed to sulfate solutions for 180 and 365 days, have the specimens with RCA and w/c=0.55 immersed in Na_2SO_4.

From the Figure 3, it can be seen that in all concrete specimens that were exposed to the sulfate solution, there was an increase in capillary water absorption over time, except for the samples with RCA, CEM I and w/c=0.55 immersed in $MgSO_4$.

3.4. Thermal analysis

Figure 4 presents TGA-DTA curves for samples with RCA that were exposed to sulfate solutions for 365 days. The thermal decomposition behaviour shows several characteristic temperature ranges that can be identified according to the DTA peaks and TGA curves. The mass changes and emphasized endothermic peaks up to 250 °C are generally assumed to be evaporation processes of physically and chemically bound water. Samples exposed to the sulfate solutions have significant peak about 150°C that are believed to be due to gypsum. The most intense peak at this point has the sample MRPC1 and also the highest loss in this temperature range (20°C-300°C). One new peak noticed at about 100°C for NRPC2 and MRPC2 and it may probably be assigned to ettringite.

Other significant peaks are between 400°C and 500°C primarily due to dehydration of portlandite. It can be seen that this peak is not present in samples with a higher water to cement factor (0.55, samples with number 1), while it is observed in samples with a lower water to cement factor (0.35, samples with number 2). Also, it is observed that samples MRPC1 and MRPC2 have one additional peak about 400°C that may be assigned to brucite (it is characteristically formed on the surface of samples exposed to the action of magnesium sulfate).

The weight loss in the range 500-900°C is probably related to the decomposition of some type of carbonates, that are inevitable. Thus, the weight loss associated with broad

peak at ≈600°C is likely due to the decomposition of amorphous carbonated phases while peak at ≈780°C is probably due to decomposition some type of crystalized calcite.

The total mass loss (from 20°C to 1000°C) for observed specimens is the highest for NRPC1 (19.6%) and MRPC1 (20.6%) but the lowest for MRMC2 (12.7%).
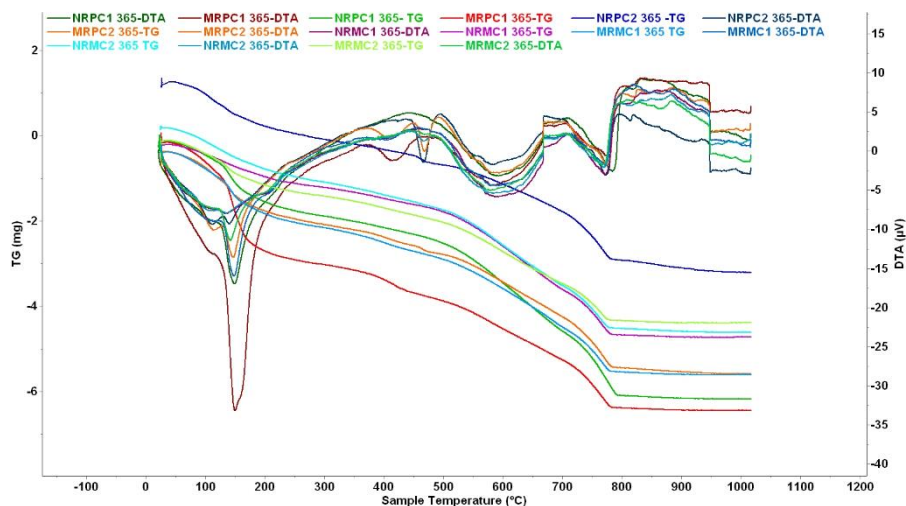
Fig. 4 TGA-DTA of samples with RCA exposed to solutions for 365 days

4. CONCLUSION

From the research that has been carried out in this study, it can be concluded that:

▪ The concretes made with CEM I and with w/c=0.55 which were immersed in both sulfate solutions have the greatest decrease of compressive strength, this is especially pronounced in samples exposed to the action of sodium sulfate. Other examined concretes showed changes in compressive strength up to 10% regardless of cement type, w/c ratio and sulfate solution type.

▪ In the case of a length change, the situation is very similar to the change in compressive strength. The concretes made with CEM I and with w/c=0.55, immersed in both sulfate solutions, have the greatest linear expansion. All other concretes have linear expansion significantly below.

▪ Due to different and complex physical processes and chemical reactions that occur during immersion specimens in sulfate solutions, it is not easy to draw a conclusion about the sulfate resistance of concrete based on the results of capillary water absorption. Generally, mixtures with natural aggregate have lower values of capillary water absorption.

▪ The results of the thermal analysis can be related to the results of the change in length. The samples with the greatest length change also had the greatest mass loss determined by TGA. As well, those samples also have the most pronounced peaks that are probably associated with the products responsible for the expansion of samples exposed to the action of sulfate solutions.

Generally, the type of cement, water to cement ratio and type of aggregate have effect on concrete sulfate resistance. The greatest influence on concrete sulfate resistance has cement type and type of aggregate. Water to cement ratio has minor influence on sulfate resistance in concrete with cement CEM III. However, in concrete with cement CEM I w/c ratio has significant influence on sulfate resistance. Satisfactory sulfate resistance of concrete with RCA can be achieved by applying CEM III and reducing w/c.

REFERENCES

1. Ali Babar, Ahsan Gulzar Muhammad, Raza Ali: Effect of sulfate activation of fly ash on mechanical and durability properties of recycled aggregate concrete. Construction and building materials, 277, 122329, 2021.
2. Zhang Hongru, Liu Wenshen, Zhang Jingbo, Liu Fujiang, Lin Xujian, Ji Tao: A new look at the resistance of recycled aggregate concrete (RAC) to the external sulfate attacks: The influence of the multiple mesoscopic material phases. Journal of Building Engineering, 64, 105653, 2023.
3. Li Yang, Zang Xianbing, Lou Peng, Wang Ruijun, Li Yanlong, Si Zheng: Sulfate attack resistance of recycled aggregate concrete with NaOH-solution-treated crumb rubber. Construction and building materials, 287, 123044, 2021.
4. SRPS EN 196-1:2017 - Methods of testing cement - Part 1: Determination of strength. Institute for standardization of Serbia.
5. SRPS EN 196-3:2017 - Methods of testing cement - Part 3: Determination of setting times and soundness. Institute for standardization of Serbia.
6. SRPS EN 196-6:2017 - Methods of testing cement - Part 6: Determination of fineness. Institute for standardization of Serbia.
7. SRPS EN 206-1:2011 - Concrete - Part 1: Specification performance, production and conformity. Institute for standardization of Serbia.
8. SRPS EN 12620: 2010 - Aggregates for concrete Institute for standardization of Serbia.
9. SRPS 12390-3:2010 - Testing hardened concrete - Part 3: Compressive strength of test specimens. Institute for standardization of Serbia.

ANALIZA OTPORNOSTI BETONA SA RCA NA DEJSTVO SULFATA NAKON JEDNOGODIŠNJE IZLOŽENOSTI SULFATNIM RASTVORIMA

Spoljašnje dejstvo napad sulfata je jedan od problema vezanih za izdržljivost betona. Uprkos percepciji da je beton napravljen od recikliranog agregata za beton (RCA) lošijeg kvaliteta, istraživanja su pokazala da RCA ima potencijal da zadovolji mehaničke i fizičke zahteve za niz primena. Ograničeni radovi su obavljeni na aspektima trajnosti RCA. Cilj istraživanja opisanog u ovom radu bio je da se proceni otpornost betona sa RCA na dejstvo sulfata u kome su kombinovane dve vrste cementa (CEM I i CEM III) i dva vodocementna faktora (0,38 i 0,55). Za procenu sulfatne otpornosti ovih betona, potopljenih u rastvore natrijum i kalijum sulfata, korišćen je pad pritisne čvrstoće, promena dužine, kapilarna vodoapsorpcija i termička analiza (TGA-DTA). Zadovoljavajuća otpornost betona sa RCA na sulfate može se postići primenom CEM III i smanjenjem vodocementnog faktora

Ključne reči: *sulfatno desjstvo, reciklirani betonski agregat (RCA), TGA-DTA, promena dužine, kapilarno upijanje vode.*

DEFINING SEISMIC PARAMETERS
FOR AN ESSENTIAL ELECTRIC POWER FACILITY

UDC 624.042.7/.8:621.17

Toni Kitanovski, Dragi Dojcinovski, Vlatko Sheshov, Marta Stojmanovska, Julijana Bojadzieva, Kemal Edip, Dejan Ivanovski

Ss. Cyril and Methodius University, Institute of Earthquake Engineering and
Engineering Seismology-IZIIS, Skopje, North Macedonia

ORCID iDs: Toni Kitanovski   https://orcid.org/0000-0003-1127-8705
Dragi Dojcinovski   https://orcid.org/0000-0003-3933-1387
Vlatko Sheshov   https://orcid.org/0000-0002-1692-2064
Marta Stojmanovska   https://orcid.org/0000-0002-5134-575X
Julijana Bojadzieva   N/A
Kemal Edip   https://orcid.org/0000-0002-4542-8911
Dejan Ivanovski   https://orcid.org/0000-0002-2012-1454

Abstract. *For the purpose of building a new electric power facility a project to determine seismic potential and seismic parameters for design is produced. Multiple in-situ geophysical investigations have been performed and soil samples have been taken to the laboratory where simple shear tests are done to determine the dynamic parameters of the soil layers. As a result, the dynamic shear modulus and damping ratio vs shear strain relationships of characteristic soil materials were defined. The response analysis was done using these curves, where the effects of the sub-surface local soil medium have a dominant influence upon the amplitude and frequency modification of the expected ground motion. Finally, the seismic design parameters, maximum accelerations at foundation level for design and maximum earthquake site-specific response spectrum have been obtained.*

Key words: *simple shear tests, response analysis, seismic design parameters.*

1. INTRODUCTION

The investigations presented in this report have been carried out for the purpose of defining the seismic potential of a site where an essential electric power facility is planned to be built. These investigations represent continuous work for the site that started with the determination of local hazard and selection of earthquakes that will be used in the analysis done by the department of Natural and Technological Hazards and Ecology part of the Institute of Earthquake Engineering and Engineering Seismology- IZIIS, Skopje [1,2,3,4,5]. Field geophysical and geotechnical surveys carried out using the seismic refraction

tomography method – SIRT were used to define the regional and local seismotectonic, geological and seismological data. A final product of these investigations is the definitions of Vp and Vs – seismic velocities and d – thickness of the layers. From the velocities, additional information can be gained such as: distinguishing of lithophysical media within the terrain structure and dynamic values of the geomechanical elastic parameters (Table 1). Soil samples were taken from three different boreholes (BH-14, BH-17, and BH-22), that were made on the site, at different depths from 4 to 12m. The laboratory testing of samples was performed in the Soil Dynamic Testing Laboratory, Department of Geotechnics and Special Structures, using a direct simple shear apparatus (DSSA) to determine the shear modulus and damping in correlation with shear strain curves. These curves have been implemented in mathematical models of the soil for the analysis of the seismic site response. The analyses have been carried out by using the software Shake2000. The results from the analysis are used to determine the seismic design parameters for different serviceability periods.

2. GEOPHYSICAL SURVEY

For the geophysical measurements 34 channel SoilSpy Rosina digital seismograph was used, also geophones with a natural frequency of 4.5 Hz were used for recording the seismic energy. Measurements using the seismic refraction method were performed along 8 seismic profiles with a total length of 740 meters: 4 seismic profiles of 80 m, 2 seismic profiles of 85 meters, 1 seismic profile of 100 m, and 1 seismic profile of 150 m. The distance between the geophones was 5-5.3 meters and the minimal offset (distance between the source and the receiver) was 5-5.3 meters. The acquisition was done by a sampling frequency of 1024 Hz and a time duration of 0.5 seconds. Seismic energy was generated by hammer blows with a hammer that weighs 8 kg upon an aluminum plate.

2D models were obtained from the analysis of the geophysical data where 5 lithological media are distinguished and are characterized by different physical-mechanical characteristics such as:

- Surface layer – clay, with values of seismic velocities: Vp=450-900 m/s; Vs=160-320 m/s
- Subsurface layer – clay, with seismic velocities values: Vp=950-1200 m/s; Vs=350-440 m/s
- Clay, with seismic velocities values: Vp=1250-1600 m/s; Vs=460-590 m/s
- Clay, coal clay, with seismic velocities values: Vp=1650-2200 m/s; Vs=610-840 m/s
- Clay, coal clay, with seismic velocities values: Vp>2200 m/s; Vs>840 m/s

The dynamic elastic parameters are calculated using empirical calculations following correlative relationships between the seismic velocities and the corresponding geomechanical parameter according to the literature [6,7,8]. The complete results for all the layers are shown in Table 1.

Table 1 Interval values of dynamic elastic parameters

Parameter	Surface layer	Subsurface layer	Clay	Clay, Coal clay	Clay, Coal clay
Vp (m/s)	450-900	950-1200	1250-1600	1650-2200	Vp>2200
Vs (m/s)	160-320	350-440	460-590	610-840	Vs>840
g (kN/m^3)	16-18	18-19	19-20	20	22
m $_{din}$	0.42	0.42	0.42	0.42-0.41	0.42
Edin (MPa)	110-570	630-1050	1130-1960	2110-3860	>4000
Gdin (MPa)	41-200	220-370	400-690	740-1370	>1400
Kdin (MPa)	230-1180	1310-2180	2350-4080	4390-7150	>7300

3. DYNAMIC LABORATORY INVESTIGATION

The behaviour of soil deposits under expected seismic loading at the site is nonlinear, this will influence the ground motion parameters during the expected earthquakes and the dynamic interaction between soil and the facilities. The nonlinearity is most commonly presented by variation of dynamic shear modulus and the damping coefficients with increasing of the amplitudes of shear deformations. The definition of nonlinear dynamic relationships of soil layers at the site was carried out based on the results of the experimental tests on the soil samples performed by cyclic simple shear tests. The DSSA (Figure 1) previously mentioned was used for testing two cylindrical models simultaneously restrained rigidly in vertical direction by three loading plates, while in radial direction with series of Polytetrafluoroethylene (PTFE) coated steel rings [9]. The dynamic excitation in the form of shear strains is applied in horizontal direction through the central loading plate placed between the two models. Through the relative horizontal displacement of the rings the dynamic excitation is uniformly applied along the entire height of the model. Due to simple cyclic shear in the element shear strains will develop and hysteresis relationships can be obtained (Figure 2).

Fig. 1 DSSA in the laboratory for soil dynamics
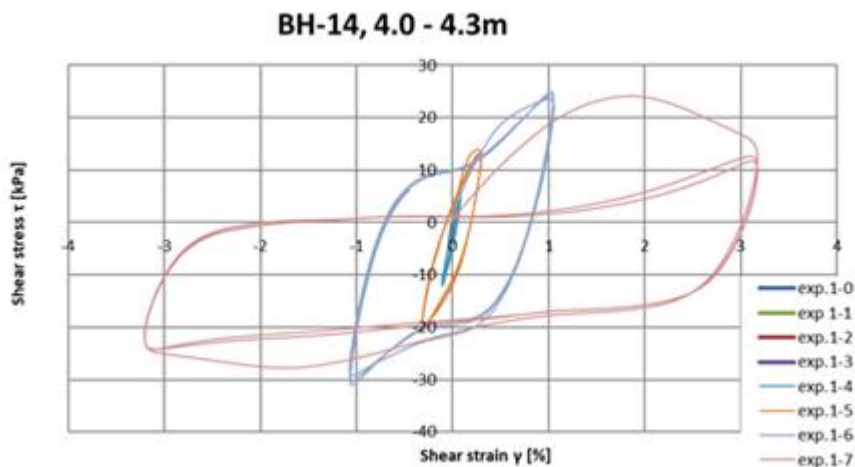
Fig. 2 Shear-strain relationship from one of the tests

The selection of the tested materials was made by careful examination of the received samples. Clay samples from boreholes BH-14, BH-17, and BH-22 were tested including characteristic horizons within each borehole. The testing material – borehole cores were received in plastic bags and placed in a wet chamber. The samples were tested as relatively undisturbed samples, with water content as preserved in the received samples and consolidated under effective pressure that corresponds to the investigated horizon. The excitation was applied step-by-step, eight steps in total, with variation of the maximum amplitude of shear strains in the range of g= 1.0x10-3% to g = 3%. The dynamic shear modulus are defined as a secant shear modulus (Gsec) that corresponds to the extreme points of the hysteretic curves for each strain level. By using the obtained values for the shear modulus

G-g diagrams are established (Figure 3 and 4). Normalized shear modulus are obtained by dividing G/Gmax for each strain level, those are the ones used in the analysis [10,11]. Damping of the soil was defined by damping ratio D that represents a percentage of the critical damping. It is determined by using the following relation:

$$D = \frac{A_H}{4\pi A_{0ab}} * 100 \ (\%)$$

where, D -damping ratio, A_H – area bounded by the hysteretic curve, A_{0ab} – Area of the triangle bounded by the secant passing through the extreme points of the curve. The damping ratios are also determined for each shear strain level and after that relationships are established (Figure 5).
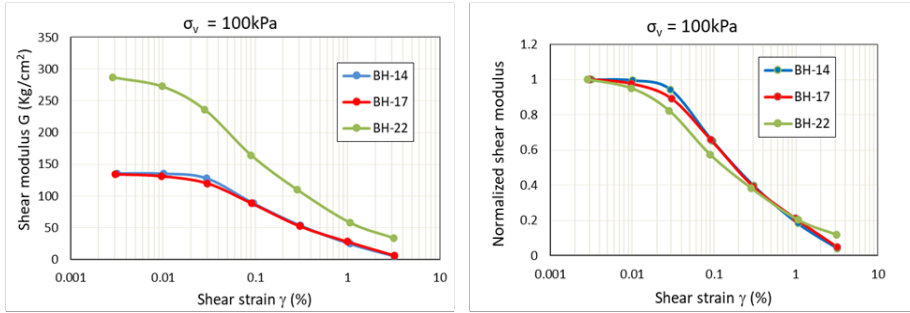
Fig. 3 Dynamic shear modulus vs shear strain for upper layers
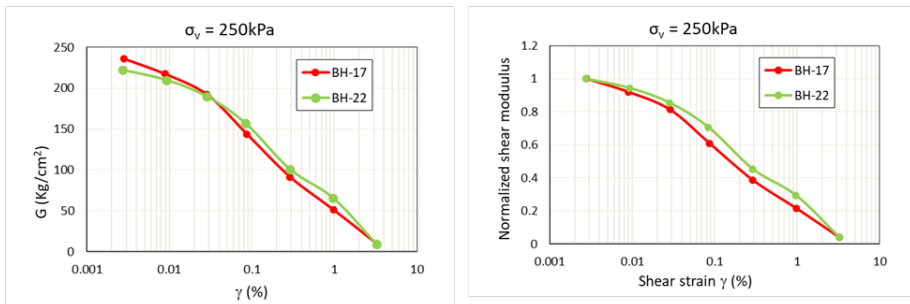
Fig. 4 Dynamic shear modulus vs shear strain for lower layers
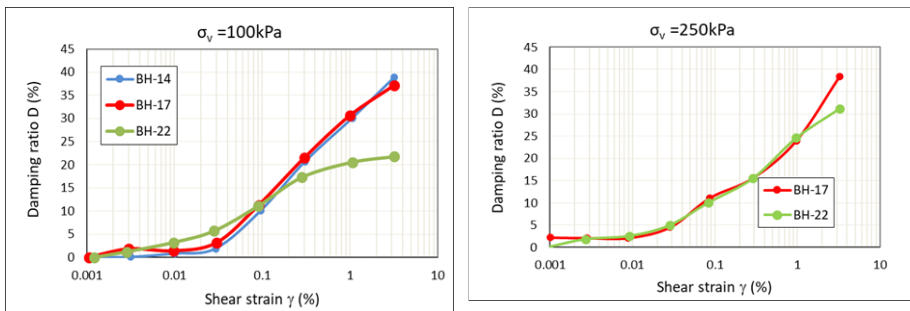
Fig. 5 Damping ratio vs shear strain for both layers

4. EFFECT OF LOCAL GEOTECHNICAL MEDIA

The local geotechnical medium has a specific effect on the characteristics of the ground motion upon the surface during the earthquake. Depending on the characteristics of the local geotechnical medium and the characteristics of the excitation at the level of the seismic subsoil, the mentioned effect can be higher or lower [12]. The effect of the local geotechnical medium has been defined by analysis of the dynamic response of the

mathematical models of soil (Figure 6), called seismic site response. The analysis has been carried out by using the software SHAKE2000 which applies the method of vertical propagation of shear seismic waves through a liner-visco-elastic system that is based on the Kanai's solution of wave equation. The physical-mechanical and dynamic characteristics of the amplification medium at the site are represented by three representative geodynamical models. The ground classification scheme was done according to recommendations in Eurocode 8, where identification of ground types (classes) is performed using the value of the average shear wave velocity $V_{s,30}$.

a) model M-1   b) model M-2

c) model M-3
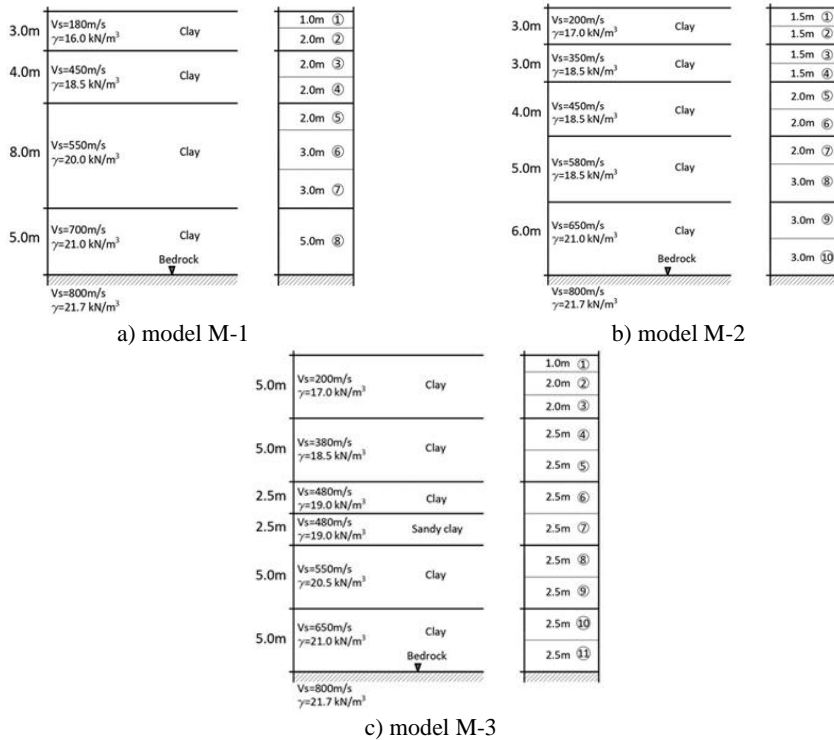
Fig. 6 Geodynamical and mathematical models at the site

Accelerograms of eight recorded earthquakes have been selected then scaled to expected ground acceleration. These time histories cover the prevailing period of the site and expected magnitudes, as well as frequency ranges with maximal amplitudes of seismic waves from the local and distant sources. The predominant periods resulting from the site response analysis for each model are given in Table 2.

Table 2 Model predominant periods

Model	Period T (s)
M-1	0.105
M-2	0.086
M-3	0.126

The accelerations along the depth of the models are presented in Figure 7. The results emphasize that the surface layers amplify the seismic effect of the earthquakes. This layer has seismic shear velocity below 300 m/s and it has significant influence on the amplification and frequency effect on the earthquake motion [13]. Therefore, this layer was discarded as an option for foundation layer and the foundation was placed in the following layer ranging from -2.0 to -5.0 m. The dynamic amplification factor for the investigated location ranges from 1.05 for model M1 up to 1.16 for model M3. For further analysis and definition of input seismic parameters, the recommended value of the dynamic amplification factor (DAF) is considered as 1.2.

a) model M-1   b) model M-2

c) model M-3
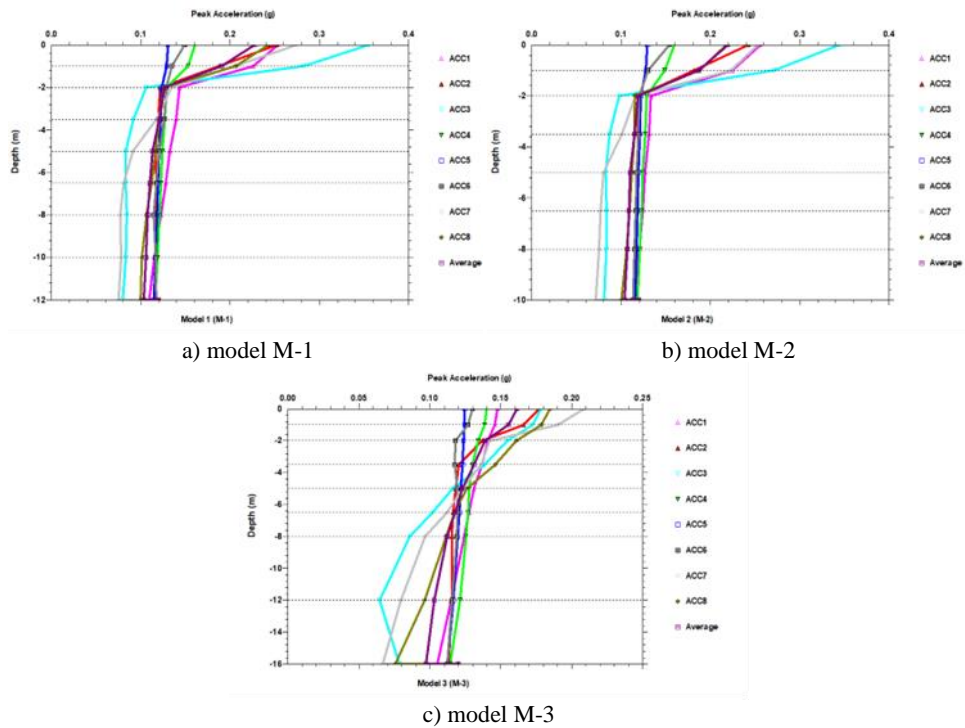
Fig. 7 Acceleration along the depth for the selected accelerograms

The acceleration response spectra have been computed for the selected earthquakes and for 5% damping with an input maximum acceleration of amax=0.12g. The obtained spectra for each model show similar results (Figure 8) where the dominant amplitudes occur in the period range of 0.2 to 0.3s.

In addition, the computed average normalized spectra have been compared with normalized spectra defined by the Eurocode8, ground type B. As can be seen the amplitudes of the calculated average site response spectra are in the range or smaller than the amplitudes of proposed spectra from Eurocode (Figure 9).

a) model M-1   b) model M-2

c) model M-3

Fig. 8 Spectral acceleration for 5% damping

a) model M-1   b) model M-2

c) model M-3
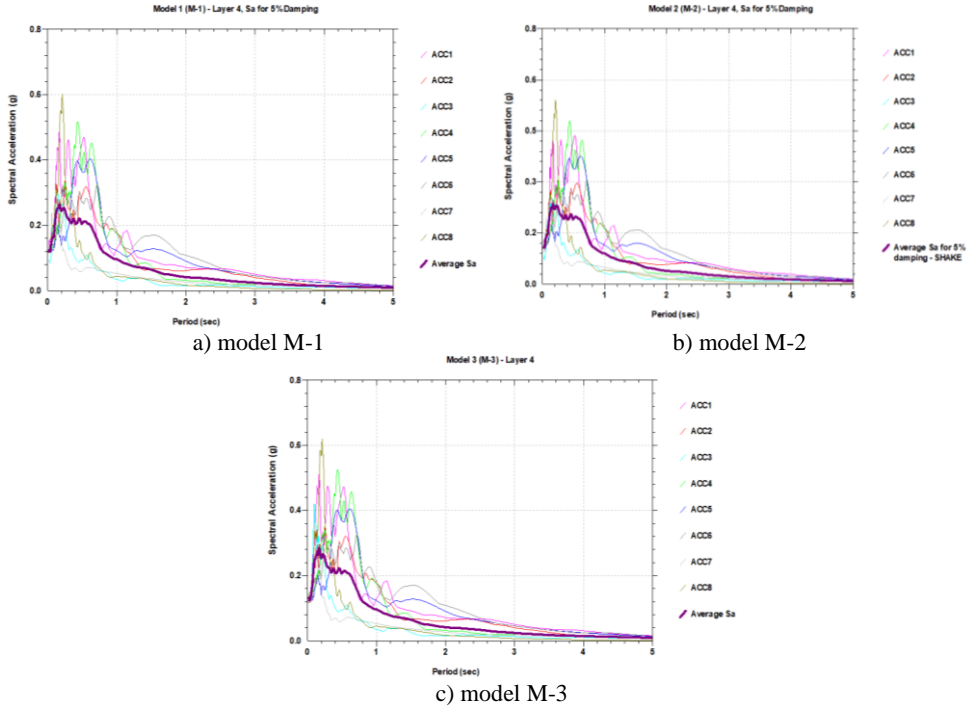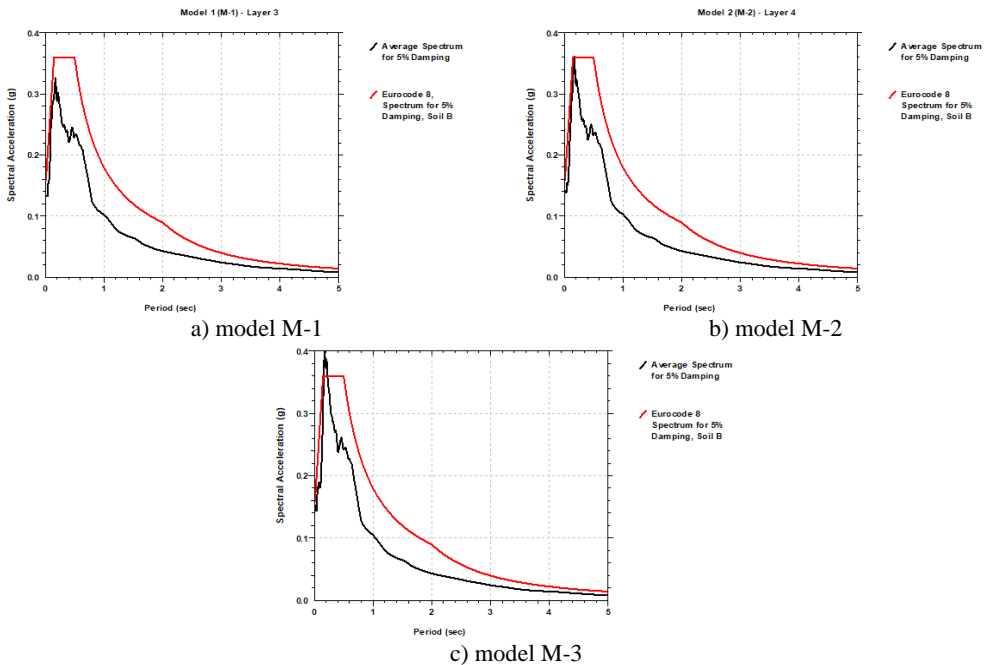
Fig. 9 Spectral acceleration for 5% damping compared with Eurocode requirements

5. SEISMIC DESIGN PARAMETERS

The seismic parameters have been defined taking into consideration the seismic hazard at the site, seismicity at the site expressed in probabilistic way, and through application of the seismic risk methodology, which includes not only technical but also economic and technological elements of design [14]. Taking into account the need for dynamic analysis and design of the structures, the seismic parameters are given in the form of expected maximum acceleration. For future structures most important are maximum accelerations at the foundation level (amax) that depend on the maximum accelerations at bedrock (a_0) and the seismic effect of the local soil medium, expressed by the dynamic amplification factor (DAF). The main seismic design parameters, the maximum accelerations, have been defined based on the results from the seismic hazard and risk analysis under the following assumptions:

- the serviceability period of the main structures is 100 years (Table 3)
- the serviceability period of the auxiliary structures is 50 years (Table 4)
- for the design earthquake the acceptable seismic risk level is 30%
- for the maximum earthquake, the acceptable seismic risk is 10%

Table 3 Seismic design parameters for foundation level for main structures

Serviceability period (years)	Seismic risk level %	Earthquake type	Max. acceleration a_{max} (g)	Corresponding return period
100	30	Design	0.124	281
	10	Maximum	0.169	950

Table 4 Seismic design parameters for foundation level for auxiliary structures

Serviceability period (years)	Seismic risk level %	Earthquake type	Max. acceleration a_{max} (g)	Corresponding return period
50	30	Design	0.108	141
	10	Maximum	0.145	475

6. SUMMARY AND CONCLUSIONS

At the request of the investors, in-situ geophysical measurements, laboratory and analytical investigations were carried out in order to define the seismic potential of the site. Based on the results the following conclusions are drawn:

- The loose surface and subsurface layers are characterized by weak physical-mechanical characteristics and represent a critical zone of the investigated location. These surface layers significantly amplify the seismic effect, therefore these layers are not recommended to be used as a foundation layer for the planned structures.

- Based on the results from in-situ geophysical measurements and the recommendations from Eurocode 8, the soil conditions of the site can be categorized as ground type B.

- The definition of nonlinear dynamic relationships of soil layers at the site based on results from experimental testing of soil samples was of great importance in the analysis. Using literature curves could significantly affect the analysis and further away from the correct results.

REFERENCES

1. Aleksovski D., Šešov V., Dojčinovski D., Kemal E., Mirakovski G, at all.; Geotechnical and geophysical field investigation on Arberia-3 site in Prishtina, Kosovo, IZIIS, Report 2006-31.
2. Dojcinovski D et. al., (2018) Kosova e Re powerplant project (KRPP), Volume 1, Seismic study, IZIIS report 2018-49/1.
3. Dojcinovski D., Aleksovski D., Sesov V., Milutinovic Z., Olumceva T., Edip K., Shalikj R., Gadza V., Zafirova I., Gjorgjeska I., Zlateski A. (2010). Seismic microzonation of Ulpijana Settlement - Prishtina Volume – I, Regional Seismotectonic and Seismological Investigations, Report IZIIS – 2010-45/1, Skopje.
4. Dojcinovski D.,Aleksovski D., Sesov V., Milutinovic Z., Olumceva T., Edip K., Shalikj R., Gadza V., Zafirova I., Gjorgjeska I., Zlateski A. (2010). Seismic microzonation of Ulpijana Settlement - Prishtina Volume – II, Geophysical investigations, Report IZIIS – 2010-45/2, Skopje.
5. Dojcinovski D.,Aleksovski D., Sesov V.,Milutinovic Z., Olumceva T., Edip K., Shalikj R.Gadza V., Zafirova I., Gjorgjeska I., Zlateski A. (2010). Seismic microzonation of Ulpijana Settlement - Prishtina Volume – III, Seismic zonation, Report IZIIS – 2010-45/3, Skopje.
6. Watanabe, T., Matsuoka, T. & Ashidi, Y., 1999. Seismic traveltime tomography using Fresnel volume approach. Kyoto University, Japan.
7. G Mavko, T Mukerji and J Dvorkin (2003), The Rock Physics Handbook, Cambridge University Press;
8. Kearey, P., Brooks, M.: An Introduction to Geophysical Exploration Blackwell Scientific Publications, Oxford,1991)
9. Dames and Moore (1981) Manual for operation of the Cyclic Simple Shear Apparatus, London UK.
10. Jianfeng Zhang et al. (2005), Normalized Shear Modulus and Material Damping Ratio Relationships,Journal of Geotechnical and Geoenvironmental Engineering, Vol. 131, No. 4, ASCE.
11. Massarsch, K. R. 2004. Deformation properties of fine-grained soils from seismic tests. Keynote lecture, International Conference on Site Characterization, ISC'2, 19 – 22 Sept. 2004, Porto, 14 p.
12. Sesov, V., Dojcinovski, D., Edip, K. and Cvetanovska, J. (2012) Evaluation of the Site Seismic Potential for Performance Based Design. Second International Conference on Performance-based Design in Earthquake Geotechnical Engineering. May 28-30, 2012 - Taormina Iitaly. Paper No.1.02
13. Ambraseys, N. N. (1995) The Prediction of Earthquake Peak Ground Acceleration in Europe, Earthquake Engineering and Structural Dynamics, Vol. 24,467-490
14. Cornell, C.A., (1968). "Engineering Seismic Risk Analysis", Seismol. Soc. Amer. Bull., Vol. 58, No. 58,pp. 1503-1606.

DEFINISANJE SEIZMIČKIH PARAMETARA
ZA KLJUČNO ELEKTRO-ENERGETSKO POSTROJENJE

Za potrebe izgradnje novog elektroenergetskog objekta izrađuje se projekat za utvrđivanje seizmičkog potencijala i seizmičkih parametara za projektovanje. Izvršeno je više geofizičkih istraživanja na licu mesta i uzorci zemljišta su odneti u laboratoriju gde se vrše jednostavna ispitivanja smicanja radi određivanja dinamičkih parametara slojeva tla. Kao rezultat, definisani su dinamički modul smicanja i odnos prigušenja u odnosu na smičnu deformaciju karakterističnih materijala tla. Analiza odziva je urađena korišćenjem ovih krivih, gde uticaji podzemnog lokalnog zemljišnog medija imaju dominantan uticaj na modifikaciju amplitude i frekvencije očekivanog kretanja tla. Konačno, dobijeni su seizmički projektni parametri, maksimalna ubrzanja na nivou temelja za projektovanje i maksimalni spektar odgovora specifičnog za lokaciju zemljotresa.

Ključne reči: *jednostavna ispitivanja smicanja, analiza odziva, parametri seizmičkog projektovanja*

LARGE DEFORMATION THEORY IN GEOMECHANICS - INFLUENCE OF KINEMATIC NONLINEARITY ON THE RESULTS OF SOME CHARACTERISTIC GEOTECHNICAL CALCULATIONS

UDC 624.042.7/.8:621.17

Borko Miladinović

University of Montenegro, Faculty of Civil Engineering, Podgorica, Montenegro

ORCID iD: Borko Miladinović   N/A

Abstract. *The geotechnical engineering calculations are usually carried out according to the small deformation and displacement theory (infinitesimal strain theory) i.e. first-order theory. A linear relationship between componental displacements and deformations is adopted. The well-known conditions for equilibrium are defined for an undeformed system i.e. undeformed structure. Therefore, the geometric and static linearity assumptions are usually valid in geotechnical engineering calculations. These linearities are collectively referred to as kinematic linearity. In other words, engineers believe that results of quite satisfactory accuracy are obtained if only material nonlinearity is taken into account in the engineering calculations, regardless of the type of geotechnical problem being analysed. Therefore, it is not necessary to apply the large (finite) deformation theory with the assumption of material nonlinearity. The main aim of this paper is to verify the previous statement in the case of some characteristic problems of Geotechnics. In the first part of this paper, the large deformation theory, which is mostly unknown to the wider professional public, is briefly presented. After that, simple numerical analyses of some characteristic problems of Geotechnics were carried out in the well-known software FLAC 2D software with the aim of comparing the results obtained for the cases of kinematic linearity and kinematic nonlinearity. The obtained results point to the fact that kinematic nonlinearity should not always be ignored in the usual geotechnical engineering calculations. Therefore, engineers are urged to be careful.*

Key words: *geotechnics, large deformation theory, kinematic nonlinearity.*

1. INTRODUCTION

In engineering practice geotechnical calculations are most often carried out according to the small (infinitesimal) deformation (strain) theory (hereinafter SD theory) with the assumption of material nonlinearity of the soil. Therefore, material nonlinearity and kinematic linearity assumptions are adopted ("material nonlinearity only"). The kinematic linearity consists of geometric and static linearity. The geometric linearity implies the adoption of the small deformation assumption. It means that the squares and higher degrees of these deformations, as well as the squares and higher degrees of their derivatives, can be completely ignored in the geotechnical engineering calculations. Adopting this assumption, a linear relationship between displacements and deformations is actually provided. The static linearity implies the adoption of the small displacement assumption. It means that the squares and higher degrees of these displacements, as well as the squares and higher degrees of their derivatives, can be completely ignored in the geotechnical engineering calculations. Adopting this assumption, the conditions for equilibrium can be defined for an initial or undeformed configuration i.e. undeformed structure.

Civil engineers consider it unnecessary to carry out usual engineering calculations according to the very complicated large (finite) deformation theory (hereinafter LD theory), because the deviations of the obtained results would be negligible in relation to the results of the calculations carried out according to the SD theory. This statement can be considered quite acceptable in the case of steel or concrete structures. However, its acceptability is more or less debatable in Geotechnics. In this paper, with the application of adequate software, an attempt will be made to verify this statement for some characteristic problems of Geotechnics. The well-known software Flac 2D (Fast Lagrangian Analysis of Continuum) was used. This software makes it possible to carry out stress-strain analysis according to the LD or SD theory for many geotechnical problems.

Generally, in continuum mechanics (mechanics of continuous media), when analyzing the motion and/or deformation of solids, or flow of fluids, two different methods (approaches, formulations, descriptions) can be used. The first formulation is so-called Eulerian formulation. The second formulation is so-called Langrangian formulation, which is directly implemented in the software Flac 2D. Therefore, only the Langrangian formulation will be described in more detail in this paper.

2. LAGRANGIAN FORMULATION IN CONTINUUM MECHANICS

The starting point for Langrangian formulation is well-known principle of virtual displacements i.e. principle of virtual work. This principle will be briefly presented in the following part of this paper. Due to the adopted material nonlinearity assumption, first the principle of virtual displacements and then Langrangian formulation will be briefly presented in the incremental form in the way it was done in [1-5].

2.1. Principle of virtual displacements

Fig. 1 shows a continuum body (hereinafter body) in the space x_i (i=1,2,3) before applying the first load increment (configuration $^0\Omega$) and the same body after applying the nth load increment (configuration $^n\Omega$). The displacement vectors for surface point E and

body (internal) point F are defined for the given body after applying the nth load increment. These are the vectors $^{n}\mathbf{u}_{i}^{E}$ and $^{n}\mathbf{u}_{i}^{F}$. According to the LD theory, the displacement of any point of the given body can be separated into two independent components. The first component represents the displacement of the point due to translation and/or rotation of the body after applying the nth load increment without changing its shape and dimensions (rigid-body displacement). The second component represents the displacement of the point due to distortion and/or volumetric deformations of the body after applying the nth load increment.
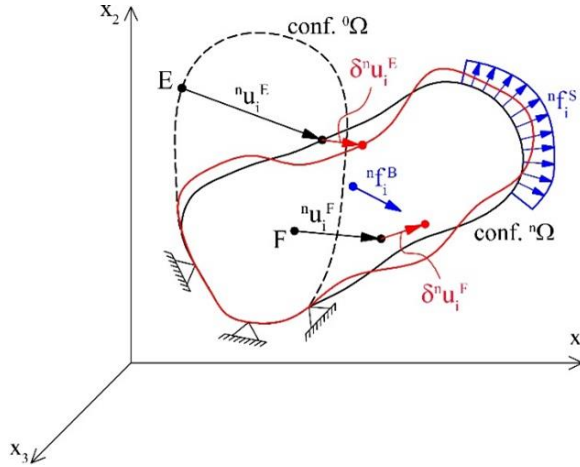
Fig. 1 Configuration of body before and after applying nth load increment in space x_i (i=1,2,3). Virtual displacement field for body after applying the nth load increment.

The configuration of the given body after applying the nth load increment $^{n}\Omega$ (hereinafter body configuration $^{n}\Omega$) is assigned a completely arbitrary virtual displacement field (red line in the image above) which satisfies displacement boundary conditions. This is just one of many possible ways of virtual displacement of the given body. The position of points E and F is additionally defined by vectors marked with $\delta^{n}\mathbf{u}_{i}^{E}$ and $\delta^{n}\mathbf{u}_{i}^{F}$. The basic equation of the principle of virtual displacements can be written in the following incremental form:

$$^{n}\mathfrak{R}_{int} =\,^{n}\mathfrak{R}_{ext} \tag{1}$$

$$\int_{^{n}V} {}^{n}\boldsymbol{\sigma}_{ij}\cdot\delta_{n}\mathbf{e}_{ij}\cdot d^{n}V = \int_{^{n}V} {}^{n}\mathbf{f}_{i}^{B}\cdot\delta^{n}\mathbf{u}_{i}^{B}\cdot d^{n}V + \int_{^{n}S} {}^{n}\mathbf{f}_{i}^{S}\cdot\delta^{n}\mathbf{u}_{i}^{S}\cdot d^{n}S \tag{2}$$

where:

$^{n}\mathfrak{R}_{int}$ - is virtual work done by all internal forces for the given virtual displacement field of the body configuration $^{n}\Omega$,

$^{n}\mathfrak{R}_{ext}$ - is virtual work done by all external forces for the given virtual displacement field of the body configuration $^{n}\Omega$,

$\delta^{n}\mathbf{u}_{i}^{B}$ - is given virtual displacement vector for all internal points for the body configuration $^{n}\Omega$,

$\delta^n \mathbf{u}_i^S$ - is given virtual displacement vector for all surface points for the body configuration $^n\Omega$,

$\delta_n \mathbf{e}_{ij}$ - is matrix (second-order tensor) of virtual deformations corresponding to the given virtual displacement field of the body configuration $^n\Omega$,

$^n\boldsymbol{\sigma}_{ij}$ - is Cauchy stress tensor,

$^n\mathbf{f}_i^B$ - is vector of body forces defined per unit volume of body configuration $^n\Omega$,

$^n\mathbf{f}_i^S$ - is vector of surface forces defined per unit surface area of the body configuration $^n\Omega$,

$^n V$ - is volume of the given body after applying nth load increment,

$^n S$ - is surface area of the given body after applying nth load increment,

i, j - are Cartesian axes for which it is valid to i=1,2,3 and j=1,2,3.

It is important to note two things. Firstly, Cartesian axes x_1, x_2 and x_3 remain stationary whereas loaded body moves through those axes. Secondly, at the end of each load increment the three fundamental conditions of Continuum mechanics must be satisfied. These are: conditions for equilibrium, compatibility conditions and stress-strain laws. All three mentioned conditions are implemented in Eq. 2.

Since virtual displacements are actually infinitesimal displacements, the well-known SD theory laws can be used for the relation between virtual displacements and their corresponding virtual deformations. In this particular case, the following equation is used to define each member of the matrix of virtual deformations of the body configuration $^n\Omega$:

$$\delta_n e_{ij} = \frac{1}{2} \cdot \left(\frac{\partial \delta^n u_i}{\partial^n x_j} + \frac{\partial \delta^n u_j}{\partial^n x_i} \right) \tag{3}$$

Eq. 2 must be rewritten because the volume $^n V$, surface area $^n S$ and Cauchy stress tensor of the given body after applying n^{th} load increment are unknown.

2.2. Total Lagrangian formulation

The problem of unknown geometry (volume and surface area) of the given body after applying nth load increment can be overcome if, instead of Cauchy stress tensor, some other type of stress tensor and an energetically compatible strain tensor is applied. In the case of Total Langrangian formulation (hareinafter TL formulation), instead of Cauchy stress tensor for unknown body configuration $^n\Omega$, a second-order Piola-Kirchhoff stress tensor $^n_0\mathbf{S}$ which is referred (defined) to the initial body configuration $^0\Omega$ (before first load increment) is used. This stress tensor is energetically compatible with the Green-Lagrange strain tensor $^n_0\boldsymbol{\varepsilon}$ which is also referred to the initial body configuration $^0\Omega$. By introducing new stress and strain tensors into the calculation with some other minor corrections, the following equation of the principle of virtual displacements according to the TL formulation was obtained for body configuration $^n\Omega$ shown in Fig. 1:

$$\int_{^0V} {}^n_0\mathbf{S}_{ij} \cdot \delta^n_0\boldsymbol{\varepsilon}_{ij} \cdot d^0V = \underbrace{\int_{^0V} {}^n_0\mathbf{f}_i^B \cdot \delta^n\mathbf{u}_i^B \cdot d^0V + \int_{^0S} {}^n_0\mathbf{f}_i^S \cdot \delta^n\mathbf{u}_i^S \cdot d^0S}_{^n\Re_{ext} \text{ - known}} \tag{4}$$

where:

$\delta^n_0\boldsymbol{\varepsilon}_{ij}$ - is variation of the Green-Lagrange strain tensor.

The 2nd Piolla-Kirchhoff stress tensor ${}_0^n\mathbf{S}$ is the symmetrical tensor that has no real (physical) meaning, so it is not suitable for practical application. It is important to note that the values of the members of this stress tensor change only in the case of deformation of the loaded body. Therefore, the members of this stress tensor do not change in the case of rigid-body motion. The Green-Lagrange strain tensor ${}_0^n\boldsymbol{\varepsilon}$ is also a symmetrical tensor. The members of this tensor are partial derivatives of displacements after applying n^{th} load increment with respect to the original coordinates i.e. coordinates of initial body configuration ${}^0\Omega$.

Assuming that all static and kinematic quantities are known for body configurations ${}^0\Omega$, ${}^1\Omega$, ${}^2\Omega$,..., ${}^{n-1}\Omega$, in order to define the Piolla-Kirchhoff stress tensor and the variation of the Green-Lagrange strain tensor, the principle of incremental decomposition is applied to the following way:

$$ {}^n\mathbf{u}_i = \underbrace{{}^{n-1}\mathbf{u}_i}_{\text{known}} + \underbrace{\Delta\mathbf{u}_i}_{\text{unknown}} \tag{5}$$

$$ {}_0^n\mathbf{S}_{ij} = \underbrace{{}_0^{n-1}\mathbf{S}_{ij}}_{\text{known}} + \underbrace{{}_0\mathbf{S}_{ij}}_{\text{unknown}} \tag{6}$$

$$ {}_0^n\boldsymbol{\varepsilon}_{ij} = \underbrace{{}_0^{n-1}\boldsymbol{\varepsilon}_{ij}}_{\text{known}} + \underbrace{{}_0\boldsymbol{\varepsilon}_{ij}}_{\text{unknown}} \tag{7}$$

where:

${}^n\mathbf{u}_i$ - is unknown displacement vector of given body after applying nth load increment,

${}^{n-1}\mathbf{u}_i$ - is known displacement vector of given body after applying $(n-1)^{th}$ load increment,

${}_0\mathbf{S}_{ij}$ - is unknown increment of the 2nd Piolla-Kirchhoff stress tensor for body configuration change from ${}^{n-1}\Omega$ to ${}^n\Omega$, which is also referred to the initial body configuration ${}^0\Omega$,

${}_0\boldsymbol{\varepsilon}_{ij}$ - is unknown increment of the Green-Lagrange strain tensor for body configuration change from ${}^{n-1}\Omega$ to ${}^n\Omega$, which is also referred to the initial body configuration ${}^0\Omega$.

Using the principle of incremental decomposition, the problem is reduced to determining the unknown increments of the corresponding stress and strain tensor. According to Eq. 3 and Eq. 5, the increment of the Green-Lagrange strain tensor is:

$$ {}_0\boldsymbol{\varepsilon}_{ij} = {}_0^n\boldsymbol{\varepsilon}_{ij} - {}_0^{n-1}\boldsymbol{\varepsilon}_{ij} \tag{8}$$

$$ {}_0\boldsymbol{\varepsilon}_{ij} = \frac{1}{2}\cdot\underbrace{\left(\overbrace{{}_0\mathbf{U}_{i,j}}^{\text{unknown}} + \overbrace{{}_0\mathbf{U}_{j,i}}^{\text{unknown}} + \overbrace{{}_0^n\mathbf{U}_{k,i}}^{\text{known}}\cdot\overbrace{{}_0\mathbf{U}_{k,j}}^{\text{unknown}} + \overbrace{{}_0\mathbf{U}_{k,i}}^{\text{unknown}}\cdot\overbrace{{}_0^n\mathbf{U}_{k,j}}^{\text{known}} \right)}_{\text{linear part by increment } \Delta\mathbf{u}_i} + $$
$$ + \frac{1}{2}\cdot\underbrace{\left(\overbrace{{}_0\mathbf{U}_{k,i}}^{\text{unknown}}\cdot\overbrace{{}_0\mathbf{U}_{k,j}}^{\text{unknown}} \right)}_{\text{nonlinear part by increment } \Delta\mathbf{u}_i} = {}_0\mathbf{e}_{ij} + {}_0\boldsymbol{\eta}_{ij} \tag{9}$$

where ${}_0\mathbf{e}_{ij}$ and ${}_0\boldsymbol{\eta}_{ij}$ are linear and nonlinear part of the strain tensor increment ${}_0\boldsymbol{\varepsilon}_{ij}$ respectively. The nonlinear part ${}_0\boldsymbol{\eta}_{ij}$ is usually neglected in SD theory in contrast to LD

theory. By taking into account the nonlinear part of the strain tensor increment $_0\boldsymbol{\varepsilon}_{ij}$ in engineering calculations, the geometric nonlinearity assumption is actually adopted. In Eq. 9, there are unknown tensors of the displacement increments. The members of these tensors are actually partial derivatives of displacement increments with respect to the original coordinates. According to the previously mentioned equations, the variation of the Green-Lagrange strain tensor for the body configuration $^n\Omega$, which is referred to the initial body configuration $^0\Omega$, is:

$$\delta \, {}_0^n\boldsymbol{\varepsilon}_{ij} = \delta(\, {}_0^{n-1}\boldsymbol{\varepsilon}_{ij} + {}_0\boldsymbol{\varepsilon}_{ij}) = \delta \, {}_0\boldsymbol{\varepsilon}_{ij} = \delta \, {}_0\mathbf{e}_{ij} + \delta \, {}_0\boldsymbol{\eta}_{ij} \tag{10}$$

Now Eq. 4 can be written in the following form:

$$\int_{^0V} {}_0^{n-1}\mathbf{S}_{ij} \cdot \delta \, {}_0\boldsymbol{\varepsilon}_{ij} \cdot d^0V + \int_{^0V} {}_0\mathbf{S}_{ij} \cdot \delta \, {}_0\boldsymbol{\varepsilon}_{ij} \cdot d^0V = {}^n\Re_{ext} \tag{11}$$

$$\int_{^0V} {}_0^{n-1}\mathbf{S}_{ij} \cdot \delta \, {}_0\mathbf{e}_{ij} \cdot d^0V + \int_{^0V} {}_0^{n-1}\mathbf{S}_{ij} \cdot \delta \, {}_0\boldsymbol{\eta}_{ij} \cdot d^0V + \int_{^0V} {}_0\mathbf{S}_{ij} \cdot \delta \, {}_0\boldsymbol{\varepsilon}_{ij} \cdot d^0V = {}^n\Re_{ext} \tag{12}$$

In order to define the unknown increment of the 2nd Piolla-Kirchhoff stress tensor $_0\mathbf{S}_{ij}$, the following relation of stress and strain tensor increment is adopted:

$$_0\mathbf{S}_{ij} = {}_0\mathbf{D}_{ijrs} \cdot {}_0\boldsymbol{\varepsilon}_{rs} \approx {}_0\mathbf{D}_{ijrs} \cdot {}_0\mathbf{e}_{rs} \tag{13}$$

where $_0\mathbf{D}_{ijrs}$ is tangential elastic tensor which is referred to the initial body configuration $^0\Omega$ and r,s are Cartesian axes for which it is valid to r=1, 2, 3 and s=1, 2, 3. Eq. 13 is obtained by writing the increment $_0\mathbf{S}_{ij}$ as a Taylor series in $_0\boldsymbol{\varepsilon}_{rs}$ neglecting higher-order members and nonlinear part of increment of the Green-Lagrange strain tensor for body configuration change from $^{n-1}\Omega$ to $^n\Omega$ which is referred to the initial body configuration $^0\Omega$. Now, the product of the increment $_0\mathbf{S}_{ij}$ and a variation of the strain tensor increment $\delta \, {}_0\boldsymbol{\varepsilon}_{ij}$ is:

$$_0\mathbf{S}_{ij} \cdot \delta \, {}_0\boldsymbol{\varepsilon}_{ij} = {}_0\mathbf{D}_{ijrs} \cdot {}_0\mathbf{e}_{rs} \cdot (\delta \, {}_0\mathbf{e}_{ij} + \delta \, {}_0\boldsymbol{\eta}_{ij}) = \overbrace{{}_0\mathbf{D}_{ijrs} \cdot {}_0\mathbf{e}_{rs} \cdot \delta \, {}_0\mathbf{e}_{ij}}^{\text{linear part by } \Delta\mathbf{u}_i} +$$
$$+ \underbrace{{}_0\mathbf{D}_{ijrs} \cdot {}_0\mathbf{e}_{rs} \cdot \delta \, {}_0\boldsymbol{\eta}_{ij}}_{\text{neglected}} \approx {}_0\mathbf{D}_{ijrs} \cdot {}_0\mathbf{e}_{rs} \cdot \delta \, {}_0\mathbf{e}_{ij} \tag{14}$$

with the brace over the second term reading "nonlinear part by $\Delta\mathbf{u}_i$".

Finally, according to the TL formulation, the following basic equation of the principle of virtual displacements for body configuration $^n\Omega$ is obtained:

$$\int_{^0V} {}_0^{n-1}\mathbf{S}_{ij} \cdot \delta \, {}_0\mathbf{e}_{ij} \cdot d^0V + \int_{^0V} {}_0^{n-1}\mathbf{S}_{ij} \cdot \delta \, {}_0\boldsymbol{\eta}_{ij} \cdot d^0V + \int_{^0V} {}_0\mathbf{D}_{ijrs} \cdot {}_0\mathbf{e}_{ijrs} \cdot \delta \, {}_0\mathbf{e}_{ij} \cdot d^0V = {}^n\Re_{ext} \tag{15}$$

By solving Eq. 15, the values of all members of the displacement increment vector Δui for body configuration change from $^{n-1}\Omega$ to $^n\Omega$ are obtained. After that, the values of all members of the total displacement vector for a body after applying n^{th} load increment $^n\mathbf{u}_i$ are simply calculated. However, it is very important to note that Eq. 15 is actually a linearized equation since the tangential elastic tensor defined for the initial body configuration $_0\mathbf{D}_{ijrs}$ is used. This means that the correct or approximately correct solution of

Eq. 15 comes iteratively. At the end of each iteration, the level of error i.e. the level of "out-of-balance" virtual work must be checked as follows:

$$\text{Error=balance virtual work} = {}^n\mathfrak{R}_{ext} - \int_{{}^0V} {}^n_0\mathbf{S}_{ij} \cdot \delta\, {}^n_0\boldsymbol{\varepsilon}_{ij} \cdot d\,{}^0V \tag{16}$$

2.3. Updated Lagrangian formulation

In the case of the TL formulation, all static and kinematic variables are determined based on the initial body configuration ${}^0\Omega$. However, in the case of the Updated Langrangian formulation (hareinafter UL formulation), all static and kinematic variables for the current body configuration ${}^n\Omega$ are determined based on the previously defined body configuration ${}^{n-1}\Omega$. For the body configuration ${}^n\Omega$ shown in Fig. 1, according to the UL formulation, the following basic equation of the principle of virtual displacements for body configuration is obtained:

$$\underbrace{\int_{{}^{n-1}V} {}_{n-1}\boldsymbol{\sigma}_{ij} \cdot \delta_n\boldsymbol{\eta}_{ij} \cdot d^{n-1}V + \int_{{}^{n-1}V} {}_{n-1}\mathbf{D}_{ijrs} \cdot {}_{n-1}\mathbf{e}_{rs} \cdot \delta_n\mathbf{e}_{ij} \cdot d^{n-1}V + \int_{{}^{n-1}V} {}_{n-1}\boldsymbol{\sigma}_{ij} \cdot \delta_{n-1}\mathbf{e}_{ij} \cdot d^{n-1}V}_{{}^n\mathfrak{R}_{int}} =$$

$$= \underbrace{\int_{{}^{n-1}V} {}^n_{n-1}\mathbf{f}^B_i \cdot \delta^n\mathbf{u}^B_i \cdot d^{n-1}V + \int_{{}^{n-1}S} {}^n_{n-1}\mathbf{f}^S_i \cdot \delta^n\mathbf{u}^S_i \cdot d^{n-1}S}_{{}^n\mathfrak{R}_{ext}\text{ - known}} \tag{17}$$

where:

$$ {}^n_{n-1}\mathbf{S}_{ij} = {}^{n-1}_{n-1}\mathbf{S}_{ij} + {}_n\mathbf{S}_{ij} = \underbrace{{}_{n-1}\boldsymbol{\sigma}_{ij}}_{known} + \underbrace{{}_n\mathbf{S}_{ij}}_{unknown} \tag{18}$$

$$ {}^n_{n-1}\boldsymbol{\varepsilon}_{ij} = \underbrace{{}^{n-1}_{n-1}\boldsymbol{\varepsilon}_{ij}}_{=0} + {}_n\boldsymbol{\varepsilon}_{ij} = \underbrace{\frac{1}{2}\cdot\left(\overbrace{{}_{n-1}\mathbf{U}_{i,j}}^{known} + \overbrace{{}_{n-1}\mathbf{U}_{j,i}}^{unknown} \right)}_{{}_n\mathbf{e}_{ij}\text{ - linear part by increment }\Delta\mathbf{u}_i} + \underbrace{\frac{1}{2}\cdot\left(\overbrace{{}_{n-1}\mathbf{U}_{k,i}}^{known} \cdot \overbrace{{}_{n-1}\mathbf{U}_{k,j}}^{unknown} \right)}_{{}_n\boldsymbol{\eta}_{ij}\text{ - nonlinear part by increment }\Delta\mathbf{u}_i} \tag{19}$$

It is important to note that, in the case of the UL formulation, functions are integrated over a known volume ${}^{n-1}V$ and known surface area ${}^{n-1}S$ of the deformed body (body configuration ${}^{n-1}\Omega$). This actually means that, the static nonlinearity assumption of the problem is adopted in the calculation. This assumption together with the geometric nonlinearity assumption, which is implemented in Eq. 19, provides kinematic nonlinearity of the problem. Eq. 17 is also a linearized equation and it solved iteratively. At the end of each iteration, the level of error i.e. the level of "out-of-balance" virtual work must be checked.

In engineering practice, Eq. 15 and Eq. 17 are usually solved numerically. In that case, the members of the vector $\Delta\mathbf{u}_i$ represent the displacement increments of nodes of the adopted numerical grid. In the case of the UL formulation, at the beginning of each load increment, the numerical grid is regenerated (updated). This means that, at the beginning of each load increment, the coordinates of all nodes of the adopted numerical grid are corrected based on the values of the displacement increments which are calculated for the previous load increment

3. Characteristic Geotechnical Calculations

3.1. Example 1 – embankment settlement

In the first example, the settlements of the embankment (Fig. 2), which are calculated according to SD theory ("material nonlinearity only") and LD theory (material+kinematic nonlinearity) using the previously described UL formulation, will be compared between each other.

3.1.1. Input data
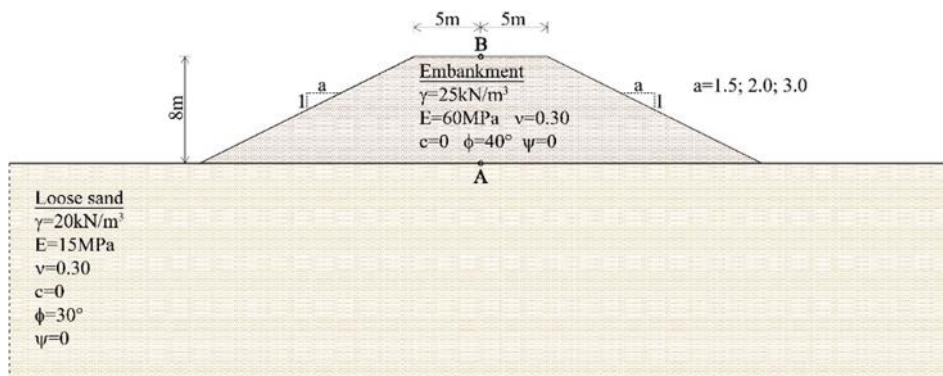
Fig. 2 Geometrical and material characteristics of the analysed embankment

3.1.2. Numerical model and calculation procedure

The formation of an appropriate numerical model in the software Flac 2D, in order to calculate the embankment settlements according to SD and LD theory, is divided into two phases. In the first phase, a numerical model is formed in order to perform a linear-elastic analysis of the foundation soil (loose sand) before the construction of the embankment. This analysis is performed to generate the initial stress state in the foundation soil. The second phase implies "adding" an embankment to the numerical model from the first phase, in order to perform the desired elasto-plastic analysis. MC material model with appropriate characteristics is used for the foundation soil and embankment in the second phase. All nodal displacements from the first phase must be canceled at the beginning of the second phase. For this cancellation, there is a corresponding option in the software Flac 2D.

3.1.3. Results and discussion

Table 1 Settlements of selected points of the embankment expressed in millimeters

Point	a=1.5			a=2.0			a=3.0		
	SD	LD	Δ (%)	SD	LD	Δ (%)	SD	LD	Δ (%)
A	222.8	225.6	1.25	229.1	231.4	1.00	233.4	236.6	1.37
B	176.3	170.3	3.52	154.1	148.3	3.91	120.8	117.6	2.72
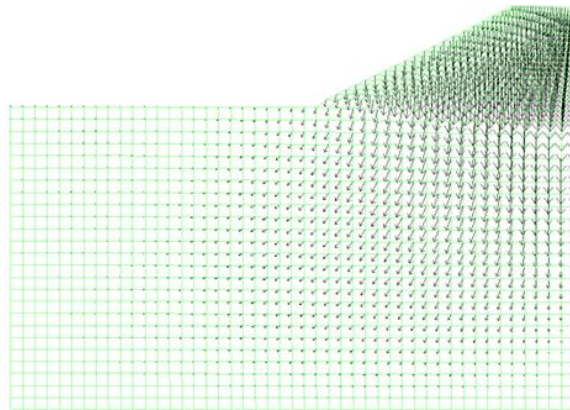
Fig. 3 Deformed shape of the analysed embankment

According to the presented results, it can be concluded that there are negligible differences between the settlement values of the selected embankment points, which were calculated according to the SD and LD theory in the software Flac 2D.

3.2. Example 2 – deformation of the tunnel opening without lining

In the second numerical example, the displacements of the points on the contour of a circular tunnel opening without lining (Fig. 4), which are calculated according to SD theory ("material nonlinearity only") and LD theory (material+kinematic nonlinearity) using the previously described UL formulation, will be compared between each other. In the calculation, the values of the Young's elastic modulus of rock mass are varied in the interval from 15 MPa to 500 MPa.

3.2.1. Input data
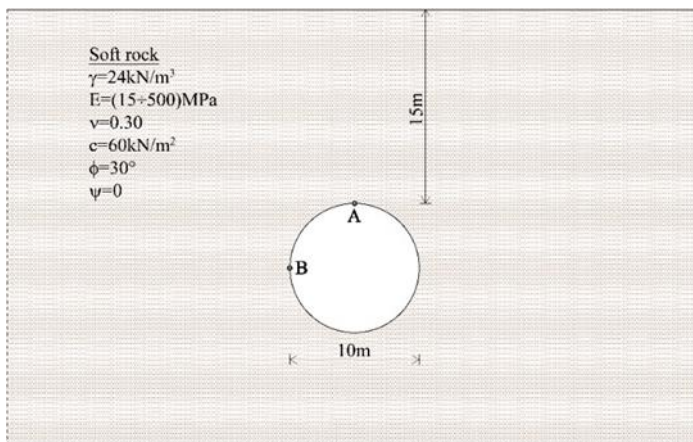
**Fig. 4** Geometrical and material characteristics of the analysed problem

3.2.2. Numerical model and calculation procedure

The formation of an appropriate numerical model in the software Flac 2D, in order to calculate the displacements of selected points on the contour of a circular tunnel opening without lining according to SD and LD theory, is divided into two phases. In the first phase, a numerical model is formed in order to perform a linear-elastic analysis of the rock mass as a homogeneous, infinite half-space (continuum) before tunnel excavation. This analysis is performed to generate the initial stress state in the rock mass. The second phase implies ''adding'' a circular tunnel opening to the numerical model from the first phase, in order to perform the desired elasto-plastic analysis. MC material model with appropriate characteristics is used for the rock masse. All nodal displacements from the first phase must be canceled at the beginning of the second phase.
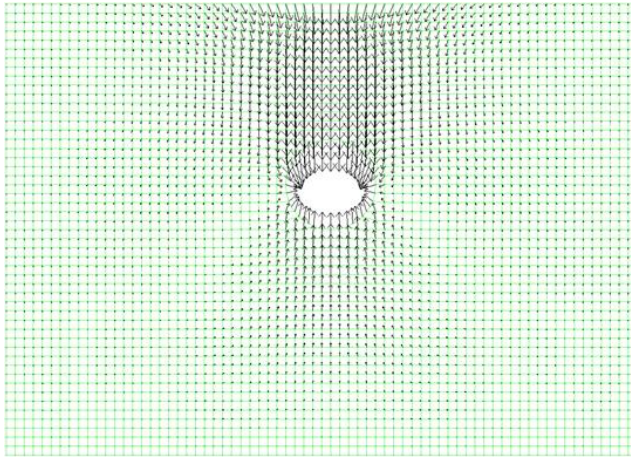
3.2.3. Results and discussion

Fig. 5 Displacements of the rock mass around tunnel opening

Table 2 Displacements of selected points on the contour of a circular tunnel opening without lining expressed in millimeters (the plus sign for ↓ and → displacements)

| E (MPa)	Point A – vertical displacement			Point B – horizontal displacement		
	SD	LD	Δ (%)	SD	LD	Δ (%)
15	695.1	565.2	22.98	257.8	191.2	34.80
25	416.7	378.3	10.10	154.3	130.7	18.05
50	210.6	201.3	4.61	77.5	71.1	9.06
100	105.6	106.9	1.32	38.7	37.4	3.47
200	51.9	52.1	0.38	19.3	18.9	2.11
500	21.2	21.0	0.95	7.7	7.7	0.00

According to the presented results, it can be concluded that in the case of very soft rocks the difference between displacements of the corresponding points on the contour of the tunnel opening without lining, which were calculated according to SD or LD theory, can be significant (maximum 35%). It is interesting that in these cases the displacements

calculated according to the SD theory are significantly larger than the displacements calculated according to the LD theory. Obviously, the previously mentioned regeneration of the numerical grid at the end of each load increment can be quite significant. However, with an increase in the value of the elastic modulus of the rock, the difference between displacements, which were calculated according to the SD and LD theory, become smaller (already for E=100 MPa become negligible).

3.3. Example 3 – soil-slope displacement due to the action of the seismic load

In the third numerical example, the horizontal displacements of the selected points on the contour of a natural and homogeneous soil-slope (Fig. 6) due to the action of the seismic load, which are calculated according to SD theory (''material nonlinearity only'') and LD theory (material+kinematic nonlinearity) using the previously described UL formulation, will be compared between each other. In the calculation, the values of the Young's elastic modulus of soil are varied in the interval from 15 MPa to 10 0MPa. The seismic load is adopted as a pseudo-static horizontal load. Its intensity is defined based on the adopted horizontal acceleration of the ground, which is $0.20 \cdot g$.

3.3.1. Input data
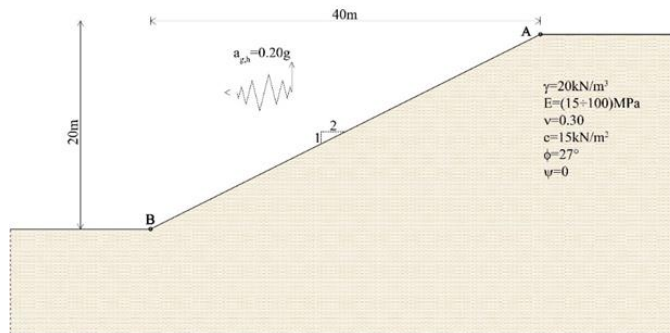
Fig. 6 Geometrical and material characteristics of the analysed soil-slope

3.3.2. Numerical model and calculation procedure

The displacement calculation of selected points on the contour of a natural soil-slope due to the action of the seismic load is divided into two phases. In the first phase, an appropriate numerical model is formed in order to perform a linear-elastic analysis of the natural soil-slope. This analysis is performed to generate the initial stress state in the soil. In the second phase, for the same numerical model, elasto-plastic analysis is performed. In the second phase MC material model with appropriate characteristics is used for the soil. All nodal displacements from the first phase must be canceled at the beginning of the second phase of the calculation. Inertial seismic forces are easy generated in softver Flac 2D by defining a horizontal ground acceleration.

3.3.3. Results and discussion
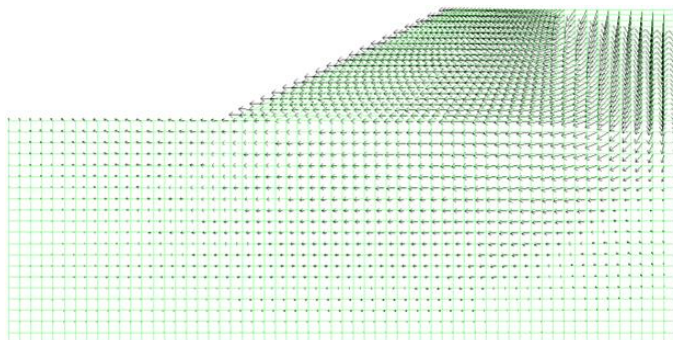
Fig. 7 Deformed shape of the analysed soil-slope due to the action of the seismic load

Table 3 Displacements of selected points on contour of the analysed soil-slope due to the action of the seismic load expressed in millimeters (the plus sign for → displacement)

E (MPa)	Point A			Point B		
	SD	LD	Δ (%)	SD	LD	Δ (%)
15	-678.8	-635.6	6.80	-434.9	-425.9	2.11
25	-403.3	-388.5	3.81	-260.6	-257.5	1.20
50	-201.6	-197.8	1.92	-130.1	-129.8	0.23
100	-100.7	-100.3	0.39	-65.2	-65.1	0.15

According to the presented results, it can be concluded that there are negligible differences between displacements of the corresponding points on the contour of a natural soil-slope due to the action of the seismic load, which were calculated according to the SD and LD theory in the software Flac 2D for different values of the soil elastic modulus.

4. CONCLUSION

By using LD theory (material+kinematic nonlinearity) in geotechnical engineering calculations, more realistic displacement (deformation) values of geotechnical constructions due to load are obtained. The differences between the amplitudes of these displacements and the corresponding displacements calculated for the same geotechnical problems according to the SD theory ("material nonlinearity only") are mostly negligible. For this reason, SD theory is recommended to engineers for practical application. However, engineers must be careful of some specific situations such as e.g. larger diameter tunneling excavation in the softer materials. The differences between the results obtained in calculations according to SD and LD theory can be significant. In these specific situations, the use of calculations according to LD theory, which simulates the real behavior of the geotechnical structure much more accurately, is recommended.

REFERENCES

1. Bathe Klaus-Jürgen: Finite Element Procedures in Engineering Analysis. Prentice-Hall, Pearson Education, Inc., Englewood Cliffs, New Jersey, 1982.
2. Jeremić Boris, Yang Zhaohui, Zhao Cheng, Guanzhou Jie, Tafazzoli Nima, Preisig Matthias, Tasiopoulou Panagiota, Pisanò Federico, Abell José, Watanabe Kohei, Yuan Feng, Sinha Sumeet Kumar, Behbehani Fatemah, Han Yang, Wang Hexiang: Nonlinear Finite Elements: Modeling and Simulation of Earthquakes, Soils, Structures and their Interaction. University of California, Davis, California, 1989-2022.
3. Itasca Consulting Group: FLAC (Fast Largrangian Analysis of Continua) User's Manuals. Minneapolis, MN, 2000.
4. Renton D. John: Large deformation theory Applied Elasticity - Matrix and Tensor Analysis of Elastic Continua (Second Edition). Woodhead Publishing Series in Civil and Structural Engineering, 129-158, 2002.
5. Bertram Albrecht: Elasticity and Plasticity of Large Deformations – An Introduction (Third Edition). Springer Berlin, Heidelberg, 2012.

TEORIJA VELIKE DEFORMACIJE U GEOMEHANICI - UTICAJ KINEMATIČKE NELINEARNOSTI NA REZULTATE NEKIH KARAKTERISTIČNIH GEOTEHNIČKIH PRORAČUNA

Geotehnički inženjerski proračuni se obično izvode prema teoriji malih deformacija i pomeranja (teorija infinitezimalnih deformacija), odnosno teoriji prvog reda. Usvojen je linearni odnos između pomeranja komponenti i deformacija. Dobro poznati uslovi za ravnotežu definisani su za nedeformisan sistem, odnosno nedeformisanu strukturu. Stoga su pretpostavke geometrijske i statičke linearnosti obično validne u geotehničkim proračunima. Ove linearnosti se zajednički nazivaju kinematička linearnost. Drugim rečima, inženjeri smatraju da se rezultati sasvim zadovoljavajuće tačnosti dobijaju ako se u inženjerskim proračunima uzme u obzir samo nelinearnost materijala, bez obzira na vrstu geotehničkog problema koji se analizira. Stoga nije potrebno primenjivati teoriju velikih (konačnih) deformacija uz pretpostavku nelinearnosti materijala. Osnovni cilj ovog rada je da se potvrdi prethodna tvrdnja u slučaju nekih karakterističnih problema geotehnike. U prvom delu ovog rada ukratko je predstavljena teorija velikih deformacija, koja je uglavnom nepoznata široj stručnoj javnosti. Nakon toga, izvršene su jednostavne numeričke analize nekih karakterističnih problema geotehnike u poznatom softveru FLAC 2D sa ciljem poređenja rezultata dobijenih za slučajeve kinematičke linearnosti i kinematičke nelinearnosti. Dobijeni rezultati ukazuju na činjenicu da u uobičajenim geotehničkim inženjerskim proračunima ne treba uvek zanemariti kinematičku nelinearnost. Zbog toga se inženjeri pozivaju da budu oprezni.

Ključne reči: *geothenika, teorija velikih deformacija, kinematička nelinearnost.*

Original Scientific Paper

SERVICE LIFE PREDICTION OF TIMBER-CONCRETE COMPOSITE FLOORS

UDC 624.016:519.21
69.059.4

Radovan Cvetković[1], Nikola Velimirović[2], Petar Knežević[2], Aleksandar Radaković[2], Milivoje Milanović[2], Nemanja Marković[1]

[1]University of Niš, Faculty of Civil Engineering and Architecture, Niš, Serbia
[2]State University of Novi Pazar, Novi Pazar, Serbia

ORCID iDs: Radovan Cvetković   https://orcid.org/0000-0002-8462-7235
         Nikola Velimirović   https://orcid.org/0000-0002-6298-8216
         Petar Knežević   https://orcid.org/0000-0003-4187-2879
         Aleksandar Radaković   https://orcid.org/0000-0002-7355-7403
         Milivoje Milanović   https://orcid.org/0000-0003-3850-6480
         Nemanja Marković   https://orcid.org/0000-0001-7289-9850

Abstract. *Timber-concrete composite (TCC) systems have application for new floors and for upgrading and enhancing of existing timber floors in residential and office buildings. In order to develop the optimal maintenance programs of structures, it is essential to predict the performance of structures over their life-cycle. The long-term behavior of timber-concrete composite floors is influenced by a combination of various factors, including material properties, load distribution, moisture effects, temperature effects and durability considerations. Timber and concrete material in the composite system, exhibit different behaviors over time due to their inherent characteristics. Deterioration prediction models are used to estimate the future degradation and condition of various types of structures. The aim of this paper is to present two probabilistic models, random variable deterioration rate model and stochastic gamma process model, that will capture uncertainty and variability associated with the deterioration of TCC floor under the service load and to estimate its service life.*

Key words: *timber-concrete composite, service life, deterioration prediction, stochastic process model*

1. INTRODUCTION

Timber-concrete composite (TCC) floors combine the benefits of both timber and concrete to create a durable and efficient flooring system. These floors typically consist of parallel timber beams that are connected with a reinforced concrete slab using different kinds of connectors. The concrete slab is placed on top of the timber elements to provide additional strength and stiffness. Timber provides a natural aesthetic appeal and also acts

as a thermal insulator, which can contribute to energy efficiency. The concrete slab in timber-concrete composite floors provides structural rigidity, fire resistance and enhanced load-carrying capacity. Timber-concrete composite floors offer good durability and can have a long service life when designed and maintained properly. Such floors are suitable for various applications, including residential, commercial and industrial buildings [1]. They are commonly used in floor systems where a balance between structural performance, thermal insulation and aesthetic appeal is desired.

Predicting the service life of timber-concrete composite floors involves assessing several factors that can affect their durability and performance over time. The choice of timber and concrete materials plays a significant role in determining the lifespan of the floor. Timber is susceptible to moisture damage, which can lead to rot, decay, and reduced structural integrity. Adequate moisture protection measures, such as moisture barriers, waterproof membranes and proper ventilation, should be implemented to prevent water infiltration and maintain the integrity of the timber. On the other hand, the concrete slab can benefit from protective finishes to enhance durability. Periodic inspections and regular maintenance are crucial for identifying and addressing potential issues before they become major problems. Environmental factors such as temperature, humidity and exposure to sunlight can impact the durability of TCC floors. Monitoring and controlling these conditions within acceptable ranges can help extend the service life of the floor. It is important to note that the service life of TCC floors can vary widely depending on the specific circumstances, including usage, maintenance and environmental conditions. While some TCC floors can last for several decades with proper care, others may require more frequent repairs or replacements.

2. DETERIORATION MODELING

Deterioration prediction models are used to estimate the future degradation and condition of various types of infrastructure such as buildings, bridges, roads, pipelines and more. These models can help in assessing maintenance and repair needs, optimizing resource allocation and making informed decisions about infrastructure management. We can distinguish deterministic and probabilistic deterioration prediction models. It is important to highlight that deterministic deterioration models rely on the assumption that all inputs and deterioration processes are known with certainty [2]. However, in practice, there is often uncertainty associated with deterioration mechanisms and environmental conditions. In such cases, probabilistic or stochastic models may be more appropriate to capture the variability and provide a more comprehensive prediction of structural deterioration [3].

2.1. Random Variable Deterioration Rate Model

A random variable (RV) deterioration rate model for structures is a probabilistic model that considers the variability and uncertainty associated with the deterioration process [4]. Instead of assuming a deterministic deterioration rate, this model incorporates random variables to represent the rate of deterioration, allowing for a more realistic representation of structural deterioration over time:

$$X(t) = \mathrm{f}(R,t) = R \cdot t^{b} \tag{1}$$

This model does not consider temporal uncertainties, but only a sample uncertainty of the deterioration process. It assumes that the deterioration of each sample follows a predictable pattern based on a known form and a constant deterioration rate over time. In our analysis, we have made the assumption that considered deterioration rate has gamma distribution. Therefore, probability density function of deterioration of X(t) could be presented by:

$$f_{X(t)}(x) = Ga(x|\eta, \delta t^b) = \frac{x^{\eta-1}}{\Gamma(\eta) \cdot (\delta t^b)^\eta} \cdot e^{-\frac{x}{\delta t^b}} \quad (2)$$

Mean, variance and coefficient of variance of $X(t)$ are given respectively:

$$E\left[X(t)\right] = \eta \cdot \delta \cdot t^b,$$
$$Var\left[X(t)\right] = \eta \cdot \delta^2 \cdot t^{2b},$$
$$Cov\left[X(t)\right] = \frac{\sqrt{Var\left[X(t)\right]}}{E\left[X(t)\right]} = \frac{1}{\sqrt{\eta}} = const. \quad (3)$$

However, in reality, the most of deterioration processes exhibit temporal uncertainties. Deterioration rates may vary over time due to various factors such as environmental conditions, maintenance activities and other external influences. To account for temporal uncertainties, a more comprehensive model would need to consider stochastic deterioration processes that incorporate variability and uncertainty over time.

2.2. Stochastic Gamma Process Deterioration Model

The stochastic gamma process (GP) is a mathematical model that can be used to describe the deterioration process of structures over time [5]. This stochastic process has independent non-negative increments that are gamma distributed with an identical scale parameter. We observe the gamma process with shape function $k(t)>0$ and scale parameter $\theta>0$, as continuous-time stochastic process $\{X(t); t \geq 0\}$ with the following properties:
- $X(0) = 0$ with probability one
- $\Delta X(t) = X(t + \Delta t) - X(t) \sim Ga(\Delta k(t), \theta)$; $\qquad \Delta k(t) = k(t + \Delta t) - k(t)$
- $\Delta X(t)$ are independent

where $k(t)$ is supposed to be a non-decreasing, right-continuous, real-valued function for $t \geq 0$, with $k(0) \equiv 0$. Probability density function of $X(t)$, according to the definition of the gamma process deterioration model could be given as:

$$f_{X(t)}(x) = Ga(x|ct^b, \theta) = \frac{x^{ct^b-1}}{\Gamma(ct^b) \cdot \theta^{ct^b}} e^{-\frac{x}{\theta}} \quad (4)$$

with mean, variance and coefficient of variation:

$$E[X(t)] = ct^b \cdot \theta, \quad Var[X(t)] = ct^b \cdot \theta^2, \quad CoV[X(t)] = \frac{1}{\sqrt{ct^b}} \quad (5)$$

3. TIME-DEPENDENT TCC FLOOR DETERIORATION

The long-term behavior of timber-concrete composite floor is influenced by a combination of material properties, load distribution, moisture effects, temperature effects and durability considerations. Timber and concrete have different material properties and behavior over time. The differential shrinkage/swelling of the concrete slab and timber beam cannot freely occur due to the connection system which restrains the possibility of either part to move relative to the other [6]. When designing medium and long-span composite floors, one of the most critical criterion to consider is the limit state of maximum deflection. Consequently, it becomes necessary to analyze and model the mid-span deflection in TCC floors over time under service load. The aim of this paper is to demonstrate how two different probabilistic deterioration prediction models can be effectively applied to estimate the service life of the TCC floor using available inspection data. Gather data on the condition of TCC floors over a specified time period may include information on observed deterioration patterns, inspection records, maintenance activities, and environmental conditions.

We have observed the TCC floor with a span of 4.5 m in indoor conditions. The concrete slab of the TCC floor with a thickness of 60 mm is constructed using concrete of the strength class C25/30. The timber beams with dimensions 100 x 200 mm are made of sawn softwood timber with a structural strength class C27. The beams are located at a distance of 800 mm. The shear connectors are glued-in steel rods $\phi 20/150$ mm. These connectors are embedded in pre-drilled holes that are positioned perpendicular to the grain of the timber and coated with epoxy resin, at constant intervals of 240 mm. The steel rods used as connectors are manufactured from steel grade S235. The relative mid-span deflection of the floor over time under normal use conditions could be defined as follows:

$$X(t) = \frac{u(t) - u_{el}}{u_{el}} \tag{6}$$

where u(t) is mid-span deflection at time t and u_{el} is the elastic deflection measured immediately after applying the service load that is assumed to be an initial deflection, deflection at time t0. Based on the definition of relative mid-span deflection, it becomes possible to establish a maximum permissible value for this parameter:

$$\rho = \frac{u_L - u_{el}}{u_{el}} \tag{7}$$

This maximum permissible value serves as a threshold beyond which the deflection of the floor under normal use conditions should not exceed. According to Eurocode 5 [7], the serviceability limit value for long-term deflection uL could be defined as l/200, where l is the span length. When the maximum mid-span deflection exceeds the proposed serviceability limit value, the observed TCC floor will reach serviceability limit state as shown in Figure 1.
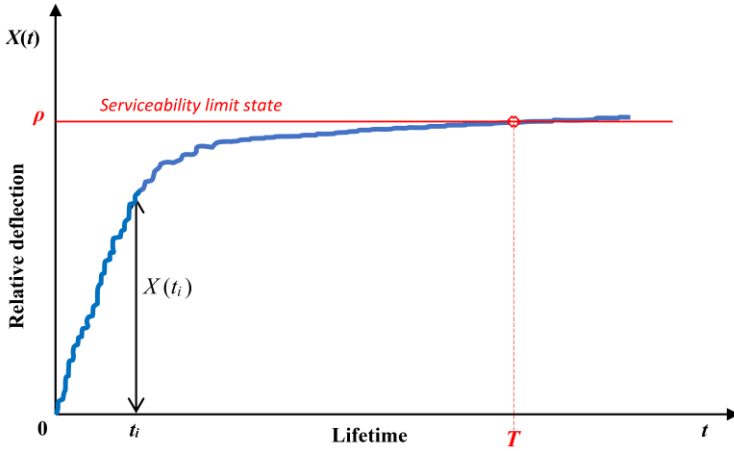
Fig. 1 Trend of the expected relative mid-span deflection increasing over time under service load

A probabilistic deterioration model for a timber-concrete composite floor would involve estimating the probability of failure of different components of the floor system over time. It is important to note that developing a comprehensive probabilistic deterioration model for a timber-concrete composite floor is a complex task that requires expertise in structural engineering, materials science and probabilistic analysis. In order to conduct a comprehensive time-dependent reliability analysis of TCC floors under normal use conditions, it is necessary to establish the limit state function. In this paper, the focus is on the serviceability limit state, specifically the maximum deflection of the TCC floor that could be expressed as:

$$g(\rho, X, t) = \rho - X(t) \tag{8}$$

According to this definition, probability of failure for considered TCC floor is given as follows:

$$P_f(t) = P[g(\rho, X, t) \le 0] = P[X(t) \ge \rho] \tag{9}$$

Since there is a lack of deterioration measurement data under normal use conditions and conducting time-consuming experiments under normal operating conditions can be costly, an alternative approach was adopted. To obtain the necessary data for the study, an accelerated aging test was performed. To obtain accelerated deterioration data, we have employed an existing deterministic model. This model is based on conducted experimental tests, presented by Fragiacomo [8]. Variation in environmental conditions will cause dispersion of mid-span deflection within the population over time. To account for the uncertainties associated with the deterioration process in a large population of structural elements, we have employed the Monte Carlo simulation technique. This approach serves to simulate the condition of the set of identical specimens exposed to indoor conditions. The observed specimens are monitored through periodic inspections at year 10 and year 20. In that way inspections reveal the progress of the deterioration of each inspected specimen, as it presented in Figure 2.
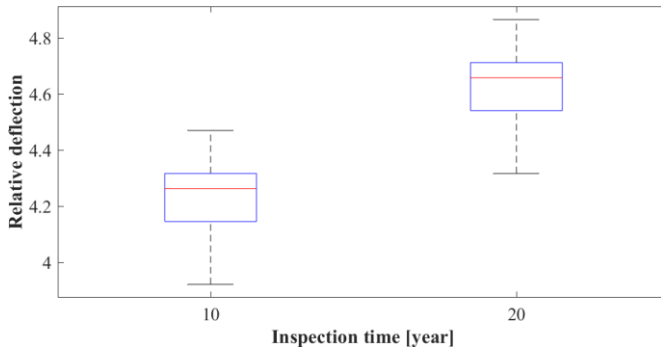
Fig. 2 Box plot of inspection data

In order to establish the relationship between the average deterioration level and time, we have utilized available inspection data and fitted it with a power function:

$$E[X(t)] = a \cdot t^b \propto t^b \tag{10}$$

where E[X(t)] presents the expected deterioration of relative mid-span deflection under indoor conditions at time t. This is performed based on the regression analysis using a least-squares fitting method, suggested by Nicolai et al. [9]. The regression analysis of the available data shows a strong fit with a power function, with a high coefficient of determination ($R^2 = 0.9175$). Based on this analysis, the relevant value of parameter b was obtained as 0.1104. By determining the parameter estimate of the power b from the regression analysis, we are able to estimate the other two parameters of the proposed random variable deterioration rate model and gamma process deterioration model. Estimation of parameters was conducted using the method of maximum likelihood and presented in table 1.

Table 1 Estimated parameters of considered probabilistic models at year 20

RV deterioration rate model		Gamma process model	
Shape (η)	Scale (δ)	Shape (c)	Scale (θ)
834.069	0.0039	699.912	0.0047

4. SERVICE LIFE PREDICTION

Maintenance management is a critical aspect of ensuring the long-term performance and safety of structures and it primarily addresses the uncertainties associated with the service life of the structures. By estimating the time when a structure is expected to reach its serviceability limit state, we can make informed decisions regarding maintenance strategies as well as risk management. Considering that the RV deterioration rate model depends on only one random variable whose mean and standard deviation are constant over time, the coefficient of variation of this probabilistic deterioration model is constant over time as well. However, coefficient of variation of GP deterioration model is variable over time and presents the function of time with the negative exponent, $t^{-(b/2)}$. According to

this fact, coefficient of variation of GP deterioration model has higher value within the first couple of years. Its value however is rapidly decreasing and quickly becomes lower than the coefficient of variation of the RV deterioration rate model, which is an indicator of quality and stability for long term predictions (Fig. 3).
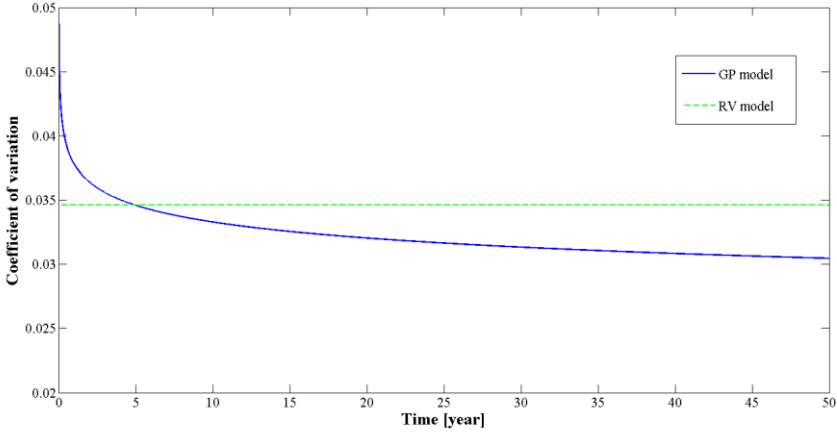
Fig. 3 Coefficient of variation of expected deterioration X(t)

Service life analysis plays a crucial role in this process by assessing the expected deterioration and determining the maximum time when the deterioration will pass the service life threshold. The service life of a structure, denoted as T, can be determined by identifying the first time when the sample path of deterioration $X(t)$ exceeds the proposed serviceability limit value of relative mid-span deflection, represented by ρ.

$$F_T(t) = P[T \leq t \,|\, X(t) \geq \rho] \tag{11}$$

When the deterioration is modelled using a random variable deterioration rate model, the cumulative distribution function of the service life can be presented as follows:

$$F_T(t) = 1 - GA(\rho; \eta, \delta t^b) = 1 - \frac{\Gamma\left(\eta, \dfrac{\rho}{\delta t^b}\right)}{\Gamma(\eta)} \tag{12}$$

where:
$$\Gamma(a, x) = \int_{t=x}^{\infty} t^{a-1} e^{-t} \, dt \tag{13}$$

is the incomplete gamma function for $x \geq 0$ and $a > 0$.

Considering the expected deterioration is represented by a gamma process deterioration model, the cumulative distribution function of the service life can be expressed as follows:

$$F_T(t) = 1 - GA(\rho; ct^b, \theta) = 1 - \frac{\Gamma\left(ct^b, \dfrac{\rho}{\theta}\right)}{\Gamma(ct^b)} \tag{14}$$

Based on Fig. 4, we can conclude that gamma process model gives a more stable prediction of expected service life than the RV deterioration rate model.
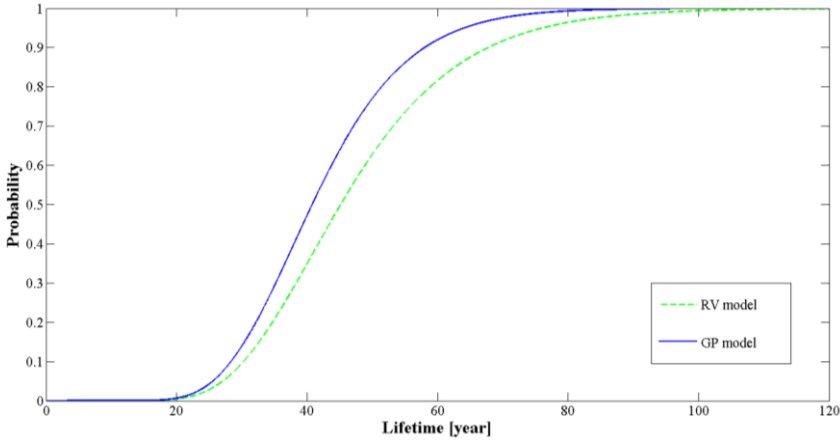
Fig. 4 Comparison of cumulative distribution function of service life, obtained from GP deterioration model and RV deterioration rate model

To effectively plan maintenance for a structure, it is crucial to determine the time at which the structure is likely to reach the serviceability limit state with specific probabilities, such as 5%, 50%, and 95%. This can be achieved by employing two presented approaches, as it shown in Figures 5 and 6.
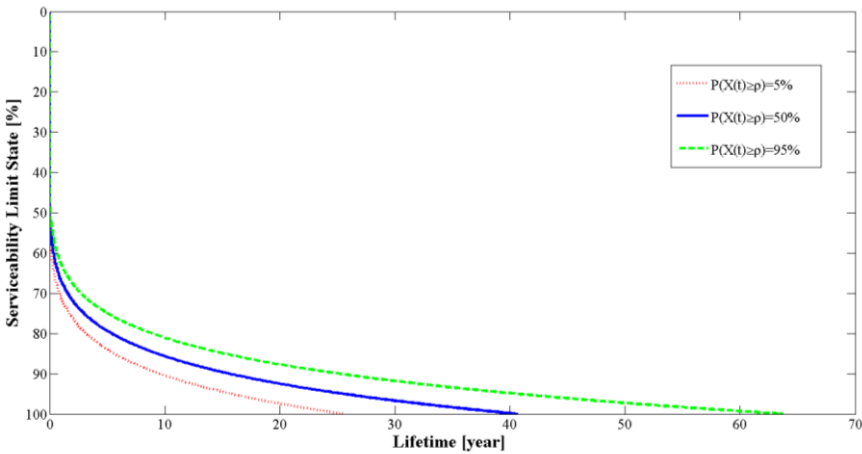
Fig. 5 Probability of achieving different levels of serviceability limit state condition during the lifetime applying GP model
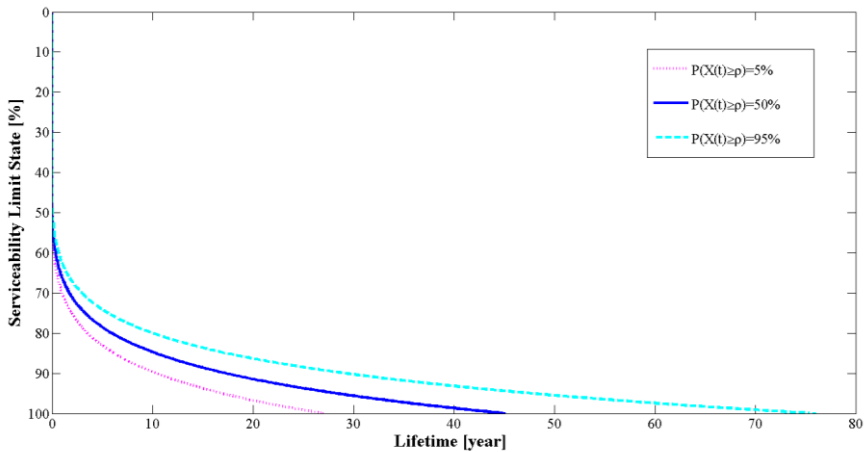
Fig. 6 Probability of achieving different levels of serviceability limit state condition during the lifetime applying RV model

5. CONCLUSION

Deterministic deterioration models are commonly employed in the maintenance management of structures. However, they have certain limitations when applied to real conditions, because the inputs and degradation mechanisms involved in structural deterioration are often uncertain and subject to variability. This work has presented the application of two probabilistic deterioration models, random variable (RV) deterioration rate model and stochastic gamma process deterioration model, to describe time-dependent timber-concrete composite floor deterioration. RV deterioration rate model does not consider temporal uncertainties, only sample uncertainty of the deterioration process. To account for temporal uncertainties, a more comprehensive model would need to consider stochastic deterioration processes that incorporate variability and uncertainty over time. The gamma process deterioration model considers deterioration increase as the sum of the series of non-negative random increments. In this model, deterioration rate in each time interval is not constant, rather it is random due to the uncertain influence of the environment over the life-cycle. Neglecting these temporal uncertainties can limit the model's ability to accurately predict the future state of the samples or make reliable projections. By considering temporal uncertainties, the stochastic gamma process model would provide a more realistic representation of the deterioration process, enabling better predictions and assessments of the samples future conditions.

REFERENCES

1. A. Dias, J. Skinner, K. Crews, T. Tannert, "Timber-concrete-composites increasing the use of timber in construction", European Journal of Wood and Wood Products, 74: 443-451, 2016.
2. F. A. Buijs, J. W. Hall, P. B. Sayers, P. H. Van Gelder, "Time-dependent reliability analysis of flood defences", Reliability Engineering & System Safety, 94(12): 1942-1953, 2009.

3. D. M. Frangopol, M. Soliman, "Life-cycle of structural systems: recent achievements and future directions", Structure and Infrastructure Engineering, 12 (1), 1-20, 2016.
4. M. D. Pandey, X. X. Yuan, J. M. Van Noortwijk, "The Influence of Temporal Uncertainty of Deterioration on Life-Cycle Management of Structures", Structure and Infrastructure Engineering, 5(2), 145–156, 2009.
5. J. M. Van Noortwijk, "A survey of the application of gamma processes in maintenance", Journal of Reliability Engineering and System Safety, 94:2-21, 2009.
6. M. Stepinac, V. Rajčić, J. Brabalić, "Influence of long term load on timber- concrete composite systems", Građevinar, 67 (3), 235-246, 2015.
7. CEN, "Eurocode 5 - design of timber structures - part 1-1: General rules and rules for building sprEN 1995-1-1", European Committee for Standardization, Brussels, Belgium. 2003.
8. M. Fragiacomo, "Long-term behaviour of timber-concrete composite beams. II: Numerical analysis and simplified evaluation", Journal of Structural Engineering, 132(1), 23-33, 2006.
9. R. P. Nicolai, R. Dekker, J. M. van Noortwijk, "A comparison of models for measurable deterioration: An application to coatings on steel structures", Reliability Engineering and System Safety, 92, 1635-1650, 2007.

PREDVIĐANJE EKSPLOATACIONOG VEKA SPREGNUTIH MEĐUSPRATNIH KONSTRUKCIJA TIPA DRVO-BETON

Spregnuti sistemi tipa drvo-beton imaju primenu kod izgradnje novih međuspratnih konstrukcija kao i kod unapređenja i ojačanja postojećih drvenih međuspratnih konstrukcija u stambenim i poslovnim zgradama. U cilju razvijanja optimalnih planova održavanja konstrukcija, neophodno je predvideti karakteristike konstrukcija tokom njihovog eksploatacionog veka. Na dugotrajno ponašanje spregnutih međuspratnih konstrukcija tipa drvo-beton utiče kombinacija različitih faktora, uključujući svojstva materijala, raspodelu opterećenja, uticaj vlage, uticaj temperature i trajnosti. Drvo i beton kao materijali u okviru spregnutog sistema, pokazuju različito ponašanje tokom vremena. Modeli predviđanja deterioracije se koriste za procenu buduće degradacije i stanja različitih tipova konstrukcija. Cilj ovog rada je da predstavi dva probabilistička modela, model slučajne stope deterioracije i model stohastičkog gama procesa, koji će obuhvatiti varijabilnosti povezane sa deterioracijom spregnutih međuspratnih konstrukcija tipa drvo-beton pod korisnim opterećenjem i proceniti njegov eksploatacionki vek.

Ključne reči: spregnuti sistem tipa drvo-beton, eksploatacioni vek, predviđanje deterioracije, model stohastičkog procesa

Original Scientific Paper

SUBBASE STABILIZATION WITH FLY ASH

UDC 625.731.6:666.952

Zlatko Zafirovski, Mite Markovski, Slobodan Ognjenovic, Vasko Gacevski, Ivona Nedevska, Riste Ristov

Ss. Cyril and Methodius University, Faculty of Civil Engineering, Skopje, North Macedonia

ORCID iDs: Zlatko Zafirovski   https://orcid.org/0000-0003-2099-0710
         Mite Markovski   N/A
         Slobodan Ognjenovic   https://orcid.org/0000-0002-4242-9169
         Vasko Gacevski   https://orcid.org/0000-0002-4731-2031
         Ivona Nedevska   https://orcid.org/0000-0002-0407-4846
         Riste Ristov   https://orcid.org/0000-0002-4996-0382

Abstract. *Due to increased activities in civil engineering, and especially in the transport infrastructure, and thus an increase in the use of additional construction materials, innovative solutions are needed in finding alternative materials for the preservation of natural resources. One of the solutions for preserving natural building materials is the application of recycled material, which will also meet the required standards in civil engineering. In the transport infrastructure, there is a great opportunity for the use of recycled material, starting from the subbase, through the embankment and all the way to the superstructure and the concrete structures. One of the recycled materials that can be used in construction is fly ash.*

Fly ash is the most promising waste material when it comes to the wide range of applications in construction. Fly ash is obtained by burning coal in thermal power plants to produce electricity.

Due to variations in the composition and characteristics of fly ash, several divisions and classifications have been created. One of the main classifications is according to the American standard ASTM C 618-05 where it is divided into class C and class F fly ash.

This research aims to investigate the application of fly ash for subgrade stabilization and to determine the difference from a financial and environmental perspective for the application of fly ash compared to natural stone aggregate.

The main research was carried out in connection with the increased use of natural stone aggregate, which appeared as a need during the rehabilitation of state road R1206, section Karpalak - Želino. Apart from the use of large quantities of stone aggregate for the stabilization of the subgrade, it also had an impact on the financial framework for the realization of the road project.

In Macedonia, an analysis of the chemical composition of 4 samples of fly ash obtained in REC Bitola was carried out. From the obtained results, it can be concluded that it belongs to the classification of F-class fly ash and with the use of an activator (lime or cement) it can be used in the stabilization of the subgrade.

Key words: *civil engineering, subbase, subgrade, fly ash, stabilization.*

1. INTRODUCTION

In order to meet the needs of the world's population, which has been in constant growth since the 20th century, the activities in construction, especially in the transport infrastructure, are increasing. Also, existing facilities require their own maintenance and innovation. All this contributes to the increased use of construction material, and especially the depletion of large amounts of natural resources. For this purpose, it is necessary to reduce the use of natural resources and to introduce the replacement of natural materials with alternative materials, that is, solutions.

One of the solutions for preserving natural material is the application of recycled material in construction. The idea of using recycled material is with the condition that the quality of the buildings is not impaired. Due to the large amount of recycled material, there is a need for its disposal and disposal, which represents a serious environmental problem.

In the transport infrastructure, there is a great opportunity for the use of recycled material, starting from the lower structure, through the embankment, and all the way to the upper structure and the concrete structures. According to data from the European Road Infrastructure Association (2018), there are over 5 million kilometers of road network in Europe. From an economic and ecological point of view, the use of recycled material in road infrastructure should be seen as a resource, not a waste material.

Fly ash is a material that is found in large coal mines, both in Europe and in Macedonia, and it can be used as an alternative solution for replacing natural resources. Fly ash is mostly used in concrete constructions, but it is also used in subgrade stabilization, as well as a filler substitute in roadway constructions. However, the application of fly ash in road infrastructure is still low, less than 2% (ASAA 2007). In the annual report of the European Aggregate Association (2017/2018) there is information that the use of fly ash and slag is less than 2.3%.

In the last decades, the tests for the application of fly ash in the road infrastructure show positive results, such as: application of fly ash in embankments, part of the mixture for cement and concrete, stabilization of the subgrade and replacement of filler in asphalt mixtures.

In industrial practice, the term "fly ash" refers to a solid non-combustible residue that is separated during the combustion of coal.

According to the place of separation, several types of fly ash are distinguished. In thermal power plants that use a classic pulverized coal combustion system, the following are distinguished:

- slag (bottom ash), the largest non-combustible residue from combustion that separates at the bottom of the boiler;
- boiler fly ash, a large class that separates from the boiler and, together with the flue gases on the way to the electrofilters, gravitationally settles under the flue gas channel and the air heater;
- electrofilter or fly ash, the smallest class that is separated from the boiler with flue gases, and the separation from the flow of flue gases is carried out by electrostatic separation in electrofilters. The term fly ash was first used in the power generation industry in 1930, and the first use of fly ash was recorded in 1937;
- in thermal power plants where the combustion is carried out in a fluidization layer, the so-called layered ash (bed ash) which is actually a mixture of the previously mentioned types;

From the point of view of disposal, the separation of slag and fly ash is important. The fly ash is actually a combination of boiler and electrofilter ash. The slag stands out

due to its specific characteristics coarseness and settling speed which are important and influence the choice of transport system.

The chemical properties of fly ash depend to a large extent on the properties of the coal and the techniques used for handling and storage. Fly ash consists of fine, powdery particles that are mostly spherical in shape, solid or hollow, and mostly glassy (amorphous). The carbonaceous material in the fly ash is composed of angular particles. The specific gravity of fly ash usually ranges from 2.1 to 3.0, while its specific surface area (measured by the air permeability method) can range from 170 to 1000 m2 / kg.

The color of the fly ash can vary from dark gray to black, depending on the amount of carbon in the ash. The lighter the color, the lower the carbon content. Ash from lignite or subbituminous coal is usually lighter in color than bituminous coal and anthracite. Bituminous coal ash is lighter shades of gray which usually indicates higher fly ash quality.

2. METHODOLOGY

The aim of this research is to improve, stabilize the subbase in the transport infrastructure using fly ash.

Professional and scientific justification of this scientific work results from the rehabilitation of the regional road R1206, section Karpalak - Želino, in the length of 12 km. The beginning of the route is at 800 m. after the exit for the village of Bojane, and ends at the exit from the village of Zelino in front of the restaurant "Dva Fazana". The object in question is an object of the 1st category.

During the construction activities on this section, due to the poor maintenance and drainage of the road section during the period of operation, there was a need to improve the existing subbase (subgrade) which did not meet the criteria for this type of building.

In the basic project for the construction of the lower structure, the following positions were foreseen:
- Mechanical excavation of an existing crushed stone in a wide trench with transport to a landfill,
- Planning and compaction the subgrade.

When starting with the construction of the subgrade of the section in question, that is, after the excavation of the existing crushed stone layer, the planning and compaction of the existing subgrade was approached. Before starting with the installation of the crushed stone layer, laboratory tests were first performed on the existing subgrade. The laboratory tests were performed by an accredited laboratory according to the technical conditions for this type of facility and the valid standards in the Republic of North Macedonia.

The following characteristics of the existing subgrade were tested by the authorized laboratory:
- Granulopetric composition of the soil (subgrade),
- Natural humidity,
- Atterberg limits,
- Proctor compactness (standard),
- California CBR Load Index,
- Content of calcium carbonate SaCO3 in soil,
- Organic and combustible substances.

Table 1 Standards according to which the existing subgrade was carried out

Experience	Standard
Determination of granulometric composition	MKS EN ISO 17892-4:2017
Determination of Atterberg limits (Casagrande's method)	MKS 1013:2016
Proctor Density	MKS EN 13286-2:2012
Determination of the California CBR Load Index	MKS EN 13286-47:2013

3. RESULTS

For the purposes of the project, 3 samples were taken, where they were examined in an authorized laboratory.

During the determination of Atterberg's limits (Casagrande's method), results were obtained for:
- Yield strength W_I (%),
- Limit of plasticity W_P (%),
- Plasticity index I_P (%),
- Consistency index I_C (%).

The data from the obtained results are shown in table 2 form in the following order:

Table 2 Overview of the results of geotechnical measurements of the existing subgrade, karpalak-želino section

Layer:	Subgrade			
Depth: 0,20-0,60 m	Trial 1 km 6+500	Trial 2 km 7+163	Trial 3 km 7+513	Criterion
Granulometric curve	Granulometric curve	Granulometric curve	Granulometric curve	/
Natural humidity	$W_{np} = 12,00\%$	$W_{np} = 10,00\%$	$W_{np} = 12,00\%$	/
Atterberg limits	$W_P = 42,30\%$ $I_P = 18,86\%$	/	$W_P = 42,30\%$ $I_P = 18,86\%$	$W_P < 30,00\%$ $I_P < 17,00\%$
Proctor Compactness (standard)	$P_{dmax} = 1,650$ Mg/m³ $W_{opt} = 21,40\%$	$P_{dmax} = 2.,60$ Mg/m³ $W_{opt} = 7,60\%$	$P_{dmax} = 1,860$ Mg/m³ $W_{opt} = 13,00\%$	$P_{dmax} > 1.750$ Mg/m³ $W_{opt} < 20,00\%$
California CBR Load Index	$CBR_{2.50} = 5,00\%$ $CBR_{5.00} = 5,05\%$	$CBR_{2.50} = 63,64\%$ $CBR_{5.00} = 83,00\%$	$CBR_{2.50} = 3,94\%$ $CBR_{5.00} = 4,00\%$	min 8%
Calcium carbonate content $CaCO_3$	/	/	7,77%	/
Organic and combustible substances	Combustible – 4,62% Organic – 0,33%	Combustible – 1,73% Organic – 0,44%	Combustible – 5,17% Organic – 0,70%	max 8%

**Note*: for sample 2, the Atterberg limits cannot be determined due to the large presence of sand, while for sample 1 and sample 2, the presence of carbonates in the soil cannot be determined due to the large reactive action that forces the liquid from the graduated tube completely.

From the obtained results in table 1, it can be noted that Tests 1 and 3 do not meet the necessary criteria according to technical conditions. Atterberg's limits for Plasticity Limit WR = 42.30%, Plasticity Index IP = 18.86% exceed the permissible limit which is for WR = 30% and IP = 17%.

The Proctor compactness for Trial 1 of the results obtained does not meet the criteria, but Trial 3 is within the range of permissible limits.

The California load index CBR value for Trial 1 and 3 does not meet the proposed technical characteristics because they are 5% and 4% which is below the limit of min 8%.

The values for organic and combustible substances in all three samples are within the permissible limit.

Only trial 2 meets the prescribed criteria. All parameters from Trial 2 satisfy the prescribed technical conditions.

Based on the laboratory report, it can be noted that the majority of the existing subgrade does not meet the required criteria for this facility.

In order to continue with the construction of the upper structure, a solution had to be found for the existing subgrade, which was in a bad condition caused by several factors, such as: inadequate maintenance of the road body during its operation, poor drainage of the existing subgrade, drainage of some sections were not resolved at all, existing channels and culverts were not maintained, etc.

Representatives from the Investor, Supervisory Authority and Contractor were involved in finding a solution for the existing subgrade. After several meetings and offered alternative solutions, it was finally decided to replace the existing mattress material with a new material and thereby achieve satisfactory results. The new material that had to be incorporated was a natural resource, that is, a material made of crushed stone.

The implementation of the new solution entailed more manufacturing positions, thereby significantly increasing the value of the project.

Fig. 1 Excavation of the existing subbase at km 11+000, karpalak - želino section

3.1. Analysis of fly ash from REK Bitola

4 samples of fly ash from the REK Bitola thermal power plant were analyzed, and the obtained results of the chemical composition of the fly ash are presented in the following table:

Table 3 Results of chemical composition of fly ash from REK Bitola, Macedonia

Trial:	1	2	3	4
SiO_2	46,83	48,61	44,85	40,49
TiO_2	0,62	0,52	0,59	0,58
Al_2O_3	25,90	24,21	23,20	24,90
CaO	6,86	8,30	11,48	13,20
Fe_2O_3	9,96	8,94	9,58	10,55
MgO	2,99	2,64	3,53	3,99
MnO	0,19	0,27	0,33	0,38
Na_2O	1,50	1,20	1,17	1,21
K_2O	2,56	2,06	1,87	1,92
P_2O_5	0.34	0,41	0,41	0,39
$SiO_2+ Al_2O_3+ Fe_2O_3$	82,69	81,76	77,63	75,94
$Mo=CaO+MgO/SiO_2+Al_2O_3$	0,13	0,15	0,22	0,23
$Ms=SiO_2/Al_2O_3$	1,81	2,01	1,93	1,63
$K=CaO+MgO+Al_2O_3/SiO_2+MnO$	0,76	0,72	0,84	1,02

According to the classification of the American standard ASTM C 618-05 and the McCarthy division, the tested samples belong to class F, because the value of $SiO_2+ Al_2O_3+ Fe_2O_3$ ranges from 75.94 to 82.69, CaO from 6.86 to 13.20.

On an annual level, REK Bitola produces 1.5 million. tons of fly ash. Part of the ash is purchased by the cement plant USJE - Skopje, which uses it in the production of cement, but most of it ends up in a landfill in REC Bitola. Additional financial resources are used for the disposal of fly ash.

The price of fly ash in REC Bitola is 125 den/ton for loading directly in a tank truck and 25 den/ton for loading in a tipper truck.

4. DISCUSSION

In order to achieve successful stabilization of the subgrade with fly ash, attention must be paid to:
- Uniform distribution of fly ash,
- Proper pulverization and thorough mixing of the fly ash with the material to be stabilized,
- Moisture content control for maximum density and strength,
- Final compaction within the prescribed time frame (usually 2 hours).

Typical design specifications call for fly ash content to be 1 to 2 percent greater than the optimum content determined in the laboratory. Tankers should be used to transport fly ash to the construction site. Careful discharge of fly ash over the exposed subgrade by conveyors is the best way to obtain uniformity of application. The amount of ash can be

calculated knowing the depth, width, length and projected percentage of fly ash. Uniform distribution can be achieved by means of transport metering ports or direct metering of the ash in the mixing drum of the mobile mixer.

Construction discs (cultivators) can effectively combine the ash with the soil. The depth that the disc cuts must be carefully monitored. Where higher degrees of stabilization are required, the use of a mobile mixer is required to ensure adequate pulverization and uniform distribution of fly ash and moisture. One or two passes of the mixer may be used to obtain good mixing.

Fugitive dust can be a problem, just like any other construction process. The maximum dust is generated at the moment when the ash is discharged from the cisterns onto the pad. Construction activity will generally minimize dust.

When a rotary mixer is used, water is added to the mixer, which minimizes dust. This is the most effective procedure for building good stabilized soil:

Weather conditions:
- Favorable
  – Wet or dry,
  – Little or no wind,
  – Temperature above 4,5 ˚C.
- Bad
  – Windy,
  – Temperature below 0 ˚C.

Transportation
Fly ash is transported to the construction site via:
– Tarpaulin trucks or
– Tanks with pressure pumping systems.

Method(s) of mixing
a. The trucks already eject fly ash in a uniform line (if there is no wind);
b. The planning of the fly ash over the pad is done
c. It is mixed with a recycler moving at a speed of 6 – 10 m/min or with a disc to increase the depth.
d. Add water if needed.
e. Final planning is done with construction machinery

Compaction procedures
a. Initial compaction – is done with a hedgehog roller
b. Final compaction – steel roller with wheels to ensure a smooth surface
c. Compaction control
d. Compaction must be done within two 2 hours because working the mixture after that can break up the hydration products that stabilize the soil.

Hardening of the soil-fly ash mixture: When self-cementing fly ash is mixed with water, the hydration of the material creates a gel that binds (stabilizes) the soil resulting in a stronger, more uniform material with less permeability. Hydration requires water. Therefore, the planned surface should be kept moist.

Construction dynamics: about 1 to 1.2 km of stabilized pad can be built in one day.
PRECAUTIONS:
1. Wind: be aware of winds if fly ash is placed on the pad.
2. Mixing: to mix fly ash as soon as possible
3. Mixing: to mix fly ash as soon as possible

Durability: With proper mix design and performance, the subgrade is expected to last at least 50 years.

Fig. 2 Mixing of soil and fly ash with recultivator

4. CONCLUSION

Although different classifications of fly ash are applied in different countries, almost all types of fly ash can be used in construction and worldwide efforts and activities are being made to exploit the use of fly ash. In the last two decades, there has been an increase in scientific research activities in the field of application of alternative materials in construction, including the application of fly ash with the intention of protecting the environment from the negative impacts of waste material, as well as saving natural resources, i.e. to the use of stone aggregate decreased.

From the research we can conclude that:

- Fly ash is a suitable and safe construction material that can be used in road infrastructure,
- The use of fly ash instead of crushed stone contributes to the preservation of natural resources in R. of North Macedonia,
- The use of fly ash reduces the amount of waste, as well as the area for its disposal,
- From an economic point of view, fly ash as a waste material not only requires large areas for depositing and construction of landfills, but also requires additional investments in protection, preservation and maintenance of landfills, i.e. waste management,
- Reduction of construction activities, by causing a reduction in the need to use construction machinery, etc.

Considering the results obtained from REC Bitola, the studied fly ash fulfills the characteristics for classification in class F. The research in this scientific work on the application of fly ash during stabilization in the subbase gave an insight that there is a big

difference from a financial aspect when using this material. However, there is still an opportunity for expansion in the research of the characteristics of fly ash from other thermal power plants located in Macedonia.

Fig. 3 Storage and maintenance of fly ash in a power plant

REFERENCES

1. Special Practices for Design and Construction of Subgrades in Poor, Wet, and/or Saturated Soil Conditions. Eugene L. Skok, Eddie N. Johnson, and Marcus Brown. (2003)
2. Skok, Eugene L., Timm, David H., Brown, Marcus L., and Clyne, Timothy R., Best Practices for the Design and Construction of Low Volume Roads. MinnesotaDepartment of Transportation, St. Paul, MN, March 2002.
3. Minnesota Department of Transportation, Geotechnical and Pavement Manual. Minnesota Department of Transportation, St. Paul, MN, April 1994.
4. Krebs, Robert D. and Walker, Richard D., Highway Materials. McGraw-Hill, New York, NY, 1971.
5. Transportation Research Board Committee on Lime and Lime-Fly Ash Stabilization, Lime Stabilization Reactions, Properties, Design and Construction State of the ArtReport 5. Transportation Research Board National Research Council Washington D.C., 1987.
6. Howley, Jack, Upgrading Unpaved Roads. Road Base Stabilization Using Lime and Fly Ash. U. S. Department of Transportation, Washington D.C., September 1981.
7. Shirazi, Hadi, Field and Lab Evaluation of the use of Lime – Fly Ash to Replace Soil Cement as a Base Course. Louisiana Transportation Research Center, Baton Rouge,LA, September 1997.
8. Fly ash facts for highway engineers (2003)
9. Soil and Pavement Base Stabilization with Self-Cementing Coal Fly Ash, American Coal Ash Association, Alexandria, Virginia,May 1999.
10. Fly Ash for Soil Improvement, Geotechnical Special Publication No. 36, American Society of Civil Engineers, New York, New York, 1993.
11. Skok, Eugene L., Best Practices for Design and Construction of Pavement Subgrades and Embankments in Minnesota. Questionnaire on Existing Projects and Practices. Minnesota Department of Transportation, St. Paul, MN, March 2002.
12. Primjena elektrofilterskog pepela u asfaltnim mješavinama - Katarina Mirković, 2019

13.   White, D. J., D. Harrington, and Z. Thomas. 2005. Fly Ash Soil Stabilization for Non-Uniform Subgrade Soils, Volume I: Engineering Properties and Construction Guidelines. IHRB Project TR-461; FHWA Project 4. Iowa State University, Ames, Iowa.
14.   White, D. J. 2006. "Reclaimed hydrated fly ash as a geomaterial." Journal of Materials in Civil Engineering. ASCE, 18(2):206-213.

STABILIZACIJA PUTNE PODLOGE UPOTREBOM ELEKTROFILTERSKOG PEPELA

Zbog pojačanih aktivnosti u građevinarstvu, a posebno u saobraćajnoj infrastrukturi, a samim tim i povećanja upotrebe dodatnih građevinskih materijala, potrebna su inovativna rešenja u pronalaženju alternativnih materijala za očuvanje prirodnih resursa. Jedno od rešenja za očuvanje prirodnih građevinskih materijala je primena recikliranog materijala, koji će zadovoljiti i zahtevane standarde u građevinarstvu. U saobraćajnoj infrastrukturi postoji velika mogućnost za korišćenje recikliranog materijala, počev od podloge, preko nasipa pa sve do gornjeg stroja betonskih konstrukcija. Jedan od recikliranih materijala koji se može koristiti u građevinarstvu je elektrofilterski pepeo. Elektrofilterski pepeo je otpadni materijal koji najviše obećava kada je u pitanju širok spektar primena u građevinarstvu. Elektrofilterski pepeo se dobija sagorevanjem uglja u termoelektranama za proizvodnju električne energije. Zbog varijacija u sastavu i karakteristikama elektrofilterskog pepela, stvoreno je nekoliko podela i klasifikacija. Jedna od glavnih klasifikacija je prema američkom standardu ASTM C 618-05 gde se deli na klasu C i klasu F elektrofilterskog pepela. Ovo istraživanje ima za cilj da istraži primenu elektrofilterskog pepela za stabilizaciju podloge i da utvrdi razliku iz finansijske i ekološke perspektive za primenu elektrofilterskog pepela u poređenju sa prirodnim kamenim agregatom. Glavna istraživanja su sprovedena u vezi sa povećanom upotrebom prirodnog kamenog agregata, koji se pojavio kao potreba prilikom sanacije državnog puta R1206, deonica Karpalak – Želino. Osim upotrebe velikih količina kamenog agregata za stabilizaciju podloge, to je uticalo i na finansijski okvir za realizaciju projekta puta. U Makedoniji je urađena analiza hemijskog sastava 4 uzorka elektrofilterskog pepela dobijenog u REC Bitola. Iz dobijenih rezultata može se zaključiti da pripada klasifikaciji elektrofilterskog pepela F klase i da se uz upotrebu aktivatora (kreča ili cementa) može koristiti u stabilizaciji podloge.

Ključne reči: *građevinarstvo, posteljica, podloga, elektrofilterski pepeo, stabilizacija*